Study of Au Ball Bond Mechanism and Reliability on Pd/Ni/Cu Substrate

by

Yan Huang

A thesis
presented to the University of Waterloo
in fulfilment of the
thesis requirement for the degree of
Master of Applied Science
in
Mechanical Engineering

Waterloo, Ontario, Canada, 2009

Declaration

I hereby declare that I am the sole author of this thesis. This is a true copy of the thesis, including any required final revisions, as accepted by my examiners.

I understand that my thesis may be made electronically available to the public.

Yan Huang

Abstract

Microelectronic wire bonding is a manufacturing process used to electrically connect integrated circuits with circuit boards or other substrates. Conventionally, balls are molten at the end of a Au bonding wire and subsequently bonded on Al metallization of a integrated circuit. However, Pd/Ni metallization has recently been used for its improved mechanical properties.

The bondability, bonding mechanism, and reliability of Au ball bonds on Pd are studied in this thesis. The substrates were produced in this project using three different materials. The base material is polished Cu in the shape of a coupon (1.0 cm × 1.0 cm × 0.5 mm). Cu coupons are plated with Ni (1.0 µm) using an electroless process, followed by electrolytic plating of a layer of Pd (0.3 µm), resulting in an arithmetic mean roughness of the surface of 0.08 µm (baseline sample, sample 0). Higher roughness values of 0.2, 0.4, and 0.5 µm are artificially produced by rolling (sample 1), sanding (sample 2), and sandblasting (sample 3), respectively, on the Cu surface before plating Ni and Pd.

A 25 µm diameter Au wire is used for bonding on the polished and roughened substrates with a process temperature of T = 220 °C, and it was found that ≈ 4 % to ≈ 18 % less ultrasonic amplitude was required for successful bonding on the roughened substrates compared to the polished substrate. Bondability is measured by shear testing the ball bonds. An average ball bond strength achieved on the polished substrate is 130 MPa. This value is lower on the roughened substrate with the exception of the sandblasted substrate.

Long-term thermal aging at 250 °C was performed with ball bonds on samples 0-3 for durations of ≈ 300 h. The reliability of the bonds is characterized by non-destructive contact resistance analysis during aging and destructive cross section analysis after aging. Contact resistance values for

the ball bonds range from 1.6 to 3.5 mΩ at 20 °C before aging, and does not correlate with roughness. For the baseline sample, contact resistance of the ball bonds decreases during aging by -6 % (median value), which indicates electrical integrity of the interconnections at high temperature. This decrease possibly is due to interfacial gap filling by Au or Pd diffusion. In contrast, the contact resistance increases for the roughened samples 1-3 and changes are 0.4, 5, and 14 %, respectively (median values). A conclusive explanation for this increase has not yet been found. After 250 h of aging, a TEM analysis showed Au to Pd diffusion in the baseline sample with a diffusion depth of ≈ 0.1 µm Au. No intermetallics, voids, or contamination is found on the interfaces after aging according to nanohardness, SEM, and TEM analyses. No bond lift-offs or electrical opens were found for the aging temperature and durations chosen. No conclusive evidence for the presence of Au-Pd intermetallics or voids is found.

Acknowledgements

I would like to thank my supervisor Michael Mayer for providing me with guidance and support throughout my time as a graduate student in the University of Waterloo. I was motivated to work hard and learned valuable skills, which will help further reach my career goals.

Special acknowledgement goes out to Michael McCracken and all the members of the CAMJ for helping me transition and adapt to the research environment. I will remember all the laughter we shared over the past two years.

This thesis would not be possible if not for the financial support from Intel Corporation, which deserves an appreciation for also giving me feedback and suggestions in order to keep me on track.

Finally, I want to thank my parents for everything they have done for me.

Table of Contents

List of Figures viii
List of Tables vi
1. Introduction 1
1.1 Motivation 1
1.1.1 Effect of Wire 2
1.1.2 Effect of Substrate 3
1.2 Objectives 4
1.3 Thesis Outline 5
2. Literature Review 6
2.1 Wire Bonding Process 6
2.2 Bond Materials 8
2.3 Film Deposition 9
2.3.1 General Plating Process 10
2.3.2 Plating Process for Ni 12
2.3.3 Plating Process for Pd 13
2.4 Bonding Mechanism 14
2.5 Bond Characterization 17
2.5.1 Wire Pull 17
2.5.2 Ball Shear 18
2.6 Ball bond Aging 19
2.6.1 Intermetallics and Interdiffusion 19
2.6.2 Kirkendall Voids 21
2.7 Some Process Modulators 23
2.7.1 Thickness 23
2.7.2 Hardness 23
2.7.3 Roughness 24
2.7.4 Contamination 24
2.7.5 Plating Chemistry 25
2.8 Summary 25
3. Development of Pd/Ni/Cu Coupon 27
3.1 Experimental 27
3.1.1 Cu Base Material 27
3.1.2 Electroless Plating of Ni 28
3.1.3 Electroplating of Pd 31
3.2 Plating Results 35
3.2.1 Electroless Ni Plating 35
3.2.2 Electrolytic Pd Plating 37

3.3 Summary 40
4. Development of Wire bonding Process 42
4.1 Experimental 42
4.1.1 Bonding Plan 42
4.1.2 Ball Bond Geometry 44
4.1.3 Ball Bond Shear Strength 44
4.1.4 Summary 45
4.2 Bonding Results 45
4.2.1 Free-Air Ball 45
4.2.2 Ball Geometry 47
4.2.3 Shear Strength 47
4.3 Summary 49
5. Reliability Study Through Destructive Analysis 52
5.1 Shear test 52
5.2 Cross-section Analysis 52
5.2.1 Nanohardness 54
5.2.2 SEM 56
5.2.3 TEM 59
5.2.4 Discussion 69
5.3 Summary 70
6. Reliability Study Through Contact Resistance Monitoring 71
6.1 Experimental 71
6.2 Results 76
6.3 Discussion 82
6.4 Summary 83
7. Roughness Modulation 84
7.1 Experiment 84
7.2 Wire Bonding Process Adjustments 87
7.3 Non-Destructive Analysis 90
7.4 Destructive Analysis 97
7.5 Discussion 97
7.6 Summary 99
8. Conclusions 100
References 101
Appendix A 104

List of Figures

Fig. 1 Schematic diagram of typical wire bonding process. 7

Fig. 2 Typical ball bond process window for Au on Al. After [21]. 8

Fig. 3 Binary phase diagram of Au-Pd [14] 10

Fig. 4 Lattice parameter of Au-Pd system [14]. 15

Fig. 5 Ball bond quality characterization methods: a) shear and b) pull test (not to scale) 17

Fig. 6 SEM image of the Au ball bond on Au/Pd/Ni cap a) after aging, and b) as bonded at magnification ×10k [28]. 19

Fig. 7 Interdiffusion between Au and Pd metallic layers at temperatures 200°C, 250°C, 312°C, and 389°C in vacuum and air [29]. 20

Fig. 8 Change in diffusion coefficient with respect to atomic fraction of Pd for thin Au/Pd alloy film with aging at 350°C over 4 h and 8 h [30]. 22

Fig. 9 Cu coupon a) before and b) after mechanical polishing with i) photo, ii) topography, and iii) roughness measurements. 28

Fig. 10 Electroless Ni setup in a) overall view and b) detailed view. 30

Fig. 11 Electro Pd setup in a) overall view and b) detailed view of Ni/Cu, and c) detailed view of anode. 34

Fig. 12 Electric field line distribution in electroplating process 34

Fig. 13 Plating thickness vs. plating time with thickness data gathered from a) z direction, and b) x direction. Fit is polynomial of 2nd degree (parabolic). Dashed lines are standard error of fit. 36

Fig. 14 SEM of Ni plated surface at magnification of a) ×5k and b) ×100k. 37

Fig. 15 SEM-EDAX of Ni plated surface cross section with FIB, at magnification of ×3k 38

Fig. 16 Curve of best polynomial fit for Pd thickness variation at input current of a) 5 mA, b) 10 mA, c) 15 mA, and d) 20 mA in the vertical (i), and horizontal (ii) directions. Fit is polynomial of 2nd degree (parabolic). Dashed lines are standard error of fit. 39

Fig. 17 SEM of the Pd plated surface at magnification of a) ×50k and b) ×100k. 40

Fig. 18 SEM thickness measurement of Pd/Ni/Cu coupon for Pd deposition time of 50s, Ni plating time of 140s 40

Fig. 19 SEM-EDAX of Pd/Ni/Cu coupon at magnification of ×5k 41

Fig. 20 a) Overview, and b) detailed view of bonding schematic for ball bond optimization. .43

Fig. 21 a) Illustration of a) FAB, and b) bonded ball bond. 44

Fig. 22 Boxplot of measured FAB diameter with respect to nominal FAB diameter. 46

Fig. 23 Measured ball bond a) BH, and b) MBD for various IF. Pd substrate. BF = 240 mN. FABnom = 45 μm. 48

Fig. 24 Optimized US for achieving a) maximum shear strength and b) shear at the ball (×200) before ultrasound enhanced deformation (UED) [27] 49

Fig. 25 Boxplot of a) MBD, and b) BH for various levels of US. 50

Fig. 26 SEM of a) bonded wire loops, b) ball bond top view and c) side view. On Pd/Ni/Cu coupon with optimized bonding parameters. 51

Fig. 27 Boxplot of shear force for various aging time. 53

Fig. 28 Optical microscope image of ground and polished as bonded ball bond. 54

Fig. 29 Topography view of cross section of interfacial layer between center of Au ball and Pd/Ni/Cu substrate after nanoindentation for an aged coupon for 250 °C over 200 h. Image size 8 μm×8 μm. 55

Fig. 30 Nano-hardness of a) across interfacial cross section of Au ball on Pd/Ni/Cu substrate for the as bonded and aged compared with Vickers of corresponding metals and b) comparison between as bonded and aged with change in distance from Pd/Au interface to pure Au region. 57

Fig. 31 SEM image of ground and polished a) as bonded, b) aged for 50h, c) aged for 100 h, and d) aged for 200h bond. 58

Fig. 32 EDX of grinded and polished as bonded ball bond. 59

Fig. 33 SEM image of ground and polished a) left edge of bond as bonded, b) right edge as bonded, c) left edge aged for 100 h, and d) right edge aged for 200h. 60

Fig. 34 SEM image of sample aged for 200h with carbon deposition on top 61

Fig. 35 SEM image of sample aged for 200h after 10 h of milling on the two sides. 61

Fig. 36 SEM image of sample aged for 200h after milling at the bottom. 62

Fig. 37 SEM image of sample after placing the manipulator tip on top, aged for 200h. 62

Fig. 38 SEM image of sample aged for 200h after being placed on the copper grid holder. 63

Fig. 39 SEM image of sample aged for 200h after additional milling to thin the sample for TEM study. 63

Fig. 40 TEM image near the Au/Pd region at increased magnification from a) to b) 64

Fig. 41 TEM image near the Au/Pd region at various (a, b, c, d) tilt angle 65

Fig. 42 Detailed TEM image near the Au/Pd region at magnifications shown in a) and b), zoom of a) 66

Fig. 43 TEM image near the Cu region at magnifications various tilt angle (a, b) 66

Fig. 44 EDX line scan across the a) Pd/Ni/Cu/Au metallic layers for x ray spectra of b) Au, c) Ni, d) Pd, and e) Cu. 67

Fig. 45 EDX line scan across the a) Au/Pd/Ni metallic layers for x ray spectra of b) O, c) Ni, d) Pd, e) Au and f) Cu. 68

Fig. 46 TEM image near the Au region at magnifications various tilt angle (a, b) 69

Fig. 47 a) Top view and b) side view of the 4-wire contact resistance measurement method. ..71

Fig. 48 Photo of plated substrate after cutting and curing on the 28-pin chip package. 72

Fig. 49 Bonding diagram for Pd/Ni/Cu on the 28-pin package (filename of bonding recipe: "YAN_INT1.REC". 73

Fig. 50 Photo of Au ball bonding process a) during and b) after bonding on Pd/Ni/Cu for contact resistance measurement. 74

Fig. 51 Wiring diagram for contact resistance measurement process of Au ball bonds to Pd/Ni/Cu substrate while in oven. 75

Fig. 52 Contact resistance measurement test for largest change and least change in resistance for coupon with Ra of 0.08 μm. T = 250 °C during phase II. 79

Fig. 53 SEM images of double ball bond for a) largest Rc change (bond #12), b) the typical change (bond #9) and c) least change (bond #10) in i) top and ii) side view for coupon with Ra of 0.08 μm. 80

Fig. 54 Contact resistance measurements for ball bond numbers 1-8, 11, and 13 through the 287 h aging at 250 °C for coupon with Ra = 0.08 μm. 81

Fig. 55 Resistivity of undeformed Au-Pd alloys at liquid nitrogen temperature (77.2 K) [44]. 82

Fig. 56 Roughness measurement samples of a) Cu after sanding with 500 grid sand paper, b) Cu after standard grinding and polishing, and c) standard Ag bondpad. 85

Fig. 57 Overview of sandblasting a) machine, b) sample, and c) fine bead. 86

Fig. 58 Optical microscope image of a) polished baseline sample with b) optical profiler roughness measurement 87

Fig. 59 Optical microscope image and corresponding optical profiler measurement of a), d) sandblasted, b), e) sandpaper, and c), f) as shipped Pd/Ni/Cu coupon 88

Fig. 60 Variation in a) FAB, b) MBD, and b) BH with change in roughness of Pd/Ni/Cu 89

Fig. 61 Au ball bond shear strength variation with roughness 90

Fig. 62 Contact resistance measurements for coupons with Ra of 0.4 μm. T = 250 °C during phase II. 91

Fig. 63 Contact resistance measurements for ball bonds 1-7, and 7-12 through 287 h aging at 250 °C.for coupon with Ra of 0.4 μm. 92

Fig. 64 Contact resistance measurements for 6 ball bond through 287 h aging at 250 °C.for coupon with Ra of 0.5 μm. 94

Fig. 65 Contact resistance measurements for 6 ball bond through 287 h aging at 250 °C.for coupon with Ra of 0.2 μm. 96

Fig. 66 Cross section of ball bonds on Pd/Ni/Cu with roughness of a) 0.2 μm and b) 0.5 μm before aging i) at the ball bond and ii) away from ball bond. 98

List of Tables

Table 1 Properties of electrolytic and electroless process 12

Table 2 Properties of electroless Ni process [37] 29

Table 3 Cleaning solution for Ni plating process [37] 29

Table 4 Properties of electrolytic Pd process [38] 32

Table 5 Calculated with change in current density and cathode efficiency 33

Table 6 Cleaning solution for Pd plating process [38] 33

Table 7 MKE Au wire properties [39] 42

Table 8 Initial parameters for the ball bonding process 45

Table 9 Bond off/wedge bond parameters 46

Table 10 FAB, ball bond parameters and responses 49

Table 11 Description of points in a typical nanohardness measurements 55

Table 12 Top ball bond and other parameters for double ball bond process. 74

Table 13 Contact resistance reading for 13 sets of double ball bonds at ambient temperature. 77

Table 14 Comparison between Rc at different stages of aging for baseline sample. 78

Table 15 Ball bonding parameters with various roughness substrate 89

Table 16 Comparison between contact resistance at different stages of aging for Ra= 0.4 μm sample (sample 2). 93

Table 17 Comparison between contact resistance at different stages of aging for Ra= 0.5 μm sample (sample 3). 95

Table 18 Comparison between contact resistance at different stages of aging for Ra= 0.2 μm sample (sample 1). 97

1. Introduction

In today's microelectronic packaging industry, wirebonding and flip chip bonding have led the way in interconnecting semiconductor devices. Wire bonding has accounted for over 70% of the total units of advanced packages of microelectronic devices for the past decade. At the same time, electronic devices are becoming smaller in size, which causes the demand for fine pitch wire bonding to rise. With the high demand, electronic packaging industry leaders are constantly investing time and money to improve the quality of the process, while attempting to reduce cost to maximize profit.

1.1 Motivation

Reliability of interconnect in wirebonding is an essential measure of its overall quality. Wirebonds with lack of reliability are deemed to fail over a short period of time. Even if all the major components in a electronic chip assembly are functional, one dysfunctional wire could cause a complete disaster for the whole system. Not only would there be additional cost incurred, the reputation of the company would be affected depending on the severity of the failure. Therefore, interconnects are required to be of the highest quality. In a typical electronic assembly, a certain amount of power is required to drive its components. Therefore, power dissipation in the form of heat is expected to occur. Reliability tests performed at elevated temperature over long period of time can simulate the actual environment the wirebonds would experience, which makes these tests a vital part of a quality assessment plan. In order to achieve reliability without the high cost of changing electrical and mechanical hardware of the bonding equipment, proper choices of the wire and substrate material are required.

1.1.1 Effect of Wire

The material of the wire used in the wire bonding process remains an interesting research topic in today's electronic packaging industry. Therefore, the property of wire is an important modulator in analyzing the reliability of the wire bond. The wires discussed in this section are those commonly used in the industry.

Au wire to Al substrate has been the most popular method in the wirebonding industry. Au wire has good electrical, thermal properties and is resistant to oxidation. Au wire is also found to have good adhesion to Al at elevated bonding temperature. However, exposure to high temperature of above 150 °C has promoted intermetallic (IMC) growth between the Au bond and the Al bond pad [1, 2]. The presence of IMC degrades the electrical conductivity, and reduces the quality of the overall electrical assembly. IMC formation can lead to crack propagation, which could result in connection failure [1, 2].

Cu wire has emerged in recent years as an alternative to the standard Au wire to Al bondpad. Even more so than Au, Cu has excellent mechanical, electrical, and thermal properties [3]. Cu is also cheaper and more readily available. Void formation due to IMC does not degrade the electrical conductivity in the Cu-Al system [4]. However, Cu is very prone to oxidation, which can be compensated by adding shielding gas during bonding, and properly storing under dry conditions. Cu-Al does produce brittle IMC, whose growth is accelerated by temperature [3]. Effects of cratering, and Al pad thinning as a result of the relatively high Cu hardness could cause chip cracking, and is a predominant issue on low-k dielectric material [5, 6]. Cu wire on Al has also shown degradation in quality over short periods of time under high humidity environment [7].

Another type of wire material commonly used in wirebonding is Al. In the Al-Al process, both wire and substrate material are the same, which makes the system not prone to IMC formation.

However, the bonding between Al and Al has reliability issues due to the high frequency of bond lift off and cracking failure [8, 9], and is exclusively used for wedge-wedge bonding, a process variation less productive than ball bonding.

1.1.2 Effect of Substrate

Au is chosen in this study on the wire side due to its useful properties in wire bonding. One remaining process modulator that can be investigated is substrate material. Similar to wire material, numerous types of substrate have been explored.

Al is the most widely used material for bonding to Au wire. Being one of the most abundant metals on earth, Al is relatively inexpensive compared to other substrate materials. Al is low in density, which reduces system weight to enhance the portability of electronic devices. The relative resistance to corrosion and oxidation properties improve the life span of the interconnect. As described earlier, Al forms IMC with Au and is prone to underpad damage.

The Au-Ag system is reliable at elevated temperature and resistant to corrosion. However, Ag is prone to contamination, causing bondability issues. The presence of oxide and organic contaminants reduces the interfacial friction and decreases the heat dissipation between bonding materials, leading to bad bond quality [10]. Therefore, Au-Ag system is used primarily in second bond formation, and elevated bonding temperatures are used to remove contaminants.

Similar to the Au-Al system, IMC formation is present in the Au-Cu system. Cleanliness of the bonding surface is imperative to improve the quality of the bonding process. Shielding gas is also required to prevent Cu from oxidation during bonding. The Au-Cu process is used mainly in second bond formation similar to the Au-Ag process. Due to the complexity for the setup of this process, it is often not preferred in the current microelectronic packaging industry.

The Au-Ni system is generally reliable at elevated temperature. Ni is a much harder material than Al, and is less likely to break under high stress, which is why it is used in direct chip bonding applications. However, Ni forms oxide and corrodes rapidly [11]. Therefore, wirebonding must take place in an inert atmosphere after plating of Ni. Alternatively, a thin film of Au can be deposited on top of the Ni layer as an oxidation barrier, but this is an additional process step and an additional cost.

The Au-Au system is deemed reliable over long times at elevated temperature. The bondability of Au-Au system is excellent as no interface corrosion, IMC formation, or other mechanism that degrades bonding are known. Although the Au on Au system shows both excellent bondability and reliability, Au is an expensive material and relatively scarce.

The properties of Pd make it an acceptable candidate for substrate material. Pd is electrically stable, and resistant to tarnish, chemical erosion, and intense heat, which makes it a good candidate for overcoming reliability issues seen in other types of substrate material. It has been reported that Pd material shows good adhesion to Au wire and improves the shelf life of lead frames during the wedge bonding process [12]. However, while the Au-Pd system is already in industrial use, studies of its bondability remain scarce in the thermosonic ball bonding community.

1.2 Objectives

The intention of this research is to form Au ball bonds of size 50 μm to 60 μm on Pd/Ni/Cu substrates and analyze the nature of bonding between Au wire and Pd. The reliability of the Au-Pd process is compared with the standard Au-Al process through aging at 250 °C over 200 h. As a process modulator, roughness is varied on the Pd/Ni/Cu substrate in an attempt to get a better understanding and possibly improve the Au-Pd process.

1.3 Thesis Outline

To explain the background of the study, the basic bonding and plating processes, bonding and failure mechanism, and techniques to characterize bondability and reliability are introduced in Chapter 2. Before bonding, the layers of Ni and Pd are plated on top of the base material Cu. The setup, and results of the material deposition process are given in Chapter 3. Bonding optimization of the Au-Pd system to analyze bondability in terms of achieving the desired geometry and shear strength are introduced in Chapter 4. The basic bonding mechanism is explored here. Chapters 5 and 6 investigate the reliability of the Au-Pd system through aging, by destructive (nanohardness, SEM, TEM) and non-destructive (in-situ contact resistance) techniques, respectively. The goal is to analyze any possible IMC and interdiffusion within the system.

The development of Pd/Ni/Cu substrates at different roughnesses, with the corresponding bondability and reliability analyses are discussed in Chapter 7.

2. Literature Review

Among the methods to make interconnections between an integrated circuits (IC) and a printed circuit boards (PCB), wire bonding is considered the most cost effective and flexible technology. The earliest reported wire bonding development was by scientists of Bell Laboratories in the 1955-1958 time period, which led to growing popularity in many semiconductor companies, and paved the way for affordable integrated circuits worldwide.

2.1 Wire Bonding Process

In order for a semiconductor device to operate, it must be electrically connected to an outside assembly. The electrical connections to this external hardware are made by wires of a few microns in diameter. Essentially, the wire bonding process is a method to bond metallic wires between two electrical devices. The ideal connection should show good conductivity and will not degrade over time.

Two variants of wire bonding process are (1) ball bonding and (2) wedge-wedge bonding. In a typical ball bonding process, there are two forms of wire bonds. The ball bond is the first bond and is responsible for connecting the first end of the wire to the bond pad of the chip. A schematic of the wire bonding process is shown in Fig 1. Initially, the tip of the wire is melted by a spark from the electrical flame off (EFO) electrode. Subsequently, a ball shape known as the free air ball (FAB) is formed from rapid solidification and surface tension at the wire tip. The shape and size of the ball formed depends on the EFO current and its duration (time). Impact force (IF) is then applied by the capillary to drive the ball to the substrate. Subsequent bond force (BF) and ultra-sound energy (US) by the attached transducer are then applied to deform the ball and create inter-facial adhesion between the bottom of the deformed ball and the bond pad on the chip. The

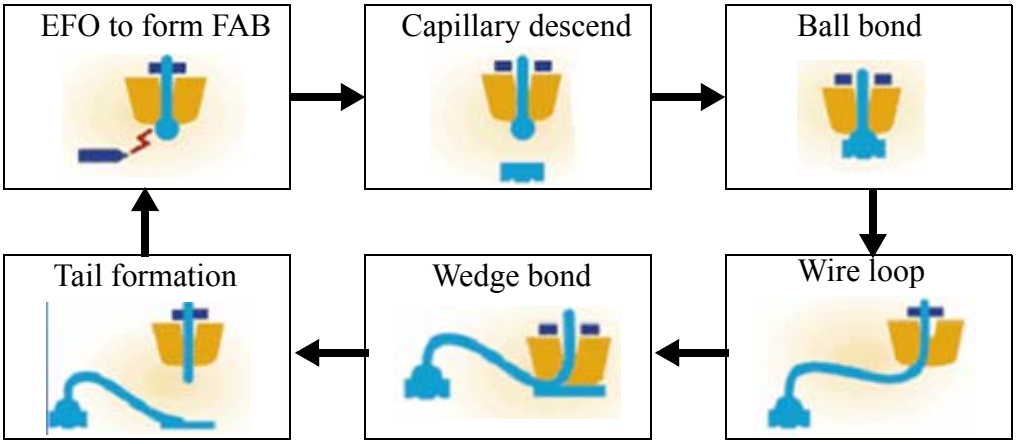

Figure 1 Schematic diagram of typical wire bonding process.

capillary then travels in a predetermined direction, while the wire feeds through. Once the capillary reaches the lead frame (2nd bond position), a wire loop is formed between the substrate and the lead frame. Subsequent IF, BF, and US are applied similarly to the ball bond process to form the second type of wire bond known as the wedge bond, which is responsible for establishing the connection between the remaining end of the wire and lead frame. The wire is cut at the 2nd bond position, leaving a tail at the end of the wire. The capillary moves back to its original position, and the next FAB is formed on the tail extruding from the capillary. The process can be repeated thousands of times per minute. There is no ball formation in the wedge bond stage and the deformation is applied directly to the wire. The shape and the amount of deformation on the ball and wedge bonds are heavily dependent on the bonding parameters, which also include bond time (BT) and temperature (T). The BT parameter defines the duration of the US generation. The ball bonds are generally stronger than the wedge bonds. In this research, the focus is on the ball bond. An example bonding process window is shown in Fig. 2 for Au on Al. The BF and US are dominant parameters during bonding. The non-shaded region indicates area acceptable for bonding, where the strength of the ball bond is above a certain required threshold. Within the shaded region, two

boundaries are known. Beyond the first boundary, excessive US deformation occurs and the strength of the ball bond drops with increase in its diameter. Beyond the second boundary, interfacial sliding is absent and US bonding cannot occur. Optimization of the bonding process is vital for achieving bondability.

2.2 Bond Materials

In typical wire bonding processes, the minimum material requirement include a wire bonding machine, a capillary, a wire spool, and the package to be bonded. In this research, a thermosonic wire bonding machine supplied by ESEC, Cham, Switzerland, is used. The machine is used mainly for bonding of Au wire. The bonding temperature used on the machine generally ranges from 100 °C to 240 °C. The desired capillary chosen in the process is the standard 60 µm pitch alumina model supplied by Small Precision Inc, Boston, USA.

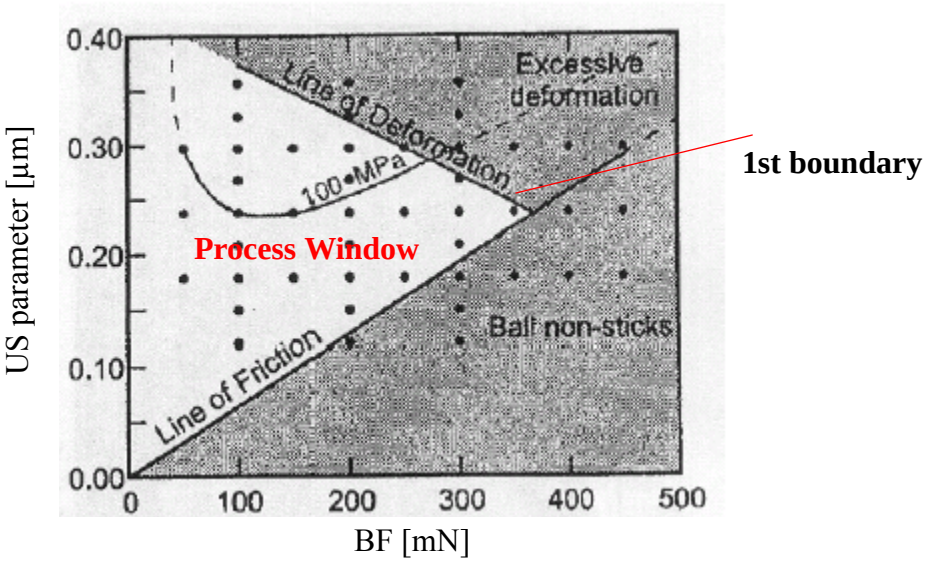

Figure 2 Typical ball bond process window for Au on Al. After [21].

In the joining process under investigation, Au wire is bonded to Pd substrate. The diameter of the wire is 25 μm. Its composition is 99.99% Au and is supplied by MKE, Yongin, Korea. The base material of the substrate is made of 99.99% high conductivity oxygen free (HCOF) Cu supplied by Goodfellow, Inc, Hungtingdon, England. To protect the Cu material from oxidation, thin layers of Pd and Ni are deposited. The goal of the Ni is to ensure the integrity of the Pd finish by preventing diffusion and migration of Cu [13]. Also, Ni is a very hard material with high Young's Modulus, which overcomes underpad damage problems seen in Al substrates. The Pd layer not only protects the Ni from oxidation, but most importantly, it provides the required wire bondability through surface adhesion and shows excellent reliability at elevated temperature over long periods of time [12, 13]. As one of the Palladium group metals (PGM), Pd is relatively inert, with respect to chemical attack by oxygen or other acids. Figure 3 shows the binary phase diagram between Au and Pd. The Au_3Pd and $AuPd_3$ phases occur at temperatures above 800°C, which is above the temperature normally experienced by the electronic components. The dotted lines indicate the two phases that cannot be confirmed. The remaining phase at about 100°C is hypothetical and may not exist [14]. In general, Au and Pd form continuous series of solid solutions, which would indicate an improvement in reliability over the Au-Al process [14]. It is of interest to analyze the bonding mechanism between Au and Pd, and to confirm the lack of IMC.

2.3 Film Deposition

Various material deposition methods were considered in the process. Some of the less novel techniques include chemical vapor deposition (CVD), physical vapor deposition (sputtering), electroplating and electroless plating. CVD is used to produce high purity and high performance solid material. However, the process is complex and requires a large amount of resources and time to find the most viable precursor for the metallic target [15]. Sputtering is a much more viable option

for metallic layers used in IC packaging as it is relatively easier and less expensive to set up than most of the deposition processes. The quality of the sputtered surface is degraded compared to other deposition processes due to impurity and contamination problems [16]. In most cases, the quality of the material deposition process is directly proportional to cost and complexity of the setup.

2.3.1 General Plating Process

Plating is a process primarily used for depositing metal on a conductive surface. The goal of typical plating processes is to provide corrosion inhibition, radiation shielding, solderability, and con-

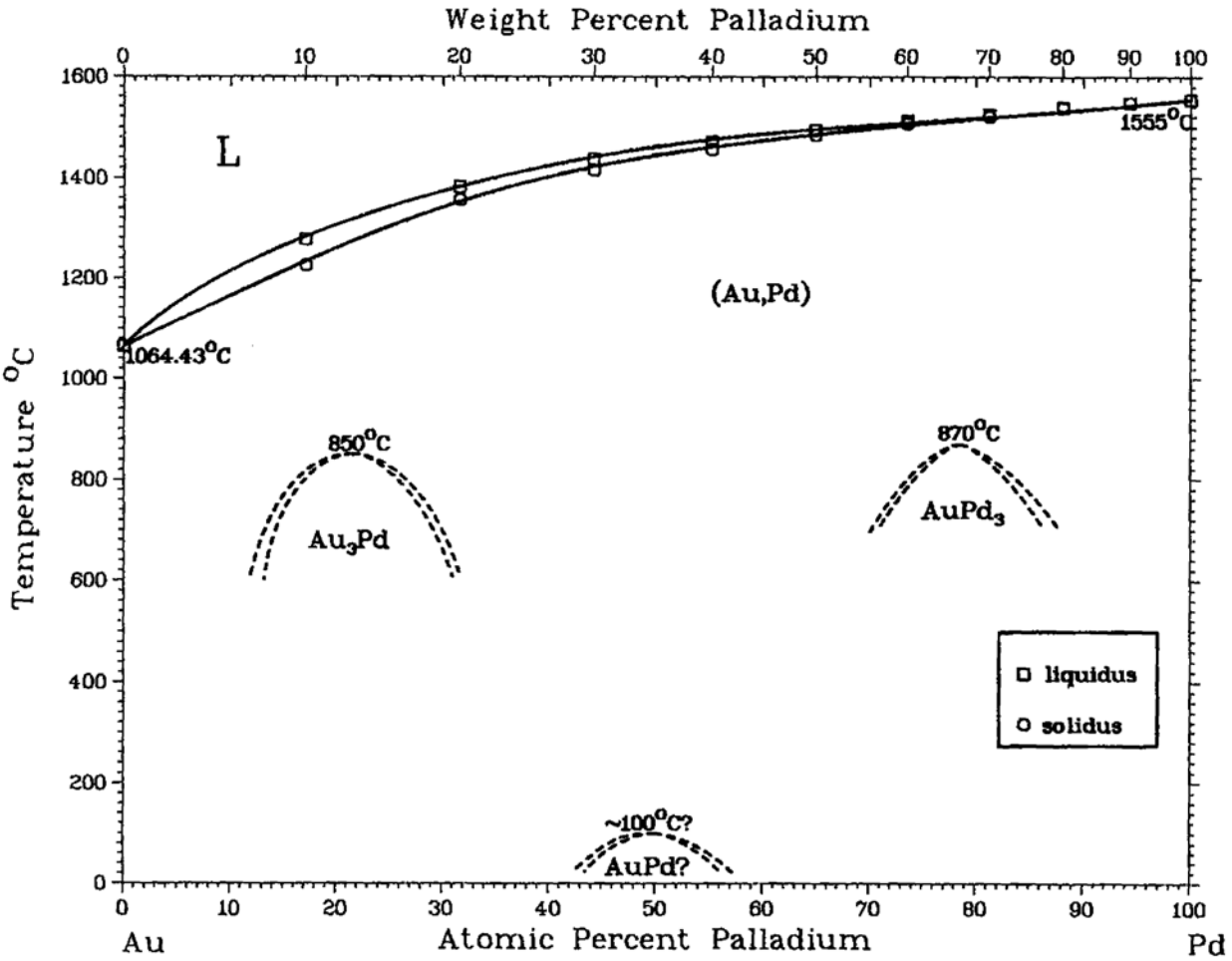

Figure 3 Binary phase diagram of Au-Pd [14]

ductivity. In general, the plated material shows good uniformity and surface adhesion to the base material [17].

There are two types of plating methods, the first type is called electroplating, which models a standard Galvanic Cell. A negative charge is applied by a constant voltage power source on an object to be plated (cathode). The positive side of the power supply is attached to an anode. Both the cathode and anode are immersed in the solution containing metallic salt. As the object to be plated is negatively charged by the constant voltage, the positive metallic ions are attracted to the surface of the cathode and reduce into metal form. The motion of the metallic ions is also a result of interaction between the electric and magnetic field within the solution medium. At the same time, the anode removes electrons from the metal salt in the solution, oxidizing it to its metallic ion state [17, 18]. Both the oxidation and reduction process occur simultaneously as long as current flows within the plating bath. Typical anode materials are metals with equilibrium potential higher than that of the metallic salt in the solution.

The second type of plating process is electroless plating, which does not require an external power source. The reduction and oxidation processes are purely chemically driven [17, 19, 20]. Similarly to the electrolytic process, metallic salt is dissolved in the plating solution. However, plating is initiated by activating the destination metal with another metal that has a higher equilibrium potential, for about 10 to 20 s. A potential difference results when both the activation and target metals are inserted in the plating bath [19, 20]. The bath types for both electrolytic and electroless plating processes include, alkaline, acidic, and neutral baths [17, 18]. The plating time is heavily dependent on temperature, pH and concentration of the bath [17-20]. Table 1 lists a comparison between the properties of the two plating processes. The step coverage is defined as the ratio of the thickness of a film over a step edge to the thickness in a flat area. For the electroplating pro-

cess, the step coverage depends on the geometry of the substrate to be plated. With a square shape Cu coupon as a substrate, the thickness of the plated layer tends to increase at the edges due to the "edge effect", generated by the interaction of an electric field with a nonuniform (gradient) magnetic field [22]. In this study, the bonding is arranged to take place at locations away from the edges to eliminate the "edge effect".

2.3.2 Plating Process for Ni

Both electroplating and electroless plating of Ni have been developed. Although electroplating of Ni provides a commercially important and versatile surface finishing method, there are a few issues that are critical for the application of interest. In a typical electroplating process, organic agents are added to maintain the pH of the bath. The presence of impurities within the bath could react with the organic agents causing a high internal stress, which reduces the ductility of the plated metal [17]. The stress can be either tensile or compressive resulting in variation in the

Table 1: Properties of electrolytic and electroless process

	Electroless	Electrolytic
Driving Force	Chemical	Electrical
External Power	None	DC power supply
Anode	None	Required
Substrate	Metal or non-metal	Metal only
Stirring	Hand stir	Magnetic stir
Step coverage	Conformal to shape of substrate	Geometry dependent
Adhesion	Good	Good
Porosity	Low	Moderate
Additional Requirements	Activation	Seed layer

shape of the metallic target. In the low current density operating range, discoloration in the final plated surface from metallic contamination has been reported [17]. When current is increased above the specified range for bath operation, excessive heat is produced resulting in burning on the metallic target. Most critically, interaction between the electric and magnetic field causes uneven distribution of thickness [17, 18]. Achieving a low roughness surface is critical for consistency of the bonding parameters, therefore it is vital that the first plated layer be as flat as possible.

The electroless Ni process has been around since the mid 1940's, and has been growing in popularity ever since. The topography of the plated surface is essentially flat with no excessive build up on the edges and projections of the target [19, 20]. The deposits are less porous than if electroplated, hence better corrosion resistance is obtained. In general, the setup time for electroless plating is less due to the absence of power supplies, electrical contacts, and other apparatus necessary for electroplating. The electroless Ni plating process has often been used with great success in the past for electrical packaging purposes, and therefore is chosen as the technique for plating Ni on the Cu layer in this study.

2.3.3 Plating Process for Pd

The quality of electroless plating of Pd is often degraded due to a high degree of solution instability within the process [17]. Development of electroless Pd plating has been ongoing with limited success in plating quality with acidic plating baths [18]. However, mixing of acidic solutions pose health and safety risks, and therefore was not considered in this project.

Unlike the electroless Pd plating process, the electroplating of Pd has a long history dating back to the early 1930's [17]. The quality of the plated surface is acceptable for electronic packaging purposes. The only known issue with electroplating of Pd is hydrogen embrittlement. If hydrogen is

introduced in the plating solution, the thermodynamic instability causes the PdH_x phase to decompose, which is accompanied by corresponding lattice contractions [17]. Cracking occurs when the tensile stress exceeds the yield point. The hydrogen embrittlement issue in electrodeposited Pd is a great concern when attempting to deposit films of technological use. However, the issue can be compensated by minimizing or maximizing the current ratio of the two simultaneous reactions occurring at the electrode interface [17, 18]. In the study of interest, the current ratio is maximized. Lastly, cleaning methods before and after plating are important in the quality of the film deposited regardless of the type of plating process.

2.4 Bonding Mechanism

The three main impediments to material joining at their faying surfaces are their roughness, lattice mismatch, and contamination. The roughness of the Cu coupon can be compensated by proper grinding and polishing methods. Different techniques in material preparation considered include electropolishing, chemical mechanical polishing (CMP), and mechanical polishing. Electropolishing is essentially the reverse of the electroplating process, where the metal work piece is immersed in a temperature controlled bath, and connected to the anode. Direct current is applied, and oxidation occurs at the anode [23]. For metals with complex geometry, manual polishing requires extensive care during the handling of the material. With electropolishing, areas that are not accessible during the mechanical polishing process are exposed to the polishing solution. However, the typical electropolishing process is very time consuming [23]. In the present case, the Cu material has a basic shape, which can be easily polished mechanically. CMP is the most desirable method for overcoming the roughness of a metallic layer. Both mechanical and chemical components are utilized [24]. The overhead cost for purchasing an automatic system and development of the slurry required for polishing are considerable. Nonwithstanding mechanical polish-

ing, the parameters IF, BF, and US used for ball bonding can reduce surface roughness by plastic flow of the ball and US friction at the interface.

Pd and Au have face centred cubic crystal structures and their lattice constants are 3.89 Å and 4.08 Å [14], respectively, which is considered a small lattice mismatch that will not interfere with adhesion. Figure 4 shows the Au-Pd lattice parameters with change in Pd composition. In the Au-Pd bonding system, the difference in lattice parameters is of no concern.

The effect of contamination is addressed by proper cleaning and storage of the materials. After each stage of grinding and polishing, the samples are cleaned with ethanol in an ultrasound bath, and dried with air blower. Before plating of Ni, the base material is airbrushed to remove the dirt on the surface. The material to be plated is immersed in two separate solutions: “Asset” and “Actimite” to remove grease and oxidation on the target material, respectively. After plating, the

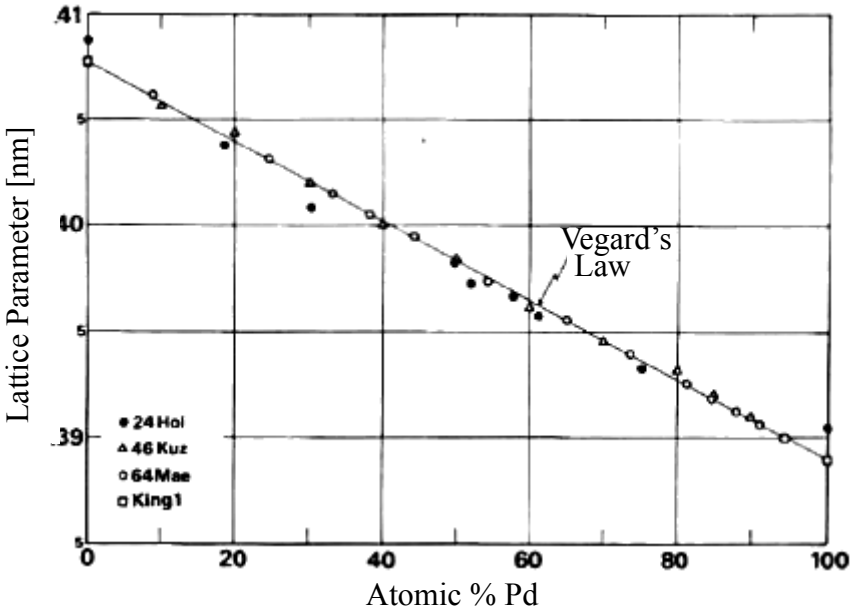

Figure 4 Lattice parameter of Au-Pd system [14].

material is cleaned with de-ionized water. To minimize surface oxidation at room temperature, the substrates used in the research are stored in a glovebox filled with N_2. The humidity in the glovebox is maintained below 10%. The Au wire is kept inside a sealed box to prevent contamination. During the bonding process, US causes wire-substrate interfacial motion, which removes contamination and oxide at various asperity points on the surface.

Thermosonic ball bonding is carried out on the ESEC 3088 wire bonder. The bonding process can be divided into stages. In a first stage, the FAB is deformed by a high enough IF. In the following stage, the US vibration is started and gradually results in interfacial friction that wears away contaminants and roughness features. In the final stage, the friction coefficient increases, which causes the US amplitude of the capillary relative to the substrate to decrease. This is because an interfacial bond is forming and the US can cause additional ball deformation. The key bonding parameters in the Au-Pd process are assumed to be the same as those of the Au-Al system, which are US, BF, and BT [21].

Wirebonding is known as a solid state process [51]. The studies of electrical conductivity and resistivity, thermal conductivity, mechanical properties, magnetic susceptibility, and optical properties have confirmed the AuPd system to be devoid of transformations in the solid state [25]. In terms of impediments to bonding, The lattice parameter changes practically linearly with the composition in at.%. The effects of contamination and roughness are minimized by the process parameters during bonding, and mechanical grinding and polishing during sample preparation. Therefore, the basic bonding type in the process is believed to be a chemical bond of metallic nature, where an electromagnetic interaction between conduction electrons and nuclei of the metals is taking place.

2.5 Bond Characterization

There are two ways to analyze the bondability of a wire bond. The first is the shear test, which characterizes the strength of the ball bond. The second is called the pull test, which can measure the strength of the wedge bond. Figures 5a and 5b show the general configuration of the shear and pull test, respectively.

2.5.1 Wire Pull

Wire pull is a destructive technique where an upward force is applied on the pull hook to the wire, pulling the wire away from the substrate. The force at which the wire failures is recorded by the machine is usually in units of gram-force. The failure modes include breaking at the wedge bond,

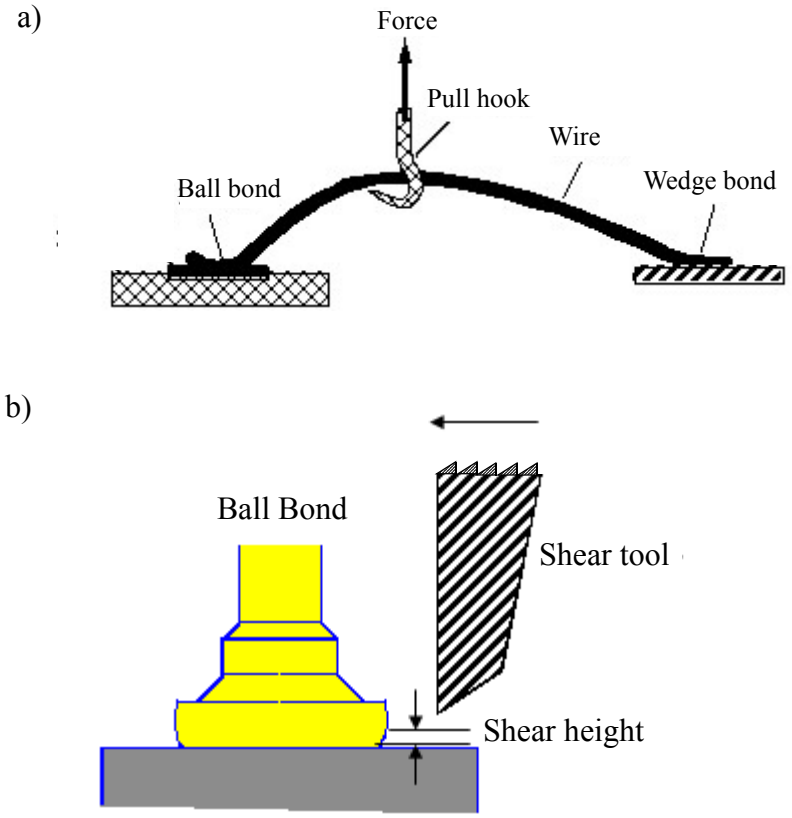

Figure 5 Ball bond quality characterization methods: a) shear and b) pull test (not to scale)

ball bond, heel, ball neck, and midspan of the wire. Typically, failure occurs at the heel of the wire, near the wedge bond side, because the wedge bond tends to be weaker than the ball bond. If failure occurs at the wedge or the ball bond, the bonding parameters can be re-optimized and an improvement might be achieved. The pull hook can be placed at various locations of the bonded wire. The common configurations are pull at the ball, wedge, and midspan, depending on the application. Typical pull tests are performed at the mid-span of the wire.

2.5.2 Ball Shear

The bulk of the bondability characterization in this study is performed using the ball shear test shown in Fig. 5b. Similar to the wire pull, the shear test is a destructive test technique that destroys the wire bond. The chisel shaped shear tool is moved to a starting location a few microns away from the ball bond. The lower end of the tool stands off the substrate surface by about one third of the bonded ball height. During the test, the shear tool moves horizontally and pushes the ball (shears) off the substrate. The shear force (SF) is defined as the force at which the ball is sheared off the substrate, and recorded by the machine in units of gram-force. The SF is directly correlated with the ball diameter. Therefore, the shear strength (*SS*) of the ball is used as a normalized measure for ball bond quality, and is given by

$$SS = \frac{SF}{A} \qquad (c)$$

where A is the area of the deformed ball bond. The failure modes in ball shear include bond lifting, bond shearing, cratering, and bond surface lifting. There is no reported *SS* in the literature for typical Au-Pd ball bonding processes as the majority of the research has focused on the second bond. The minimum *SS* required for acceptable ball bond in the Au-Al system is 90 MPa [26], with a typical *SS* of 110 MPa reported in literature [27]. Therefore the goal in this research is to achieve a *SS* above that of the standard Au-Al process of 110 MPa [27].

2.6 Ball bond Aging

2.6.1 Intermetallics and Interdiffusion

One common way in industry to analyze the reliability of the ball bonding process is to age the wire bond in air at elevated temperature over a sufficiently long period of time. For the Au-Al system, aging temperatures range from 50 to 250°C. Ratchev [28] performed Au ball bonding on Au/Pd/Ni capped bond pads, and aged the bonds in an oven at 150°C over 120 days. Figures 6a and 6b show SEM images of the ball bonds aged and as bonded. No IMC formation was observed before and after aging. Interdiffusion is another effect, which can occur during the aging process. Interdiffusion usually does not degrade the bond quality, and is preferred in some cases as it could increase the overall bond strength. Figure 7 shows the amount of interdiffusion between thin film

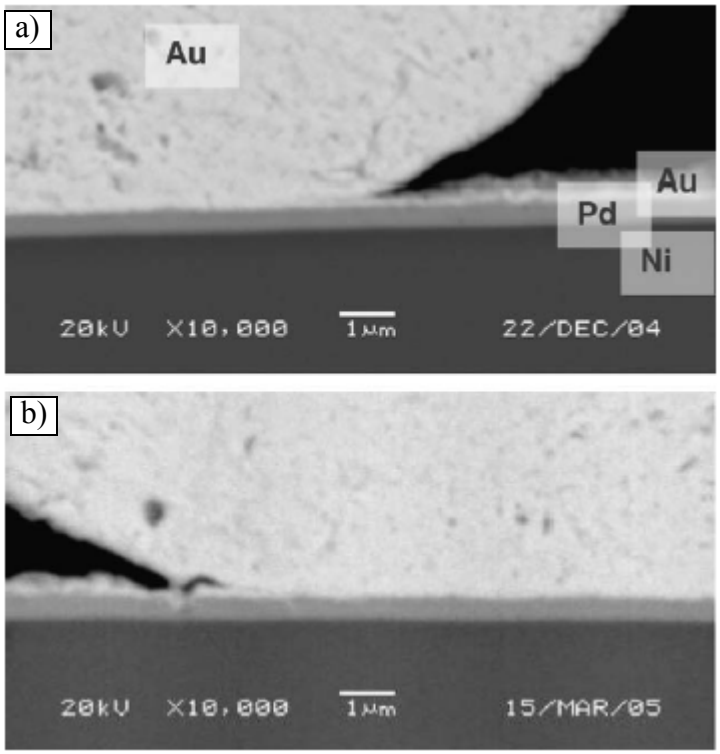

Figure 6 SEM image of the Au ball bond on Au/Pd/Ni cap a) after aging, and b) as bonded at magnification ×10k [28].

Au and Pd in vacuum and air. For an aging temperature of 250°C, 2 h of aging, and about 0.5 μm from the interface, there is approximately 0.3 at% concentration of Au diffused into Pd, and about 0.4 at% of Pd diffusion into Au [29]. Therefore, interdiffusion between Au and Pd can be a significant phenomenon in this research. In a similar study, Mirakami *et al.* [30] reported the presence of diffusion in Au-Pd alloy, but the amount of diffusion changes with atomic concentration of Pd

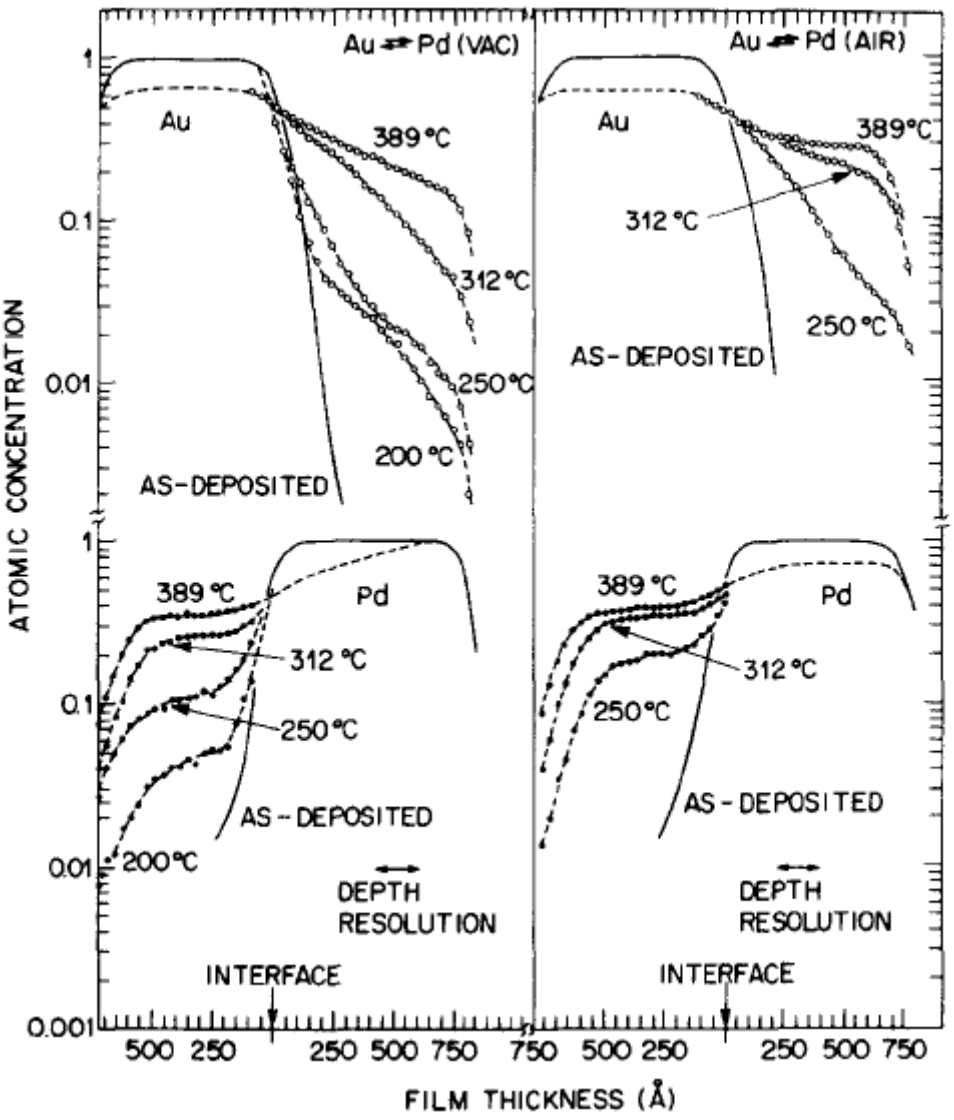

Figure 7 Interdiffusion between Au and Pd metallic layers at temperatures 200°C, 250°C, 312°C, and 389°C in vacuum and air [29].

in the Au-Pd thin film alloy as shown in Fig. 8. Interdiffusion between Au and Pd decreased with increase in Pd concentration, until at about 50% at. Pd, the diffusion rate saturates. The diffusion rate is consistent with time within 8 hours of aging at 350°C. Compared with the standard Au-Al process, which forms IMC phases including but not limited to $AuAl_2$, Au_2Al, Au_4Al and Au_8Al_3 at similar aging temperature and time, the Au-Pd is expected to be a more reliable system.

2.6.2 Kirkendall Voids

The effect of interfacial voids can lead to irregular formation of IMC and/or degration of the ball bond quality. Kirkendall voids can occur between two metals that have different interdiffusion coefficients and sometimes can be attributed to contamination on the surface of the substrate material after bonding [31]. However, Kirkendall voids can usually observed due to stress on the weakened area in the bond during thermal cycling. The voiding was found to develop faster with elevated temperature [50]. Figure 8 shows the diffusion coefficient in pure Pd is two magnitudes less than that in pure Au. The difference in diffusion coefficient between Au and Pd could result in Kirkendall voids in the Au-Pd bonding process. Also, the degree to which possible voids in the Au-Pd process can lead to IMC is not known. Void formation in the Au-Al system leads to the formation of IMC [32-34]. The voids in the Au-Al system are known to be formed by passive regions resulting from contamination by Al oxide, with IMC formation at the bottom of the passive region [32]. Another source of void formation is attributed to improper bonding, where an inhomogenous weld is produced at the interface [34]. As a result, a non welded region is widely spread and is the source of an initial interfacial void before aging.

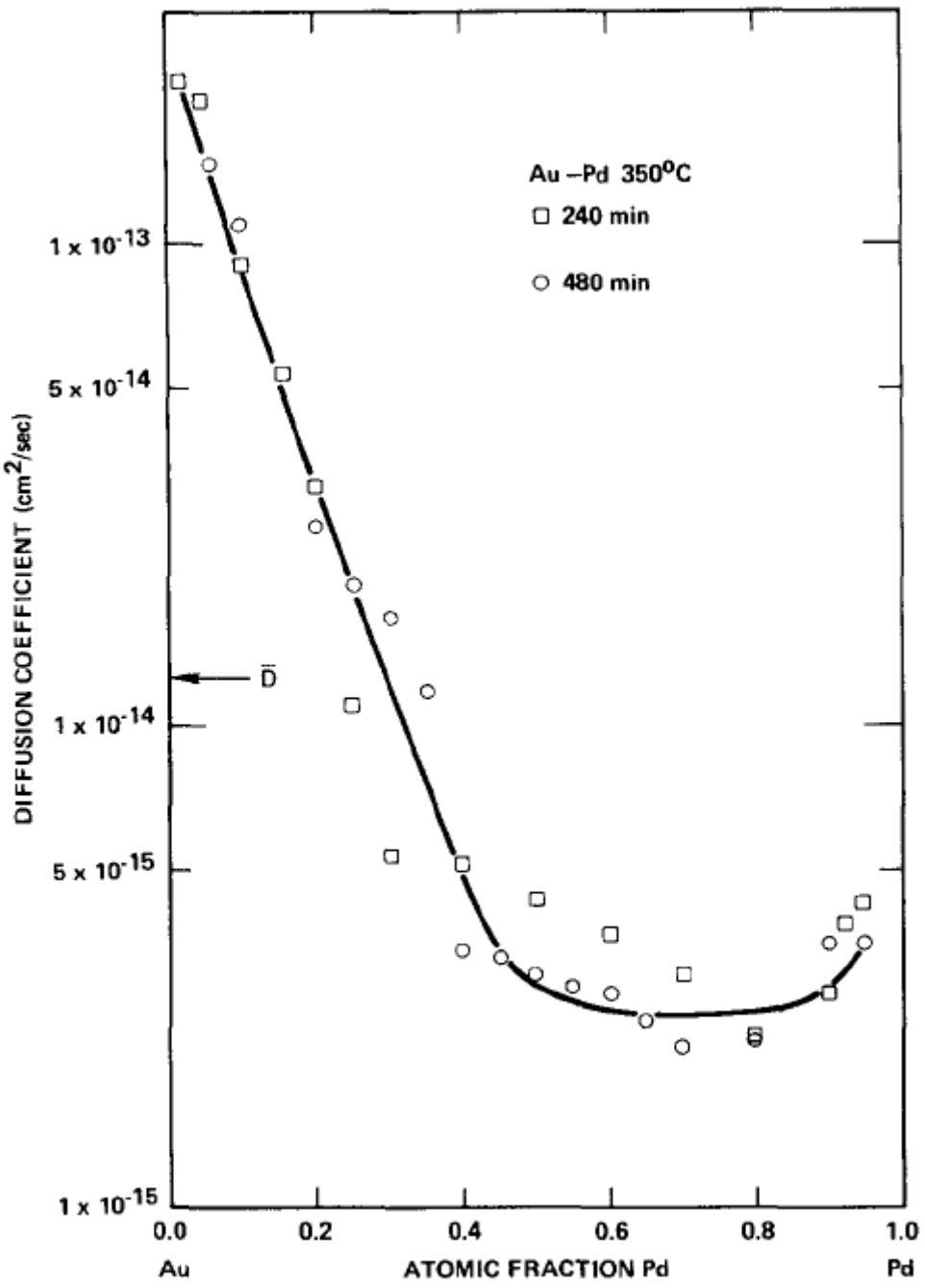

Figure 8 Change in diffusion coefficient with respect to atomic fraction of Pd for thin Au/Pd alloy film with aging at 350°C over 4 h and 8 h [30].

2.7 Some Process Modulators

In order to get a thorough understanding of the Au-Pd ball bonding process, process parameters can be varied to analyze how the overall system responds. The bonding parameters are optimized for the type of process. A standard Au wire is used and no other wires are tested. The properties of the substrate material including roughness, thickness, hardness, chemistry and contamination have been adjusted in the past [35], and are discussed in more detail in the subsections that follow.

2.7.1 Thickness

Thickness of the substrate can be adjusted by varying the parameters of the deposition process. In this study, the thickness of the deposited layer is directly proportional to the length of the deposition time and the magnitude of the current density. So far, there has been no reported variation of ball bond strength and quality with thickness of the metallization on the ball bond side. The strength of the Au wedge bonding increases with thickness of substrate metallization as the metal impurities migrate and diffuse less to the surface. In the Au-Pd process, the Ni layer is thick enough to minimize any Cu migration into Pd. Therefore, the effect of Ni thickness on the bonding strength is negligible.

2.7.2 Hardness

Metal hardness can be adjusted by presence of hydrogen and other impurities, which introduces hardening on the metallization [35]. However, the degree of change in hardness is hard to control, and the repeatability of the result is difficult. It has been reported [35] that the ball bond strength is inversely proportional to hardness. However, a soft coating is more likely to deform and spread to create more contact area for bonding. As a result, the best bondability occur when the hardness of the wire and metallization are the same. In this study, hardness is inherently varied by aging, which anneals the material over elevated temperatures.

2.7.3 Roughness

Various methods can be employed to change the surface roughness of the substrate. In the past, plasma bombardment has been used in both metallic and non-metallic materials [36]. However, the roughness variation obtained with this method is in the nanometer range, which is too small to have any effect in the wire bonding application. Other ways to vary the roughness includes various degrees of sandblasting, sanding, or rolling. The methods employed determines the orientation of the final roughness. In general, a rough surface provides more contact area for welding, resulting a stronger bond possibly aided by mechanical interlocking. However, a large roughness substrate may require a higher energy or force for successful bonding. Therefore, proper adjustment of the bonding parameters must be made for bonding on rough substrates in order to achieve bonding quality and strength.

2.7.4 Contamination

The possibility of contamination is always present in wire bonding. As one of the impediments in welding, contamination should always be minimized. However, the ability to vary contamination would allow a better understanding of the process behavior. Controlling the amount of impurities in a bonding process in a repeatable way can be difficult as contaminants are usually introduced in a system unintentionally. Depending on applications, impurities have been added in the past [53] during plating to increase the hardness, wearability, brightness and ductility of the final deposited material. However, the amount of impurities vary after repeated use of plating chemical or improper rinsing, handling and storing of the samples. Therefore, the end effects are likely difficult to reproduce. The variation in the amount of Al oxide on standard Al pads was reported [48]. The thicker the oxide, the lower the bond quality. A comparable modulation of the Pd surface is impractical because no Pd oxide can be formed easily in a repeatable way. In any case, contamination always reduces the bond quality, and therefore is not further considered as a modulator in

this study. However, the effect of contamination if any, can be promoted through the aging process, with subsequent discoloration [53] on the surface of the substrate.

2.7.5 Plating Chemistry

In the Au-Pd process, the electroless and electrolytic processes are used for plating Ni and Pd, respectively. The plating chemistry can be changed if other types of bath with different pH levels are considered in the process. Variations in chemistry can cause changes in the plating quality and subsequent bonding quality due to metallic impurities and contamination. Hardness and roughness of the final plated layer can also be altered with plating chemistry. Kim *et al.* [35] reported an increase in bond strength of 160% by plasma cleaning the Au substrate before plating with Ni due to removal of organic contamination and inorganic compounds on metallic bond pad [35, 47]. Due to the time required and the complexity for the development and optimization of the different plating processes associated with change in chemistry, this modulator is not considered.

2.8 Summary

Based on the literature study, several points can be generalized before conducting the Au-Pd ball bond study. Electrolytic and electroless plating are the preferred option for plating thin metallic layers of Pd on Ni and of Ni on Cu, respectively. The bondability of Au on Pd is expected to be similar to that of Au on Al, where US and IF are expected to be the dominant parameters for bonding. The bonding mechanism of the Au-Pd process is believed to be a chemical bond of metallic nature, and will be confirmed in the analyses of the report. Proper cleaning and storage of the material in the process is required. Ball shear is the most common method for analyzing and optimizing the *SS* of the ball bond. The reliability of the bonds after aging is expected to be better in the Au-Pd process compared to that of the standard Au-Al process due to lack of IMC formation. However, both voids and interdiffusion could occur in the Au-Pd process. In general, Au and

Pd form continuous series of solid solutions. Parameters which can lead to the improvement of the overall process includes thickness, hardness, roughness, chemistry, and contamination of the substrate material. However, roughness is the modulator of choice in this research as it can be easily reproduced and is expected to have a significant impact on the overall process.

3. Development of Pd/Ni/Cu Coupon

This section describes the production of Pd and Ni layers on Cu coupons as bonding substrates using electrolytic and electroless plating processes. The substrates produced will mimic the actual Pd/Ni/Cu substrate used in the industry, which is a silicon microchip with Pd/Ni pad metallization on the Cu layer for signal and power distribution. Target thicknesses of 1 μm and 0.3 μm were chosen for the Ni and Pd layers, respectively.

3.1 Experimental

3.1.1 Cu Base Material

The base material is an oxygen free high conductivity (OFHC) Cu foil with thickness of 0.5 mm supplied by GoodFellow Corporation, and is cut into coupons with dimension of 1.0 cm×1.0 cm. A WYKO NT1100 Optical Profiler is used to measure the original roughness of the coupon under vertical scanning interferometer (VSI) mode with vertical resolution of 3 nm. The parameter R_a is the arithmetic average of absolute distances to the mean line, and is used to quantify roughness in this work. The R_a of the coupon after cutting is 0.2 μm, which is above that of the chip metallization used in industry. The coupon is grounded with silicon carbide abrasive paper starting with 600, followed by 800, 1200, and 1200 fine grit. Polishing with 0.1 μm, 0.25 μm, and 0.05 μm diamond slurry is performed after grinding. The polished sample are cleaned with ethanol and dried with an air blower. The grinding and polishing are performed on the Fischione Instrument Model 160 Grinder supplied by Fischione Instrument, Pittsburgh, USA. Figures 9a and 9b show the coupon before and after polishing with the corresponding optical profiler measurements, respectively. The magnitude of R_a is reduced by one order, which is comparable to that of the substrate used in industry.

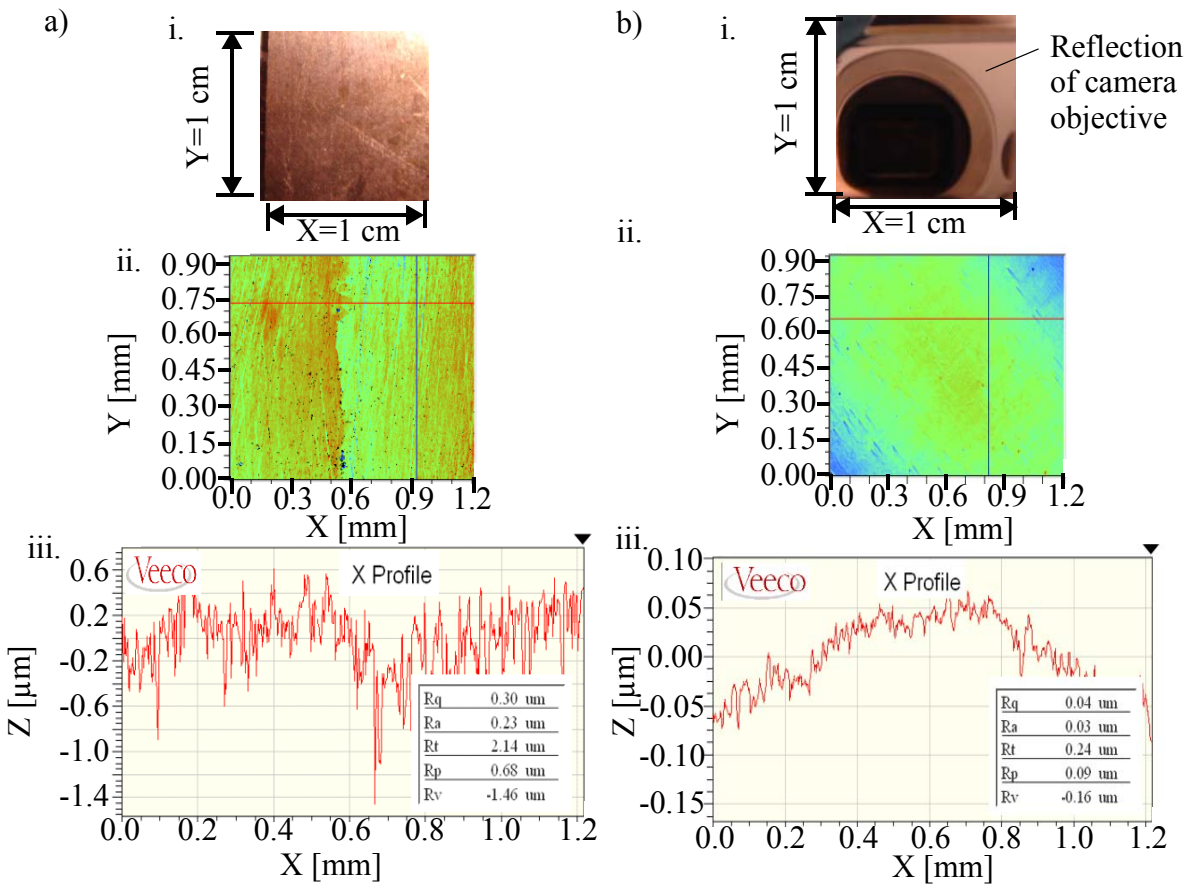

Figure 9 Cu coupon a) before and b) after mechanical polishing with i) photo, ii) topography, and iii) roughness measurements.

3.1.2 Electroless Plating of Ni

The general principle for electroless Ni plating follows the standard oxidation and reduction reactions, which occur simultaneously. The reduction and oxidation of this process uses Ni^{2+} ion as salt in the plating solution to be reduced, and the Cu metal is oxidized. The total number of electrons transferred is 2. Steel is used as the activation agent in the plating process. The electrode potential of Fe is -0.447 V, when connected to Cu, which has a electrode potential of -0.257 V, the resulting potential difference activates the plating process [17]. Table 2 lists the recipe [37] and the plating conditions of the electroless Ni process. Before plating, the coupon is airbrushed, and

Table 2: Properties of electroless Ni process [37]

Target thickness	0.3 μm
Substrate size	1cm×1cm×0.5mm
Solution	Alkaline bath
Salt	Nickel sulphate ($NiSO_4.6H_2O$)
Reducing agent	Sodium hypophosphate ($NaH_2PO_2.H_2O$)
Replenishing agent	Ammonium hydroxide (NH_4OH)
Deposition rate	0.42 μm/min
Temperature	90 °C
pH	8-10
Activation	Steel

rinsed with solutions listed in Table 3 in order to minimize grease and oxide on the surface of the Cu coupon [37]. A temperature of 35 °C is recommended for the cleaning process. The Ni plating and cleaning solution are supplied by Cadwell Inc, Kennewick, WA, USA.

Figures 10a and 10b show illustrations of the plating setup. The Cu coupon is held by an alligator clip on one side and has a steel clip on another side. Both the alligator clip and steel are kept as close to the edge of the coupon as possible to reduce any influence on the central area on the Cu

Table 3: Cleaning solution for Ni plating process [37]

Name	Composition	Purpose
Asset	Potassium hydroxide, sodium metasilicate, citric acid, alcohol alcoxylate	remove grease
Actimite	Sodium bifsulphase, sodium flouride	remove oxide

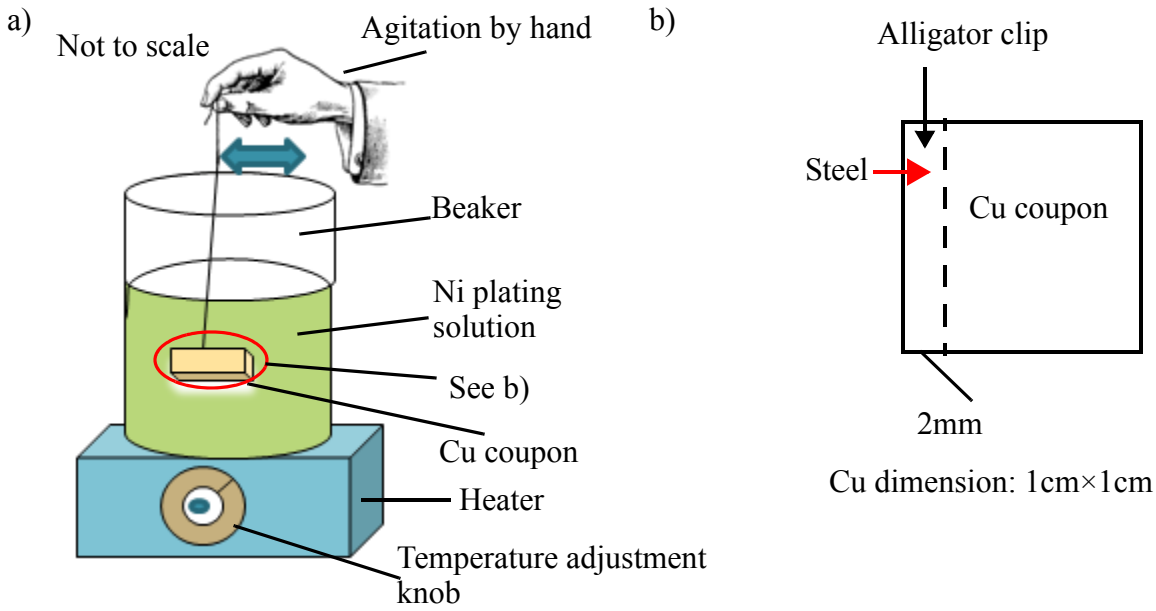

Figure 10 Electroless Ni setup in a) overall view and b) detailed view.

coupon. The coupon is kept in a horizontal position in order to achieve uniform plating across its surface. When the coupon is plated vertically, the thickness varies by up to 50 % between measurements in the vertical and horizontal directions, which can be attributed to the change in depth experienced by the coupon across its surface. Once the temperature reaches 90 °C as measured by an immersed thermometer, and the pH is between 8-10 as measured by an immersed pH meter, the coupon is immersed in the plating solution as shown in Fig. 8a. For consistency, the Cu coupon is kept at about the same depth in the beaker during every plating experiment. The time required to plate 1 µm of Ni, is given by

$$T_{dep}^{Ni} = t/R \qquad (2)$$

where, t represents the thickness to be deposited, and R represents the deposition rate. The T_{dep}^{Ni} in the electroless Ni process is approximately 140 s. Air bubbles can accumulate on the coupon, pre-

venting Ni ion to be deposited. Therefore, when a bubble builds up on the coupon during plating, the coupon is shaken manually to remove the bubble. The Ni credit is defined as

$$Ni_{credit} = A\ (in^2) \times T_{dep}\ (min) \tag{3}$$

and is a measure of Ni concentration in the plating solution. where A is the area of the coupon. Ni_{credit} is in unit of $in^2 min$, both A and T_{dep} are not in their SI unit. The Ni_{credit} required to plate one coupon is about 0.37 in^2min. The bath is generally replenished when the amount of Ni credit falls below 1100 in^2min. After replenishing the bath, the Ni_{credit} is 1300 in the plating solution. If Ni_{credit} is below 1100, the plating quality and deposition rate reduces drastically. After plating, the coupon is rinsed with de-ionized water and dried with an air blower.

3.1.3 Electroplating of Pd

Table 4 shows the properties of the Pd plating solution [38]. The deposition time T_{dep}^{Pd} can be adjusted with current density (I), and is defined by

$$T_{dep}^{Pd} = \frac{had}{ZI} \tag{4}$$

$$Z = \frac{A_{wt}}{nF} \tag{5}$$

$$F = N_A e \tag{6}$$

where h is the thickness of the deposit, a and d are the area and density of the cathode, respectively. T_{dep}^{Pd} is inversely proportional to I and Z. A_{wt} is the atomic weight of the cathode, n is the number of valence electron of the metallic ion in valence state, N_a is Avagadro's number, and e is the charge of an electron. Assuming a cathode efficiency (η) = 95%, T_{dep}^{Pd} is approximately 70 s for I = 1 A/dm^2. From eqn. (2), T_{dep}^{Pd} for I = 1 A/dm^2 is 0.25 μm/min.

Table 4: Properties of electrolytic Pd process [38]

h	0.3 μm
Substrate size	1cm×1cm×0.5mm
Solution	Neutral bath
Salt	Palladium chloride (PdCl2)
Stabilizer	Ammonium chloride (NH4Cl)
Adjust pH	Ammonium hydroxide (NH4OH)
Reducing agent	Ammonium sulfamate (NH4O SO2 NH2)
Anode	Plantinized Titanium
I	5-20A/ft^2
T_{dep}^{Pd}	Varies with current
Temperature	40 °C
pH	7.8
Cathode efficiency	95%
Pd concentration	10g/gallon
Total concentration	1 gallon
Agitation	Magnetic stir

A basic design of experiment (DOE) is setup to analyze the deposition time required for various I in the actual Pd plating experiment. Table 5 lists the calculated deposition time for different I, starting with 0.5 A/dm^2 in steps of 0.5 A/dm^2, up to the maximum allowable [38] 2.0A/dm^2. The T_{dep}^{Pd} at different η is computed [17] and shown in Table 5.

Before plating, the Ni plated coupons are cleaned. Table 6 shows the ingredient for the cleaning solution. Both the plating and cleaning solutions are supplied by Technic, Inc., Florida, USA. The

Table 5: Calculated T_{dep}^{Pd} with change in current density and cathode efficiency

η [%] / I [A/dm^2]	**85**	**90**	**95**	**100**
0.5	100s	110s	120s	130s
1.0	50s	60s	70s	80s
1.5	30s	40s	50s	60s
2.0	20s	30s	40s	50s

Ni/Cu coupon is first cleaned with dish detergent to remove any grease build up on the surface, and then immersed in 20 %v/v sulfuric acid at room temperature for plating activation. Figures 11a, 11b and 11c show an overview and detailed illustrations of the plating process. Before plating, the one gallon solution is shaken to re-distribute the Pd salt accumulated at the bottom of the container. About 800 ml of the one gallon plating solution is poured into a 1000 ml beaker, which is about 2 g of Pd salt. The mass of Pd required for plating one coupon is defined by

$$m = V\rho \qquad (6)$$

where V is the volume of the cathode and ρ is the density of Pd, which is 58.7 g/cm^3. The amount of Pd in the 800 ml beaker can plate about 340 Ni/Cu coupons of size 1cm×1cm×0.5mm. The

Table 6: Cleaning solution for Pd plating process [38]

Name	Composition	Purpose
Dawn Detergent	Biodegradable cleaning ingredients (detailed not shared	remove grease
Activate	20%v/v Sulphuric acid, sodium flouride	remove oxide

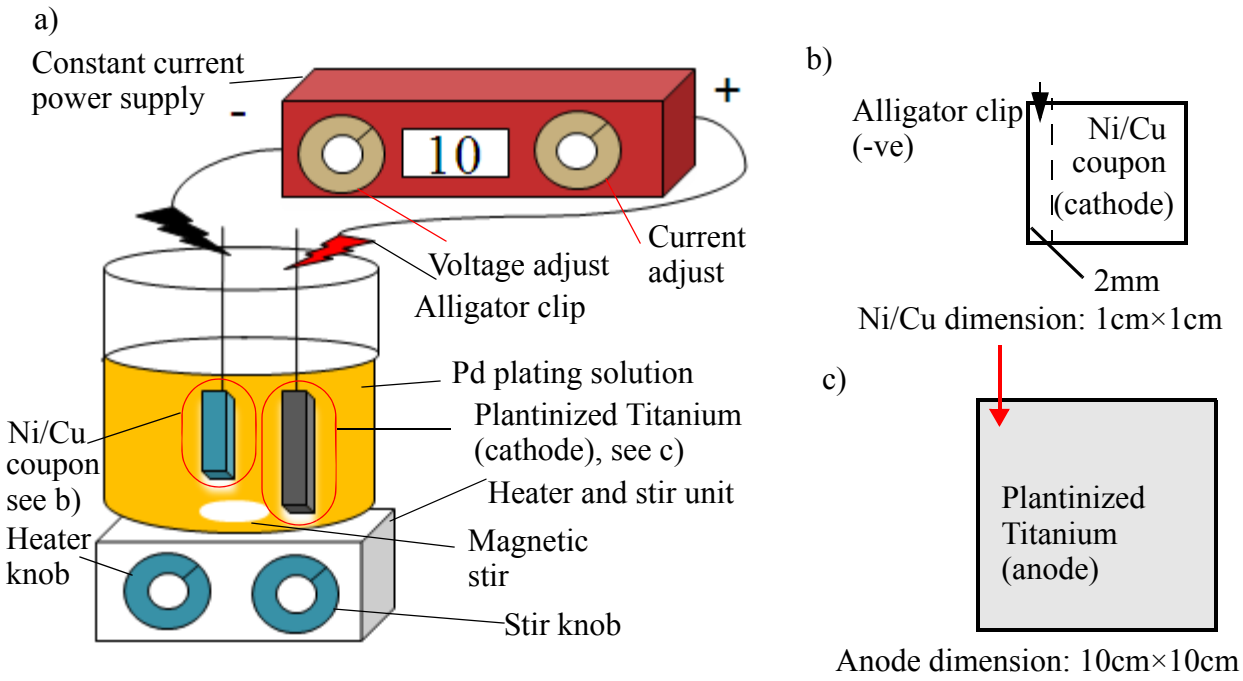

Figure 11 Electro Pd setup in a) overall view and b) detailed view of Ni/Cu, and c) detailed view of anode.

anode and the cathode are connected to the positive and negative ends of the constant current power supply, respectively. The stir knob is adjusted to have mild stirring for agitation, which minimizes the porosity during plating [53]. Once the desired temperature, *I,* and pH are reached, both the anode and cathode are placed vertically inside the beaker. The side of the Ni/Cu coupon to be plated must face the anode directly, in order to get the maximum electric field exposure as illustrated in Fig. 12. The other side of the coupon will be plated with an undesired thickness due

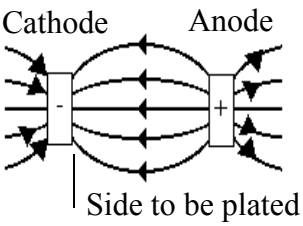

Figure 12 Electric field line distribution in electroplating process

to the weak strength of electric field line, combined with possible electroless plating taking place. The process is repeated for each current level at the specified plating time.

3.2 Plating Results

The Fischerscope x-ray fluorescence (XRF) machine, Fischer Inc., Windsor, USA, is used to measure the thickness of the plated layers. Five measurements are made across the horizontal and vertical directions for each coupon and plated layer. The lateral tolerance of a single measurement is ≈ 2% of the measured value. The XRF can be programmed to measure specific points on single or double coated layers with tolerance below 10 % of the measurement range. The surface quality of the plated layer is analyzed by a JEOL 6480 tungsten filament scanning electron microscope (SEM), JEOL, Tokyo, Japan along with the energy dispersive x-ray (EDX) analysis for measuring the chemical composition of the plated layers. SEM images of cross sections of the plated layers are also used to confirm the thickness measured by the XRF.

3.2.1 Electroless Ni Plating

Figures 13a and 13b show the thickness of the plated Ni layer measured across the horizontal and vertical directions, respectively. The plating times of 130s, 140s and 150s were used. The blue and pink lines in Fig. 13 are the average and +/- standard deviation of the thickness measurements. The difference between the measurements in vertical and horizontal directions are within 25%, and the difference between maximum and minimum thickness measurements in the same direction are within 30% for both horizontal and vertical directions. Therefore, the Ni thickness has no significant directional dependence during the plating process. As expected, an increase in plating time results in an increase in plating thickness. In order to get a Ni plating thickness of about 1 μm, the desired plating time should be between 140s and 150s. Figures 14a and 14b show

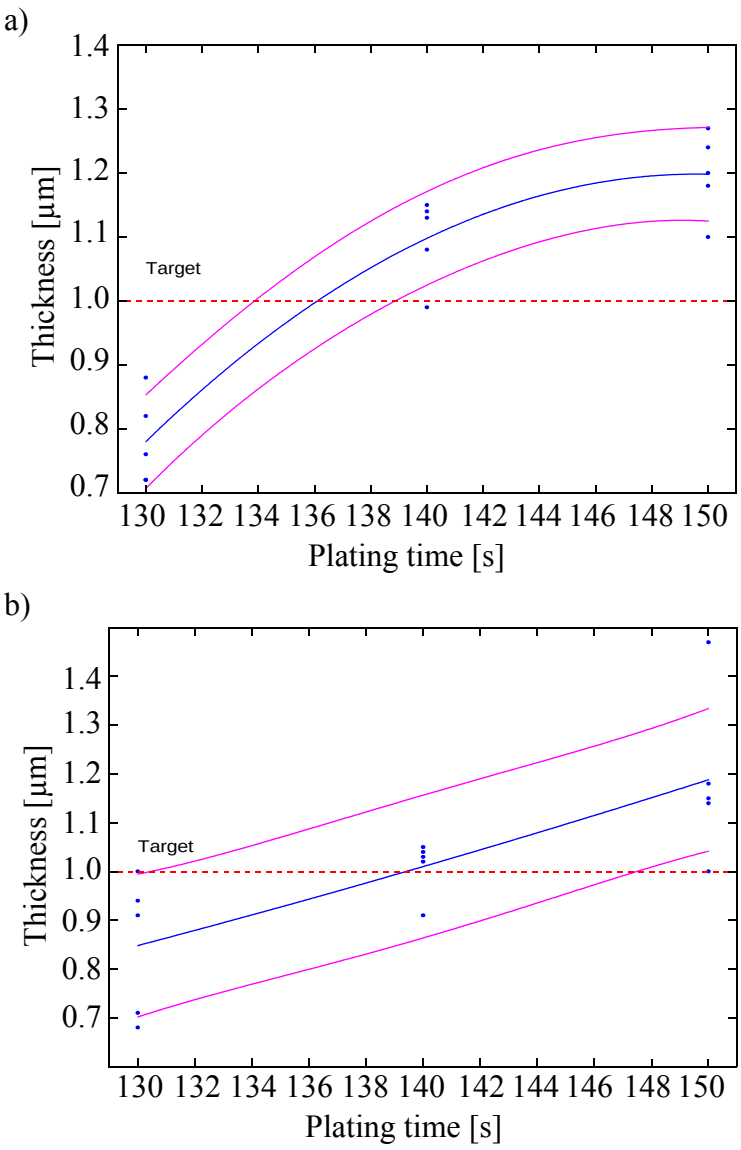

Figure 13 Plating thickness vs. plating time with thickness data gathered from a) z direction, and b) x direction. Fit is polynomial of 2nd degree (parabolic). Dashed lines are standard error

SEM micrographs of the Ni plated surface at magnifications of ×5k, and ×100k, respectively. The surface of the plated layer is smooth. Focused ion beam (FIB) is used to cut through the surface of the Ni/Cu layer, and measure the thickness on the cross section of the cut sample for deposition times of 130s, 140s and 150s. Figure 15 shows a sample cross section thickness measurement at deposition time of 140s under the SEM. EDX analysis to confirm the chemical composition of the

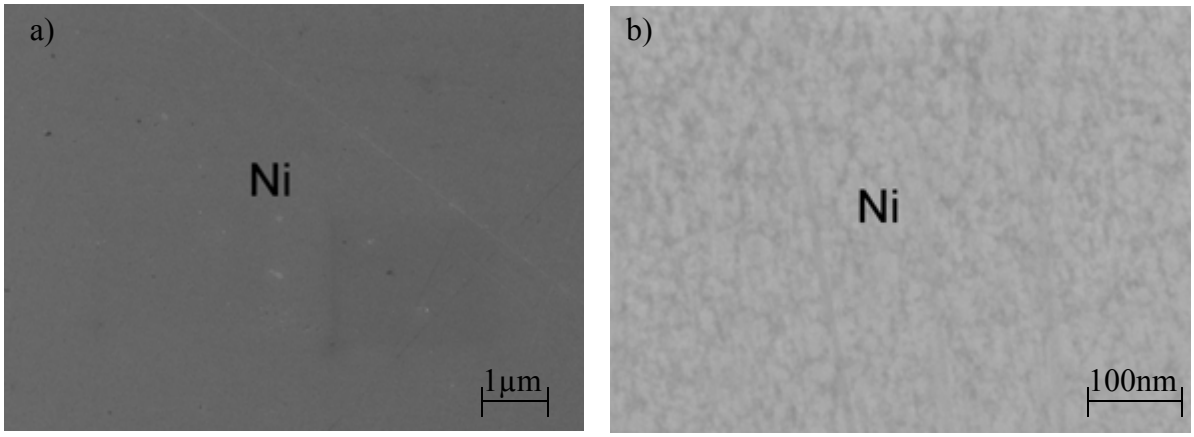

Figure 14 SEM of Ni plated surface at magnification of a) ×5k and b) ×100k.

plated layer is performed at the cross section shown in Fig. 15. At the Cu and Ni side, the chemical composition is predominately Cu and Ni, respectively. The oxygen and phosphorous components in the Ni region are from the plating solution. The cross section thickness measurements obtained with the SEM are within 10% of the XRF measurement results.

3.2.2 Electrolytic Pd Plating

Figures 16a to 16d show the Pd thickness measurement for values of I varied from 5 mA to 20 mA in steps of 5 mA. For I below 20 mA, h is below the thickness specification by using the calculated deposition time. At I = 20 mA and T_{dep}^{Pd} = 50 s, h reaches 0.3 μm on average over 5 samples, and remains consistent along the vertical and horizontal directions. As expected, t increases with both T_{dep}^{Pd} and I.

Figures 17a and 17b show SEM images of the plated surface. Similar to the Ni plated surface, the Pd plated surface is smooth, with visible corrosion pits of sizes between 20 nm and 200 nm. Corrosion pits have been reported [51] to occur in the Pd electroplating process. Although Pd has excellent corrosion resistance, electrolytic process is more prone to surface pore than the electro-

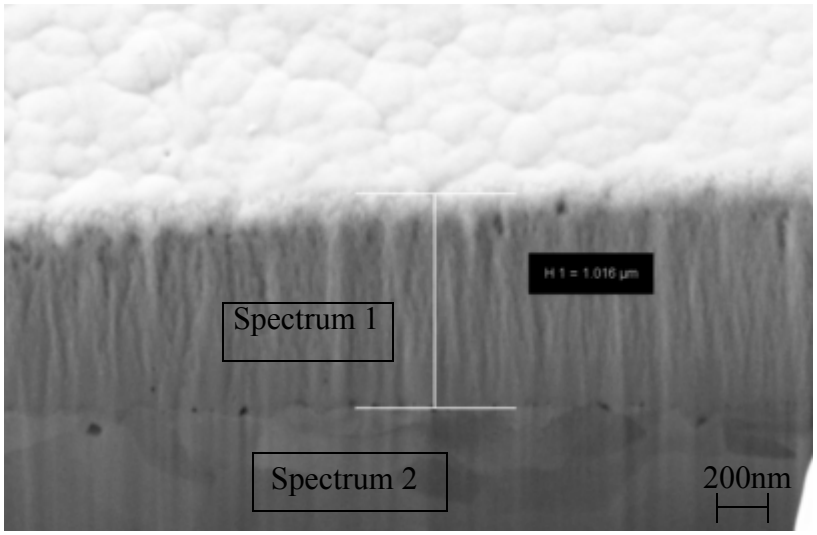

Spectrum	In stats.	C	O	P	Ni	Cu
Spectrum 1	Yes	6.08	4.43	7.86	81.63	
Spectrum 2	Yes	7.73				92.27
Max.		7.73	4.43	7.86	81.63	92.27
Min.		6.08	4.43	7.86	81.63	92.27

Figure 15 SEM-EDAX of Ni plated surface cross section with FIB, at magnification of ×3k

less process [17]. Cross sections are made on the Pd/Ni/Cu coupons by mounting them in epoxy. Grinding and polishing procedures similar to that of the preparation for lower roughness Cu coupon are carried out, and *h* is measured to confirm the XRF results. Figure 18 shows an example thickness measurement from a Pd/Ni/Cu coupon cross section with Pd deposition time of 50s and Ni plating time of 140s after a Au ball bond has been made. Both Pd and Ni thicknesses are within 10% of the results measured by XRF. Figure 19 shows an SEM image of the surface with chemical analysis to confirm the composition of the plated layers.

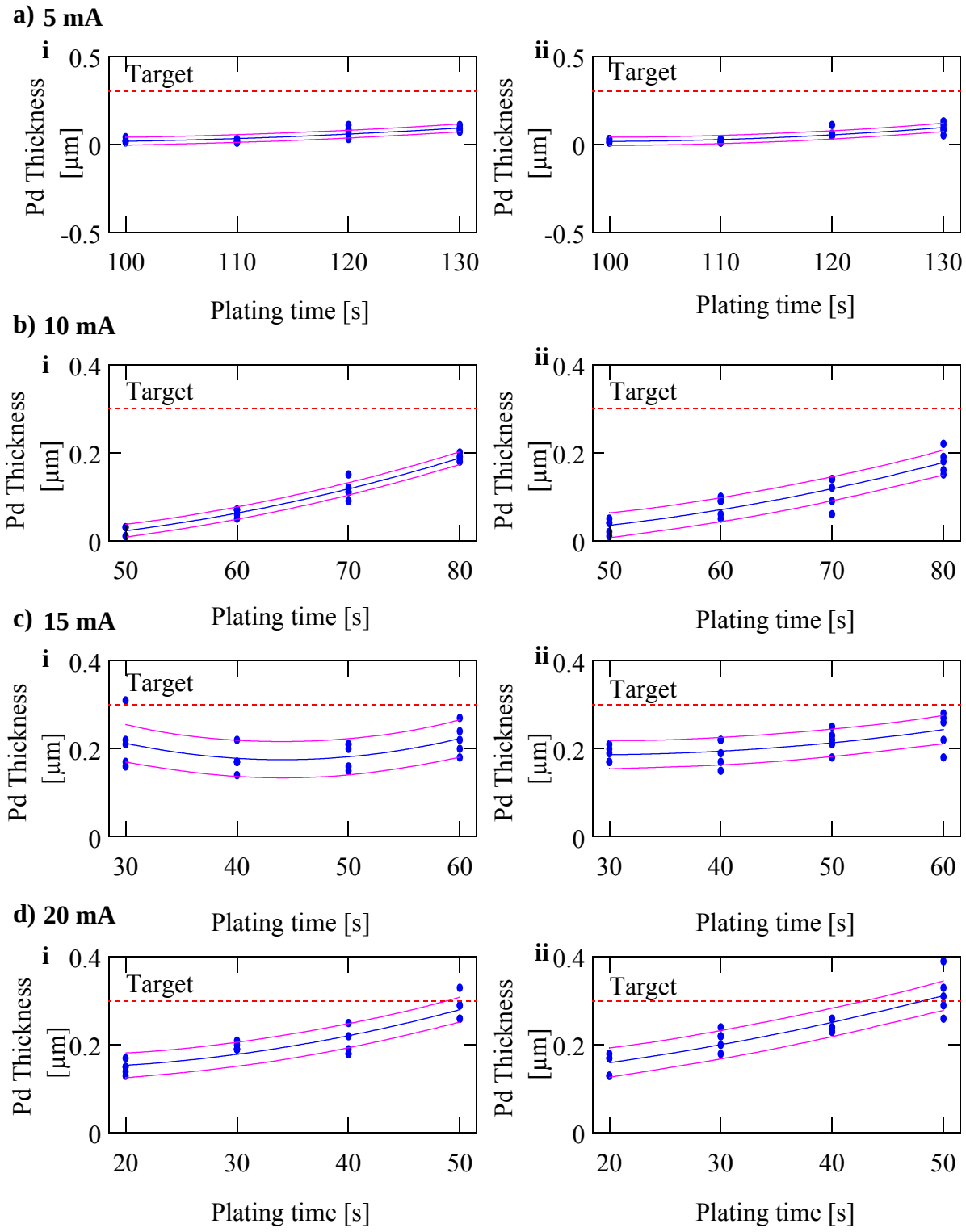

Figure 16 Curve of best polynomial fit for Pd thickness variation at input current of a) 5 mA, b) 10 mA, c) 15 mA, and d) 20 mA in the vertical (i), and horizontal (ii) directions. Fit is polynomial of 2nd degree (parabolic). Dashed lines are standard error

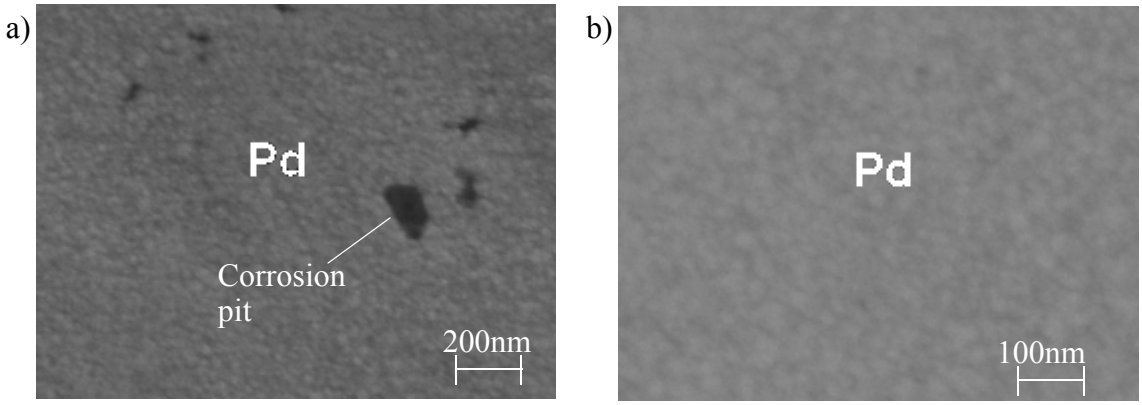

Figure 17 SEM of the Pd plated surface at magnification of a) ×50k and b) ×100k.

3.3 Summary

Processes to plate thin layers of Ni and Pd have been developed. The electroless Ni deposition time of 140s, and electrolytic Pd deposition time of 50s are required to consistently plate 1 μm and 0.3 μm of Ni and Pd, respectively. The current of the electroplating process used is 20 mA. The thicknesses are measured nondestructively by XRF and confirmed by SEM cross section

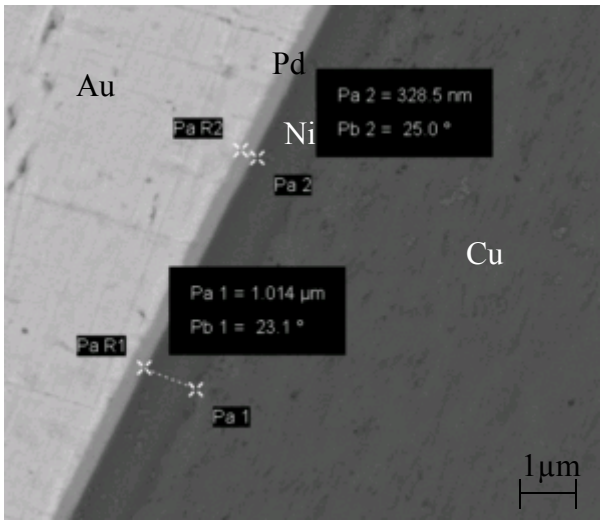

Figure 18 SEM thickness measurement of Pd/Ni/Cu coupon for Pd deposition time of 50s, Ni plating time of 140s

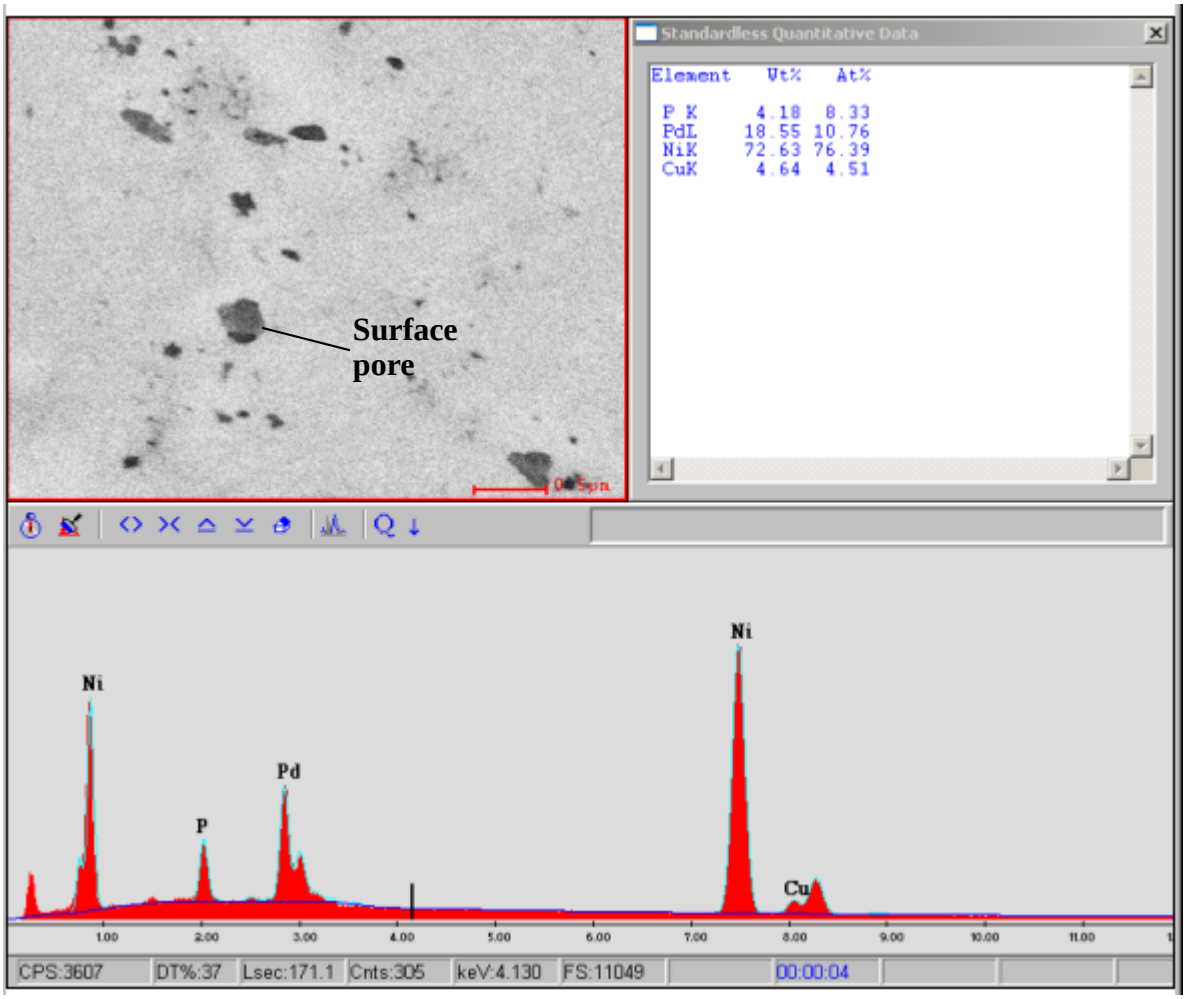

Figure 19 SEM-EDAX of Pd/Ni/Cu coupon at magnification of ×5k

measurements. The surfaces of both Ni and Pd plated layers are smooth with surface pores on the Pd layer with sizes ranging from 20 nm to 200 nm, the degree for which the pores have on the bonding and reliability of the Au ball bonds are to be determined in subsequent sections of the report. Chemical analysis confirms the materials deposited on the bulk Cu.

4. Development of Wire bonding Process

The plating processes for the Cu coupon have been developed with consistent thicknesses. In this section, the bondability of Au on the Pd/Ni/Cu substrate in terms of achieving the specified ball geometry and maximizing shear strength is reported. The specified ball diameter is between 50 µm to 60 µm, and the ball height is between 7 µm to 12 µm. The maximum shear strength (*SS)* is desired to be comparable to that of a typical Au-Al process, 110 MPa.

4.1 Experimental

4.1.1 Bonding Plan

An ESEC 3088 ball-wedge automatic bonder supplied by Oerlikon ESEC, Cham, Switzerland, is used in this experiment. The US frequency of the bonder is 130kHz. The wire bonder used is capable of bonding 10 wires per second. Cu and Au wire bonding are preferred applications for the bonder. The ESEC 3088 offers a maximum process temperature (T) of 300°C. A 25 µm diameter 4N Au bonding wire is supplied by MKE, Yongin, Korea, with properties shown in Table 7. A ceramic capillary with hole diameter (H) and chamfer diameter (CD) of 35 and 51 µm, respectively, is provided by SPT, Inc., Petaluma, USA. The coupon is placed in the center of the bond area on the heater plate of the wire bonder. Both vacuum and heat are supplied by the machine through the heater plate to fix and heat the coupon, respectively.

Table 7: MKE Au wire properties [39]

Content	Breaking load (gf)	Elongation (%)	Vickers hardness (HV)
99.99% Au	10.0	2.8	50.0

Figures 20a and 20b show an overview and a detailed illustration of the bonding diagram. Both the ball and wedge bonds are placed on the coupon. Bonding takes place away from the edges of the coupon to minimize contamination and any other "edge effect" during bonding. Equal spacing between the ball and wedge of the same wire bond, and subsequent ball and wedge bonds are maintained. The wire loops are bonded parallel to the direction of US.

While only the ball bonds are of interest in this study, a consistent bond off on the coupon is required for FAB formation, and is achieved by setting up proper second bond parameters. The FAB diameter for achieving desired ball geometry is optimized by properly adjusting the EFO current and time. To achieve the desired ball geometry, the IF is varied with all other parameters kept constant. Finally, the *SS* is maximized by increasing the US while maintaining all other parameters fixed. To avoid complexity and time during the optimization process, the BT, T and BF are kept constant throughout the process, as they are factors minor to US and ball bond geometry. The ranges of BT, T and BF parameters are comparable to those used in Au-Al processes [27].

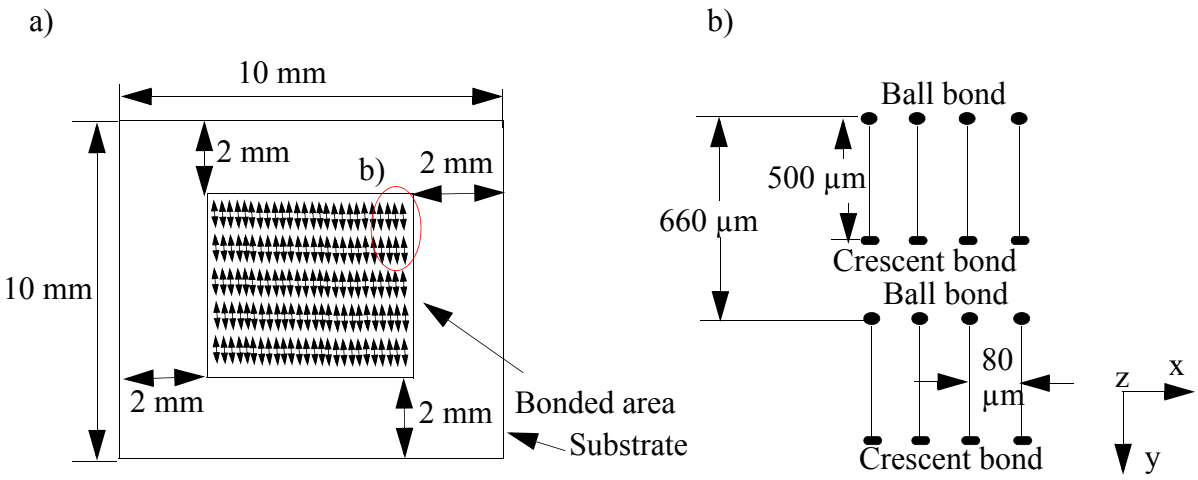

Figure 20 a) Overview, and b) detailed view of bonding schematic for ball bond optimization.

4.1.2 Ball Bond Geometry

Figures 21a and 21b show the definitions of FAB and ball bond geometric features, respectively. The ball diameter as conveniently measured optically at the capillary imprint and at the ball peripheries are defined as BDC and MBD, respectively. The ball diameter at the interface (BDI) cannot be measured without cross sectioning the ball or otherwise removing it from the substrate. The ball height (BH) is measured by taking the absolute difference in height between the focus at the bottom and the top of the ball bond under the microscope. In general, only one of the three ball diameters and the BH are required to determine the ball dimensions. In this work, the MBD and BH are chosen to classify the ball geometry.

4.1.3 Ball Bond Shear Strength

The Dage 4000 ball shear tester supplied by Days, Buckinghamshire, UK, is used for the shear testing. The ball shear is performed using a shear tool (chisel) placed at a height of about 1/3 of the BH, to ensure the shear height is above any IMC. The travel speed of the chisel is 250 µm/s. The shear direction is parallel to the direction of the US during bonding.

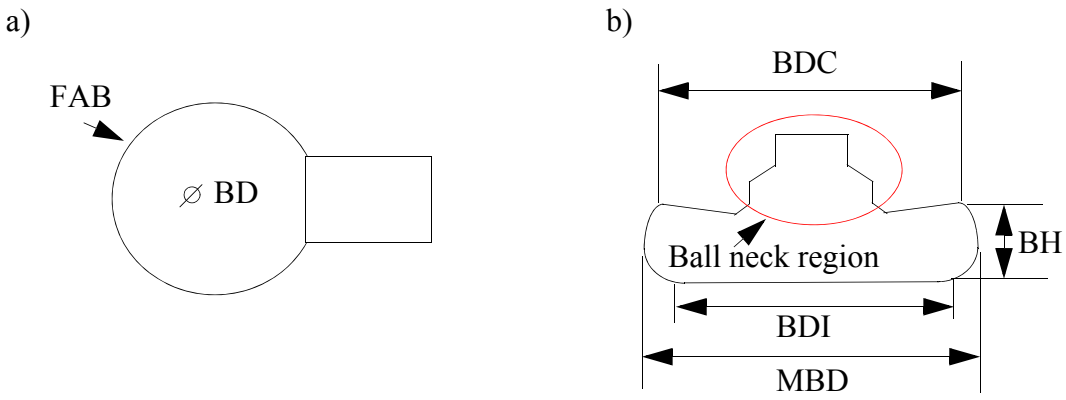

Figure 21 a) Illustration of a) FAB, and b) bonded ball bond.

4.1.4 Summary

Table 8 summarizes the settings for the initial bonding process. The crescent bond parameters used for bond off are derived from the Au-Al process reported in literature [27]. The FAB diameter of about 45 µm is desired for the range of ball shape specified in this process. The parameter on the wire bonder is the nominal FAB diameter (FAB_{nom}), which usually is different from the actual measured FAB diameter.

4.2 Bonding Results

4.2.1 Free-Air Ball

Table 9 lists the actual crescent bond parameters, used for ten consecutive bond offs on the coupon. Between each bond off, a FAB is formed. Figure 22 shows the measured FAB (FAB_{act})

Table 8: Initial parameters for the ball bonding process

Class	Parameter	Unit	Value
Heater stage	T	°C	220[a]
Crescent bond or bond off	IF	mN	700
	BF	mN	350
	US	%	65
	BT	ms	20[a]
Ball bond	IF (ball geometry)	mN	500-1100 (steps: 50)
	BF	mN	240[a]
	NSOP US	%	0 - 10 (steps: 1)
	US for maximum SS	%	NSOP-45 (steps: 2)
	BT	ms	20[a]
To get 45 µm FAB	FAB Diameter (ESEC 3088)	µm	47

a. Maintained constant;

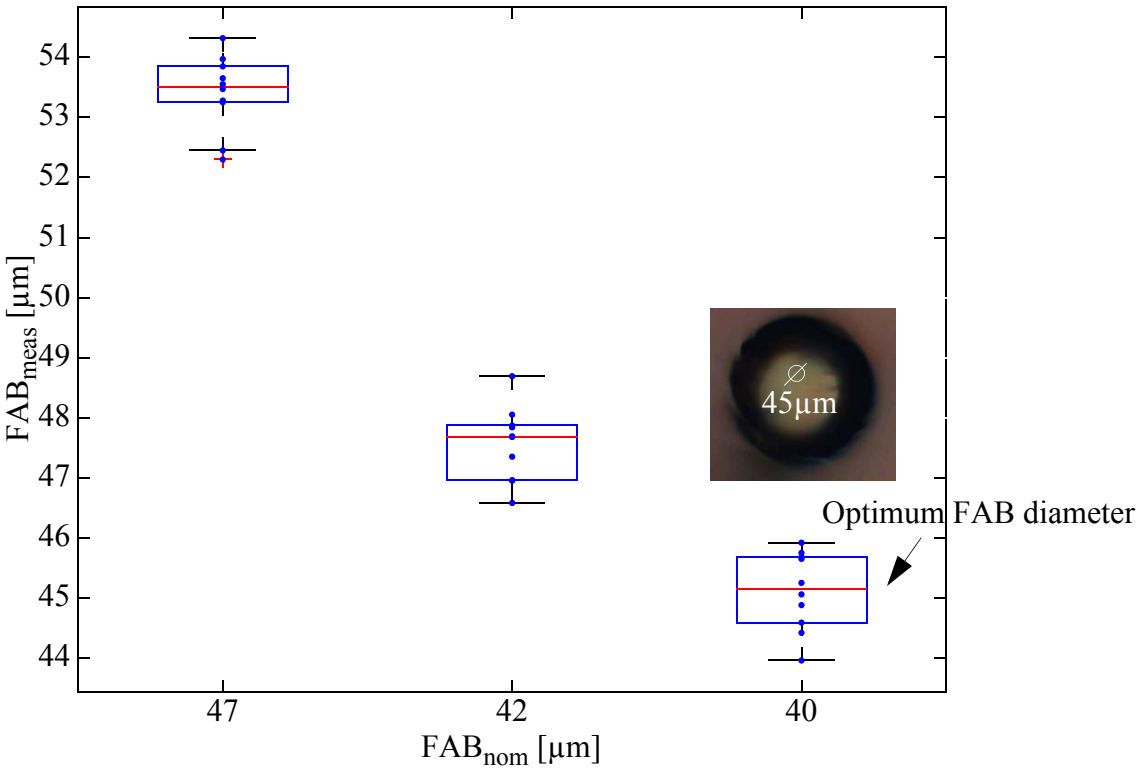

Figure 22 Boxplot of measured FAB diameter with respect to nominal FAB diameter.

diameters for various FAB_{nom} values. The initial attempt of FAB_{nom} = 47 µm gives an average of FAB_{act} = 53.5 µm (ten samples). At FAB_{nom} = 40 µm, the average FAB_{act} is approximately 45 µm. An example FAB micrograph is shown in Fig. 22. The US for consistent ball bond sticking is determined to be 10 % after 5 successful ball were bonded on the Pd/Ni/Cu substrate with that value.

Table 9: Bond off/wedge bond parameters

IF (mN)	**BF (mN)**	**US (%)**	**Time (ms)**	**Temperature (°C)**
500	300	18	20	220

4.2.2 Ball Geometry

Figures 23a and 23b show the variations in BH and MBD, respectively, with change in IF. The US parameter for consistent ball bond sticking is maintained from the previous step, and all other bonding parameters are fixed. The range of IF for both average MBD and BH to be within the specified ranges is 850 mN to 1000 mN. IF of 950 mN is used arbitrarily in order to achieve the median of the BH range, which is 10 µm. The IF of 950 mN gives a MBD of 58µm, which is within its range. The ball geometry is measured over five ball bonds. The micrograph of an example ball bond is shown in Fig. 23b.

4.2.3 Shear Strength

After determining the ball geometry, the US is varied from the magnitude required to get consistent ball bond sticking to 45%, which is about the same US magnitude to achieve maximum *SS* in the Au-Al process [27]. All the other parameters are kept constant. The *SS* is shown in Fig. 24. The corresponding MBD and BH are measured before shearing, and are shown in figures 25a and 25b, respectively. The *SS* for US above 36% decreases due to the ultrasound enhanced deformation (UED) [27] kicking in and causing an additional rise in the MBD. The US of 36% in this process is defined as the UED limit. The maximized *SS* is achieved at the UED limit and is approximately 130 MPa, averaged over ten ball bonds. The *SS* is above the minimum standard for the ball bonds, 65.2 MPa [4] and the typical Au ball bond shear strength of 110 MPa [5]. The shear occurs at the ball, with Au residue remaining on the surface of the coupon as shown in Fig. 24.

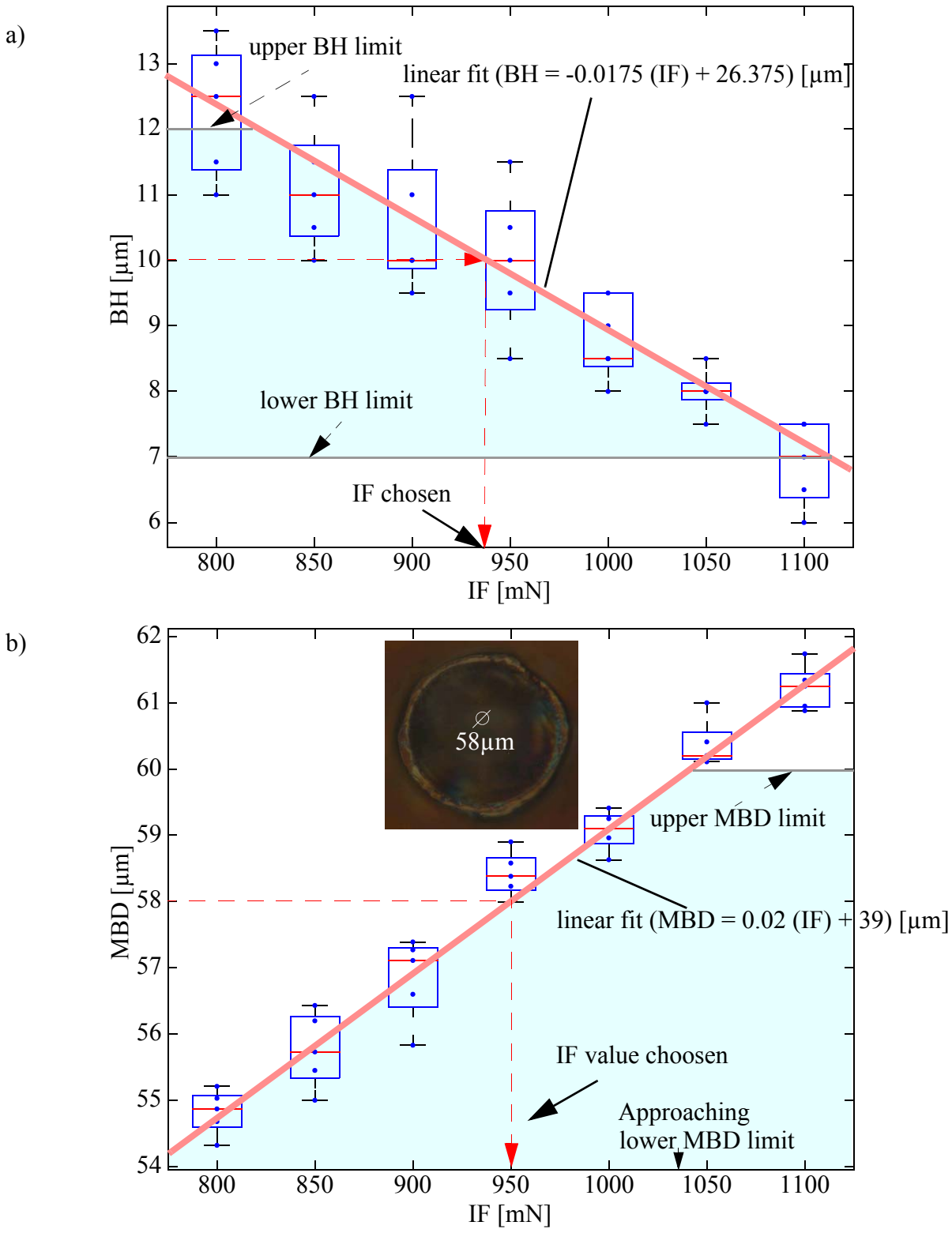

Figure 23 Measured ball bond a) BH, and b) MBD for various IF. Pd substrate. BF = 240 mN. FAB_{nom} = 45 µm.

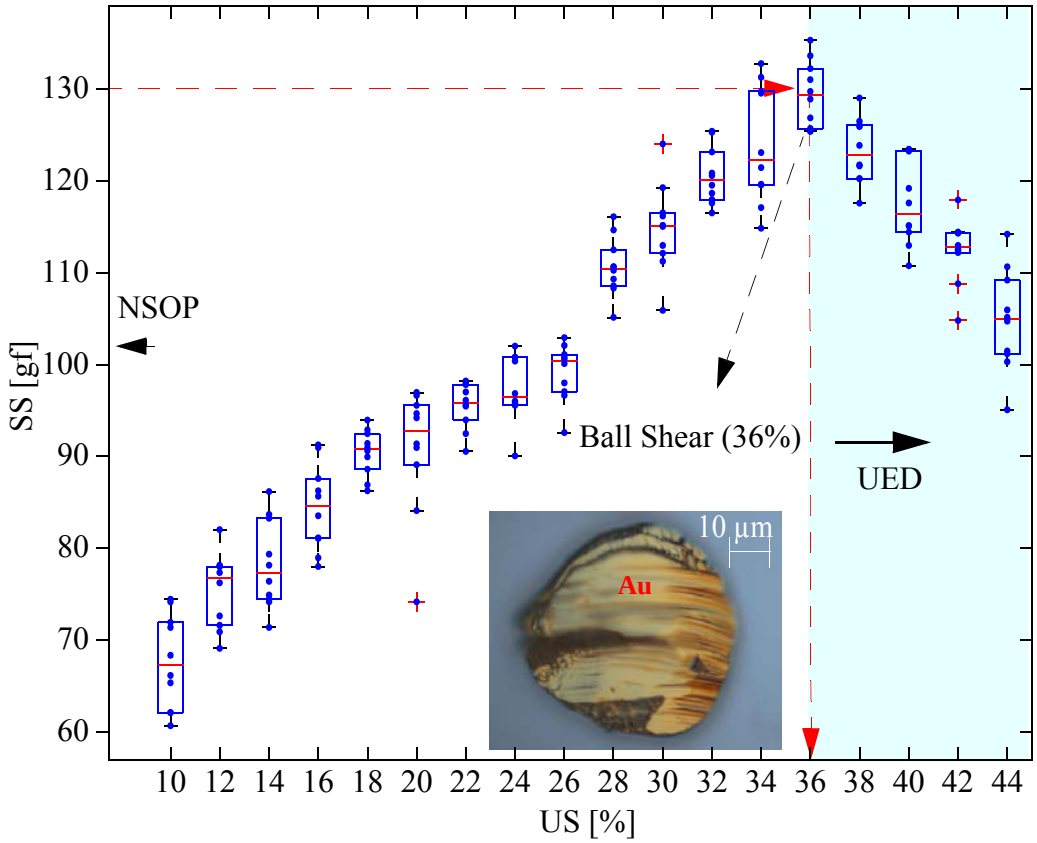

Figure 24 Optimized US for achieving a) maximum shear strength and b) shear at the ball (×200) before ultrasound enhanced deformation (UED) [27]

4.3 Summary

The optimized process parameters include nominal FAB diameter, ball bonding parameters, geometry and shear strength, all summarized in Table 10. Figures 26a, 26b and 26c show the SEM

Table 10: FAB, ball bond parameters and responses

Parameters						Responses		
FAB (µm)	**IF (mN)**	**BF (mN)**	**US (%)**	**Time (ms)**	**T(°C)**	**MBD (µm)**	**BH (µm)**	***SS* (MPa)**
40	500	300	18	20	220	58	10	130

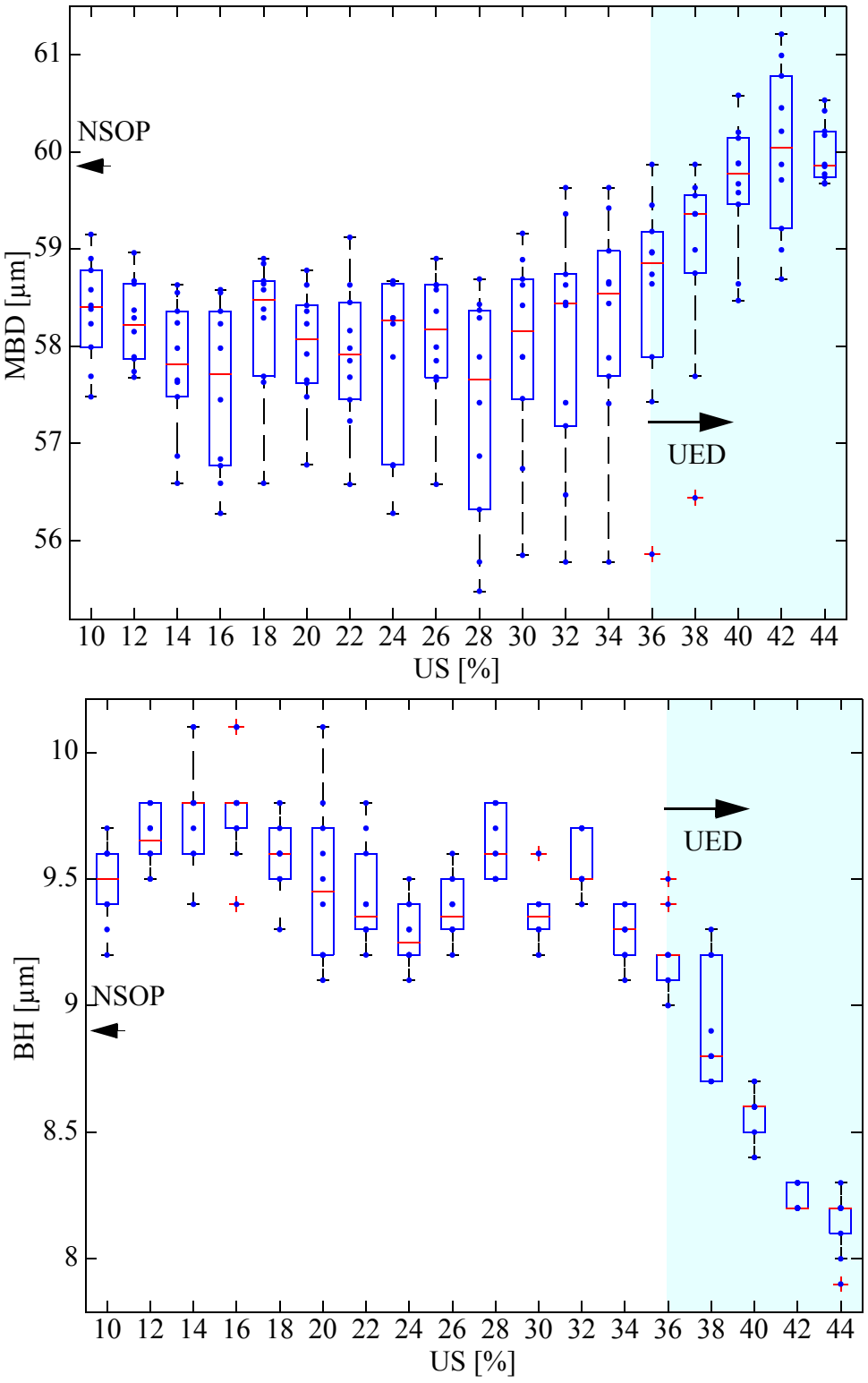

Figure 25 Boxplot of a) MBD, and b) BH for various levels of US.

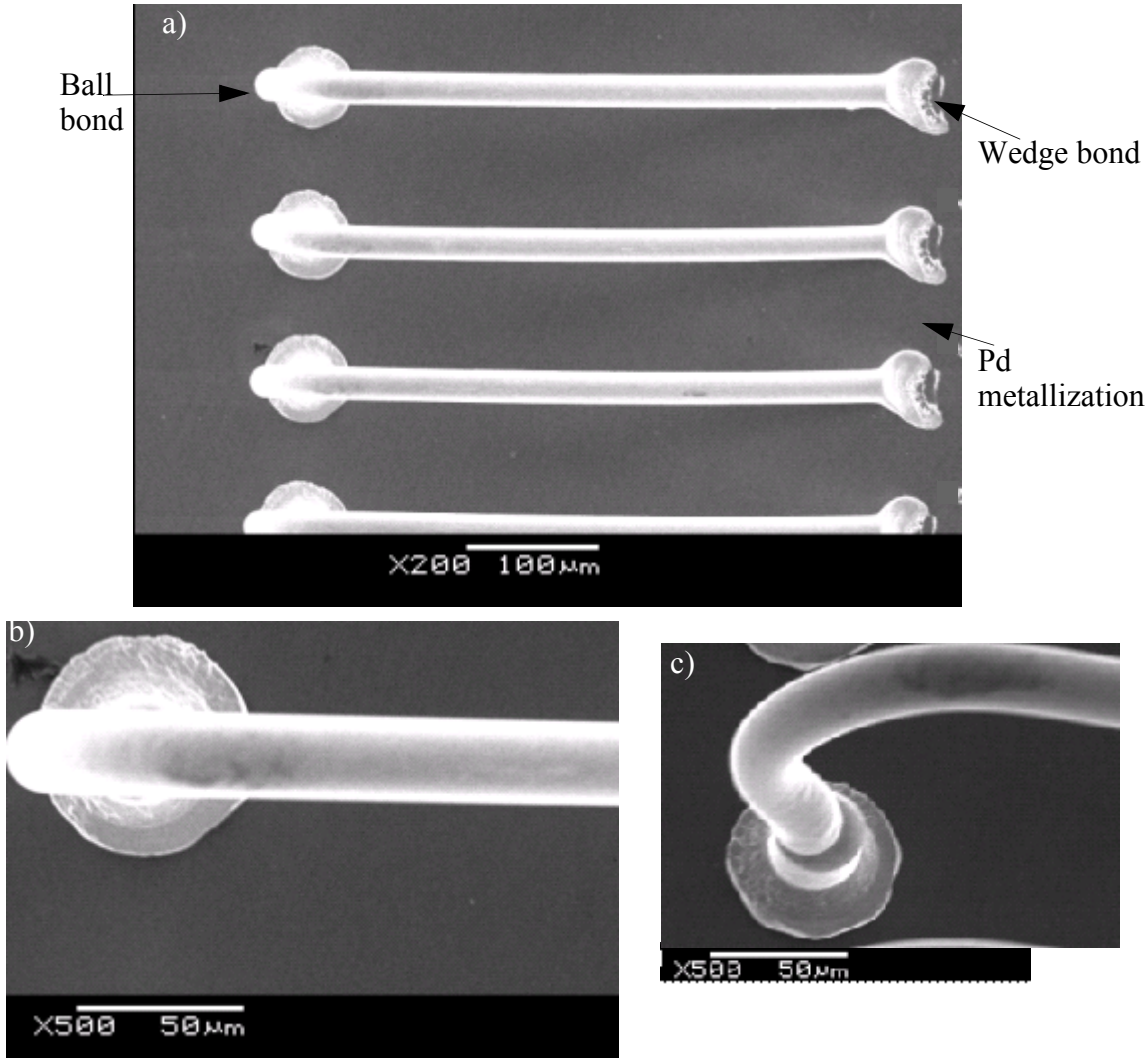

Figure 26 SEM of a) bonded wire loops, b) ball bond top view and c) side view. On Pd/Ni/Cu coupon with optimized bonding parameters.

images of the ball bond overview, detailed top view, and detailed side view, respectively. The geometry of the ball is achieved to be within the specified range. The ball bond shape is similar to that of the standard Au-Al process. However, the bondability of Au-Pd system is better (increase in *SS*) than that of a typical Au-Al process.

5. Reliability Study Through Destructive Analysis

After successful bonding on the Pd/Ni/Cu coupons, it is of interest to analyze the nature of the bond. The possibility of IMC formation and interdiffusion is studied in detail. A standard aging process is used in an attempt to thermally increase the possible voids and diffusions near the interfaces of Pd/Ni/Cu coupons.

The ball bonds are aged at a temperature of 250°C over 50 h, 100 h and 200 h. Cross section analysis is performed on the ball bonds, and nanohardness, SEM and TEM techniques are used to compare aged and as bonded ball bonds on the Pd/Ni/Cu coupons.

5.1 Shear test

The same shear test setup used previously for ball bonds before aging is used in this study. Figure 27 shows the *SS* variation with aging time. Ten ball bonds were sheared for each aging time. The average shear strength of the ball bond for aging of 100 h and 200 h show increase in magnitude compared with the as bonded and 50 h samples. The MBD and BH remain the same during aging. The increase in *SS* for the aged samples above 100 h over the as bonded samples is significant according to the t-test. Such increase can be attributed to the expansion of effective bonded area through surface diffusion filling interfacial gaps, which promotes the strength of the ball bond. Similar to the as bonded failure type, the shear occurs at the ball in all aged samples.

5.2 Cross-section Analysis

Mechanical grinding and polishing are used to prepare the ball bond cross sections. The coupons before and after aging are held by epoxy hardened in a cup holder for 12 h. The mounted sample is removed from the cup to be ground and polished. The epoxy allows for grip, and minimizes smear during polishing of the coupon. The grinding starts near the second bond. Similar to the

previous grinding process, 300 and 600 grit paper are used to quickly grind away the material remote from the wire bond. Silicon carbide paper of 800 grit is used when the wedge bond has been reached, until the top of the wire loop is exposed, which is near the edge of the ball bond under the microscope. Grit paper of 1200 and 1200 fine are used to grind from there to the ball center.

The same polishing procedure as used for lowering the roughness of the as bonded sample is employed for the cross section of the ball bond. After polishing with diamond slurry, an additional polishing stage is used to minimize smear of Cu. The solution in this final polishing stage is a

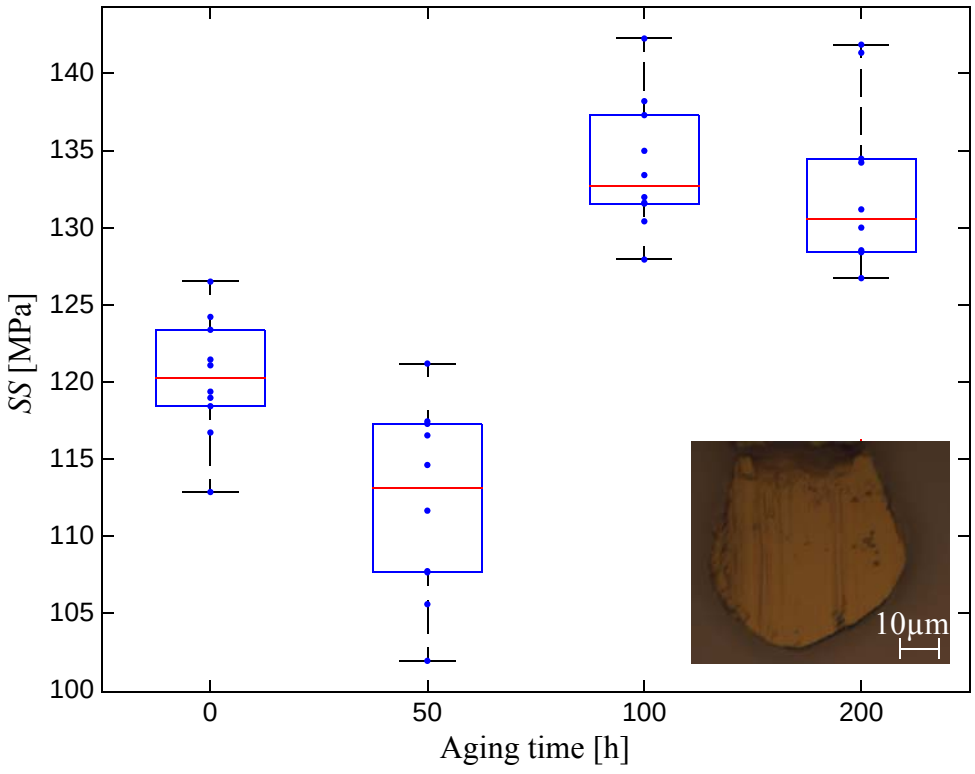

Figure 27 Boxplot of shear force for various aging time.

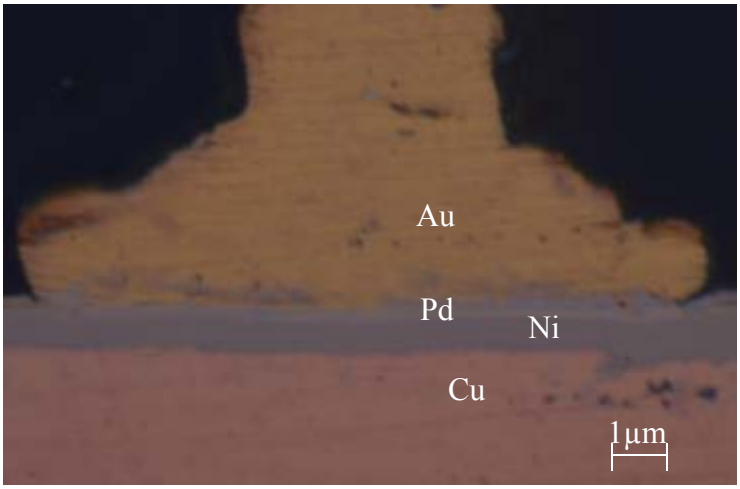

Figure 28 Optical microscope image of ground and polished as bonded ball bond.

mixture of colloidal silica, ammonia, and hydrogen peroxide. Figure 28 shows an example micro-graph of the ground and polished as bonded ball bond.

5.2.1 Nanohardness

A Hysitron TriboIndenter supplied by Hysitron, Minneapolis, USA, is used for nanoindentation testing to identify possible hardness differences between the as bonded and aged sample. The cross section is placed on an adhesive, and inserted in the machine. No additional modification is performed to address possible surface hardening due to mechanical polishing since the relative hardness of the various metallic layers is sufficient for comparisons. The goal in this stage is to see whether IMC or interdiffusion can be detected by means of change in nanohardness next to the Au/Pd interface.

Figure 29 shows the topography of the cross section at the interfacial layer between the Au ball and Pd/Ni/Cu substrate after indentations are made for a sample aged for 200 h. The process is repeated for an as bonded sample. Table 11 lists descriptions of the fourteen nanohardness points

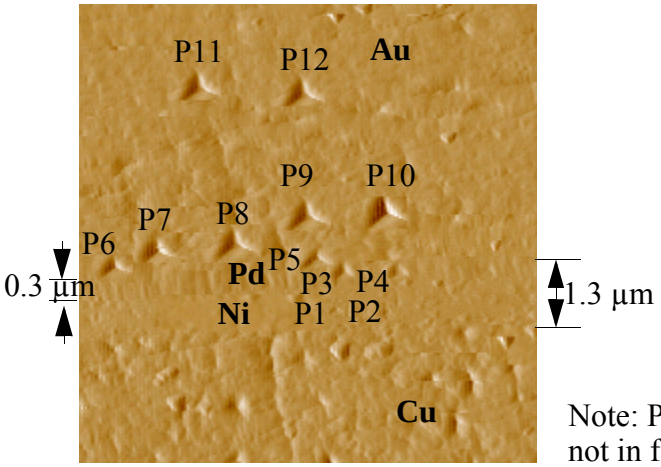

Figure 29 Topography view of cross section of interfacial layer between center of Au ball and Pd/Ni/Cu substrate after nanoindentation for an aged coupon for 250 °C over 200 h. Image size 8 µm×8 µm.

Table 11: Description of points in a typical nanohardness measurements

Point (P)	Description
P1	Center of Ni layer I
P2	Center of Ni layer II
P3	Center of Pd layer I
P4	Center of Pd layer II
P5	Au/Pd interfacial layer I
P6	Au/Pd interfacial layer II
P7	0.2 µm vertically from Au/Pd I
P8	0.2 µm vertically from Au/Pd II
P9	0.4 µm vertically from Au/Pd I
P10	0.4 µm vertically from Au/Pd II
P11	1.5 µm vertically from Au/Pd I
P12	1.5 µm vertically from Au/Pd II
P13	Cu (3 µm away from Ni/Cu) I
P14	Cu (3 µm away from Ni/Cu) II

taken. Ideally, the points taken at the same region should be close to each other, but there are indents and scratches from the sample preparation stage, so the locations of the points were carefully chosen to avoid these features.

Figure 30a shows a plot of nanohardness results for the as bonded and aged coupons compared with Vickers hardness [40] of the corresponding metals. Similar to the Vickers, the overall pattern of aged and as bonded nanohardness over separate metal layers shows Ni has the highest nanohardness, followed by Pd, Cu and Au. Compared with nanohardness test of aged coupon, there is an increase in magnitude for the Au/Pd, Ni, and Pd regions in the as bonded coupon, attributed to the effect of aging, which counteracts annealing and softening. The nanohardness for Au is an average of the points P7, P8, P9, P10, P11, P12 taken away from the Pd/Au interfacial region in the Au side. All other data are an average of two sampling points. To verify the possibility of interdiffusion between Au and Pd, nanohardness taken at the Au region in steps of 0.2 μm away from the Pd/Au interfacial is performed for the aged and as bonded samples. Figure 30b shows a comparison of the change in nanohardness with distance from the Pd/Au region. The overall trends of the two curves are the same regardless of aging time. At a distance of 0.4 μm from the Pd/Au interface, the nanohardness saturates to that of bulk Au as measured at 1.5 μm away from the Pd/Au interface. Total of two measurements were made at each position interval for each coupon.

5.2.2 SEM

The LEO FESEM 1530 with ultra high resolution is used with EDAX EDS Sapphire Si(Li) 10mm^2 detecting unit supplied by Carl Zeiss, Peabody, MA, USA for imaging and chemical analysis of the cross sections.

Figures 31a to 31d show detail SEM views of the ball bond center for the as bonded, aged in 50 h, 100 h and 200 h, respectively. Different metallic layers are discernible by distinct contrast differ-

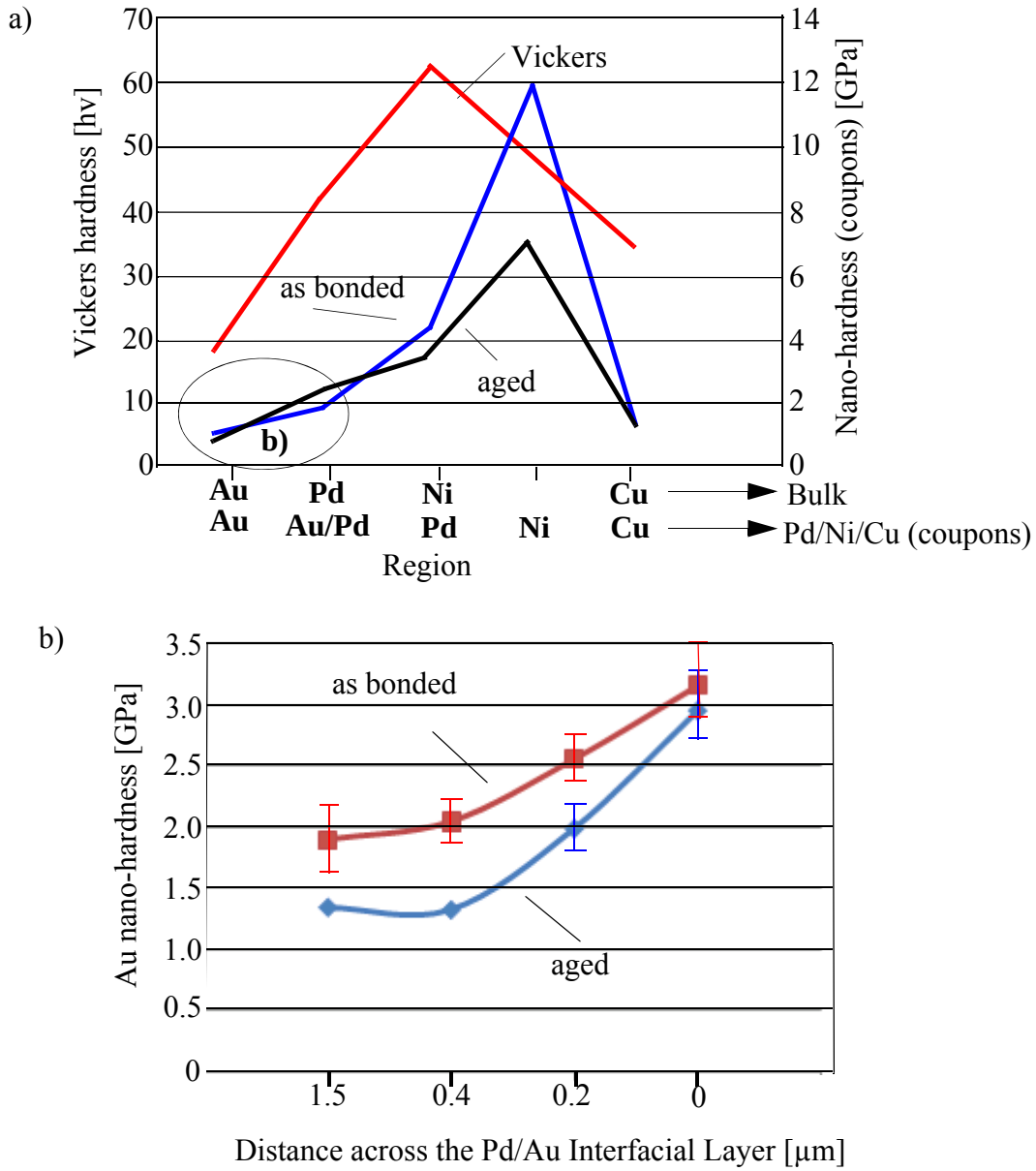

Figure 30 Nano-hardness of a) across interfacial cross section of Au ball on Pd/Ni/Cu substrate for the as bonded and aged compared with Vickers of corresponding metals and b) comparison between as bonded and aged with change in distance from Pd/Au interface to pure Au region.

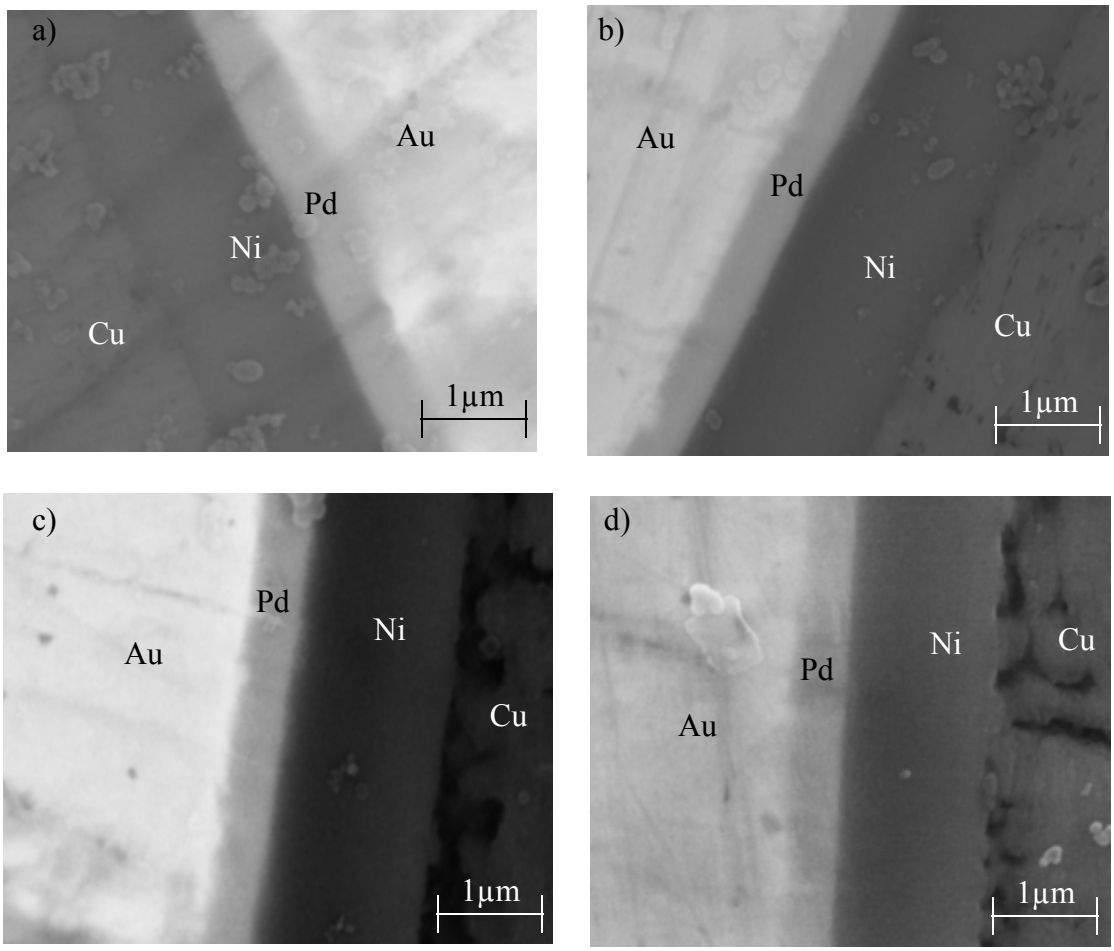

Figure 31 SEM image of ground and polished a) as bonded, b) aged for 50h, c) aged for 100 h, and d) aged for 200h bond.

ences on the images. The thicknesses of the plated layers are consistent with previous measurements. Figure 32 shows a typical EDAX of the aged sample at 200 h confirming the chemical composition of the material. Figures 33a and 33b show the left and right edges of the as bonded ball in comparison to Fig. 33c and 33d, which shows the left and right edges of ball bonds aged for 200 h. Similar to Fig. 31, separate metallic layers are distinguishable. There is no conclusive evidence of diffusion, IMC or voids near the interfaces in the SEM analyses.

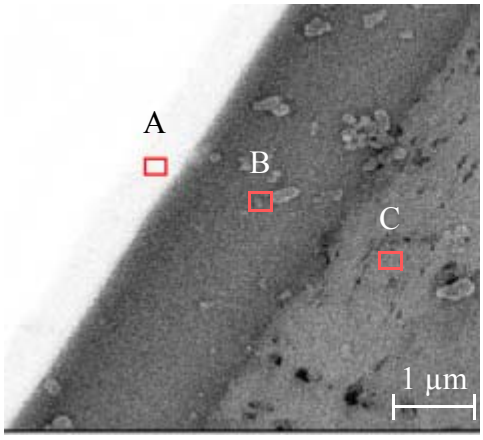

Spectrum	Ni	Cu	Pd	Au	Total
A	7.91	4.01	74.10	13.98	100.00
B	76.61	2.56	20.01	0.81	100.00
C	1.26	87.25	-0.62	12.11	100.00
Mean	28.60	31.27	31.16	8.97	100.00
Std. dev.	41.72	48.48	38.59	7.12	
Max.	76.61	87.25	74.10	13.98	All weights in %
Min.	1.26	2.56	-0.62	0.81	

Figure 32 EDX of grinded and polished as bonded ball bond.

5.2.3 TEM

The JEOL 2010 field emission TEM/Spectroscopy TEM (STEM) of the Brockhouse Institute of Material Research at McMaster University in Hamilton, Ontario, is used with maximum magnification in transmission mode of 1.5 million and the information limit of 1.4 Å to further characterize the bond cross section interface. In STEM mode its spot size has been optimized to 1 nm. This allows for high magnification imaging (X 8 million) and energy dispersive analysis of materials. The small spot size enables elemental analysis with special resolution limited by the scattering in the specimen.

Before analyzing the sample under TEM, carbon film deposition is performed perpendicular to the ball bond cross section with SEM micrograph shown in Fig. 34 The sample chosen for TEM analysis has been aged for 200 h at 250 °C. Once the deposition is completed, FIB milling is performed to cut out a thin Au-coupon interface. The milling direction is perpendicular to the ball bond cross section. The milling process is continued for 45 min until the front and back surfaces of the cross section are exposed with SEM micrograph as shown in Fig. 35. Any effect of smear-

ing in the mechanical preparation of the sample is removed in the process. Figure 36 shows the area to be analyzed in the TEM after milling the bottom section of the ball bond cross section. The manipulator tip is positioned on top of the carbon film, and lifts the free lamina away from the cross section sample using carbon film deposition shown in Fig. 37. The milled section of the sample is placed on a copper grid by the manipulator tip shown in Fig. 38. After fixing the lamina to the Cu grid holder, the manipulator tip is released by additional FIB milling. The lamina is thinned for 2 h, with the final extracted sample shown in Fig. 39 for TEM analysis. The region near the Au/Pd region, and the Cu/Ni shown in Fig.39, are of interest in the study.

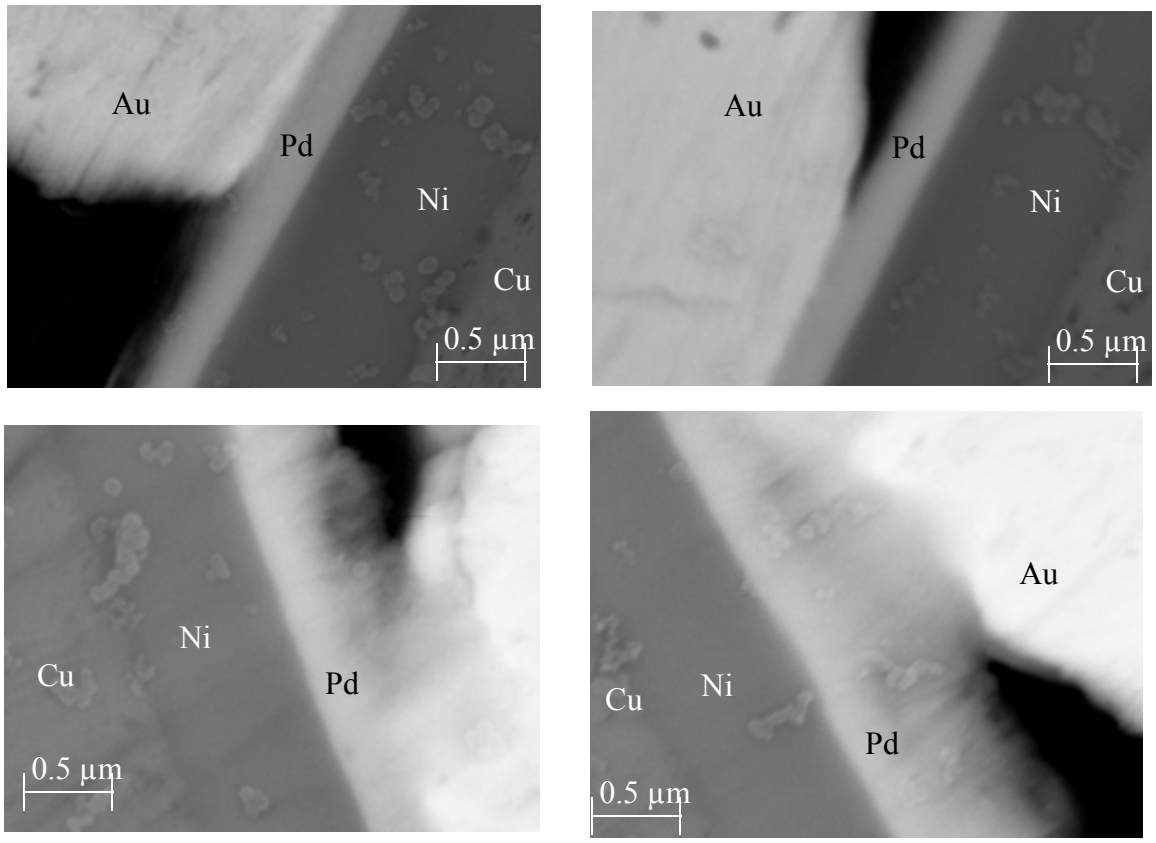

Figure 33 SEM image of a) left edge of bond as bonded, b) right edge as bonded, c) left edge aged for 100 h, and d) right edge aged for 200h.

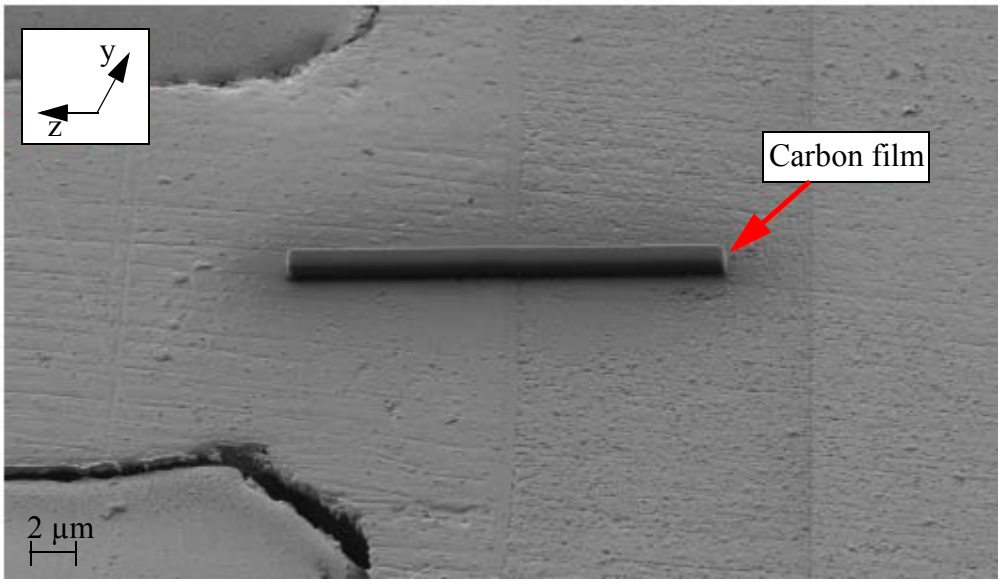

Figure 34 SEM image of sample aged for 200h with carbon deposition on top.

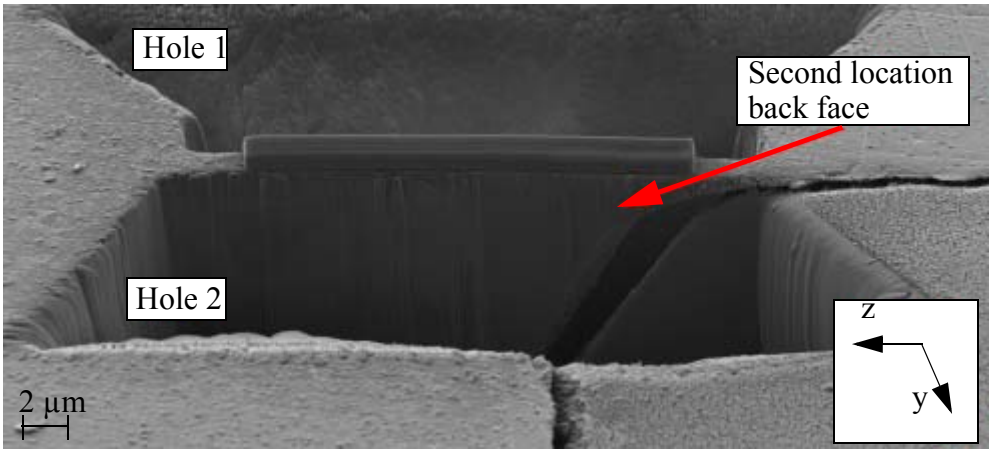

Figure 35 SEM image of sample aged for 200h after 10 h of milling on the two sides.

Figures 40a and 40b show detailed representation of the Au/Pd region at different magnifications. The interface between Au and Pd is distinguished from the contrast in the figures. In order to resolve the interface between Ni and Pd, which is of less interest in the study, a different set of

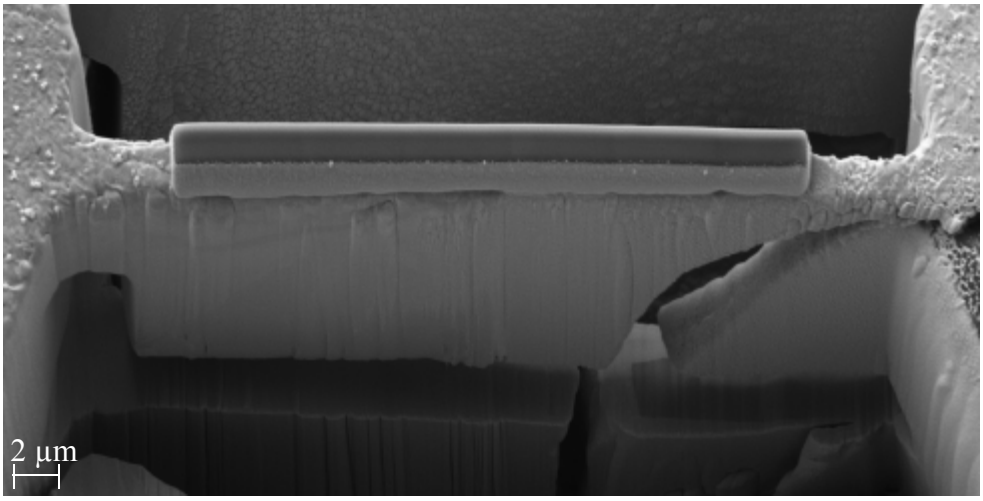

Figure 36 SEM image of sample aged for 200h after milling at the bottom.

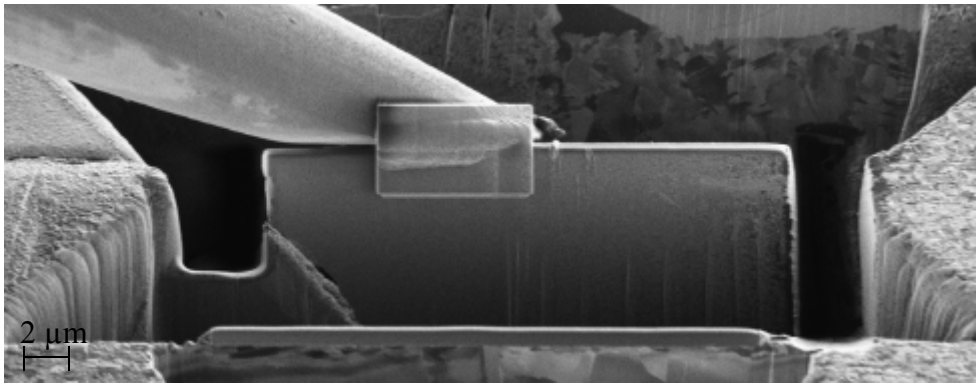

Figure 37 SEM image of sample after placing the manipulator tip on top, aged for 200h.

milling process is required. Dislocations and grain boundaries are visible throughout regions near the Au/Pd interface.

Figures 41a, 41b, 41c and 41d show TEM micrographs near the Au/Pd interface at different tilt angle. The Au/Pd boundary can be identified through the contrast of the images in Fig. 41, and is used as reference to identify dislocations near the Au/Pd interface. The presence of dislocation near the Au/Pd interface is confirmed when a change in dislocation plane (change in tilt angle) oc-

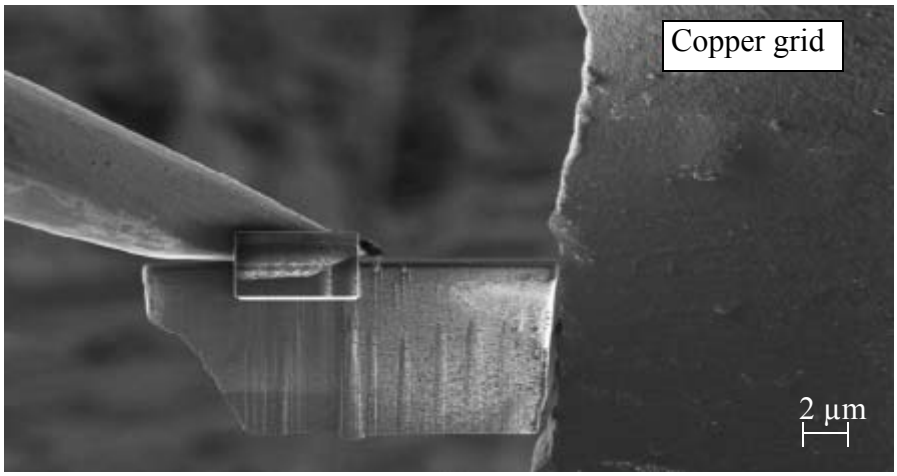

Figure 38 SEM image of sample aged for 200h after being placed on the copper grid holder.

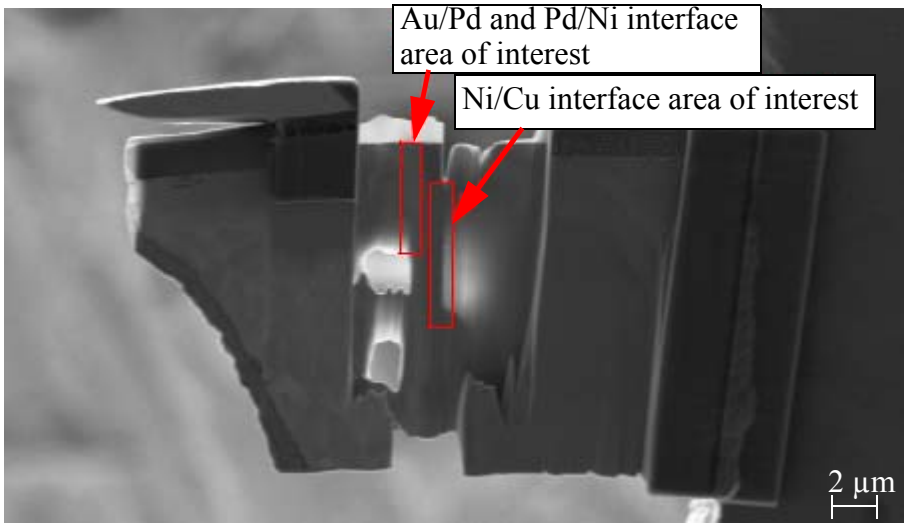

Figure 39 SEM image of sample aged for 200h after additional milling to thin the sample for TEM study.

curs as shown in Fig. 41. However, The presence of IMC formation and/or interdiffusion in the system is not clear. In an attempt to analyze the microstructure at the Au/Pd interfacial line, TEM micrographs are shown in Figs. 42a and 42b with higher magnification of the regions near the Au/Pd interface. The dark region varies in shape and intensity with change in tilt angle, which indicates the presence of dislocations near the Au/Pd interface. Figures 46a and 46b show an overall

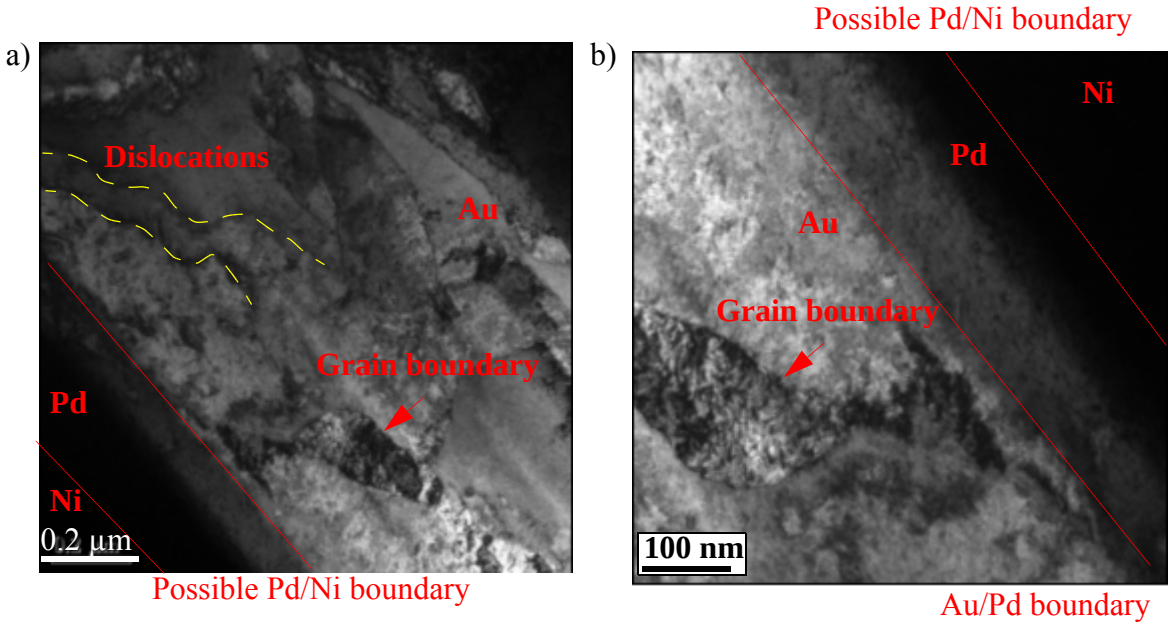

Figure 40 TEM image near the Au/Pd region at increased magnification from a) to b)

TEM image at the Au region where “oval” shapes in the dislocations are present. For comparison, TEM micrographs near the Cu/Ni side are shown in Fig. 43, away from the bonding region. Figures 43a and 43b show grain boundaries and dislocation to have "flake" patterns on the Ni/Cu interface, which differs from that of Au/Pd interface.

A TEM-EDS analysis was conducted in a similar way to that of the SEM-EDS. Figure 44a shows the Cu, Ni, Pd, and Au metallic layers with Figs. 44b to 44e showing x-ray spectra plots for Au, Ni, Pd, and Cu. The gap between Cu and Ni is due to sample preparation (ion milling) during which all of the Cu was removed in the region. Figure 45a shows the EDX scan over a higher resolution TEM micrograph with focus on the Pd layer. The x-ray energy scans of O, Ni, Pd, Au, and Cu are shown in Figs. 45b to 45f, respectively. Similar to the lower resolution analysis, Cu exists through all metallic layers. With the exception of Au, Ni, Pd, or Cu in the sample, there is no other

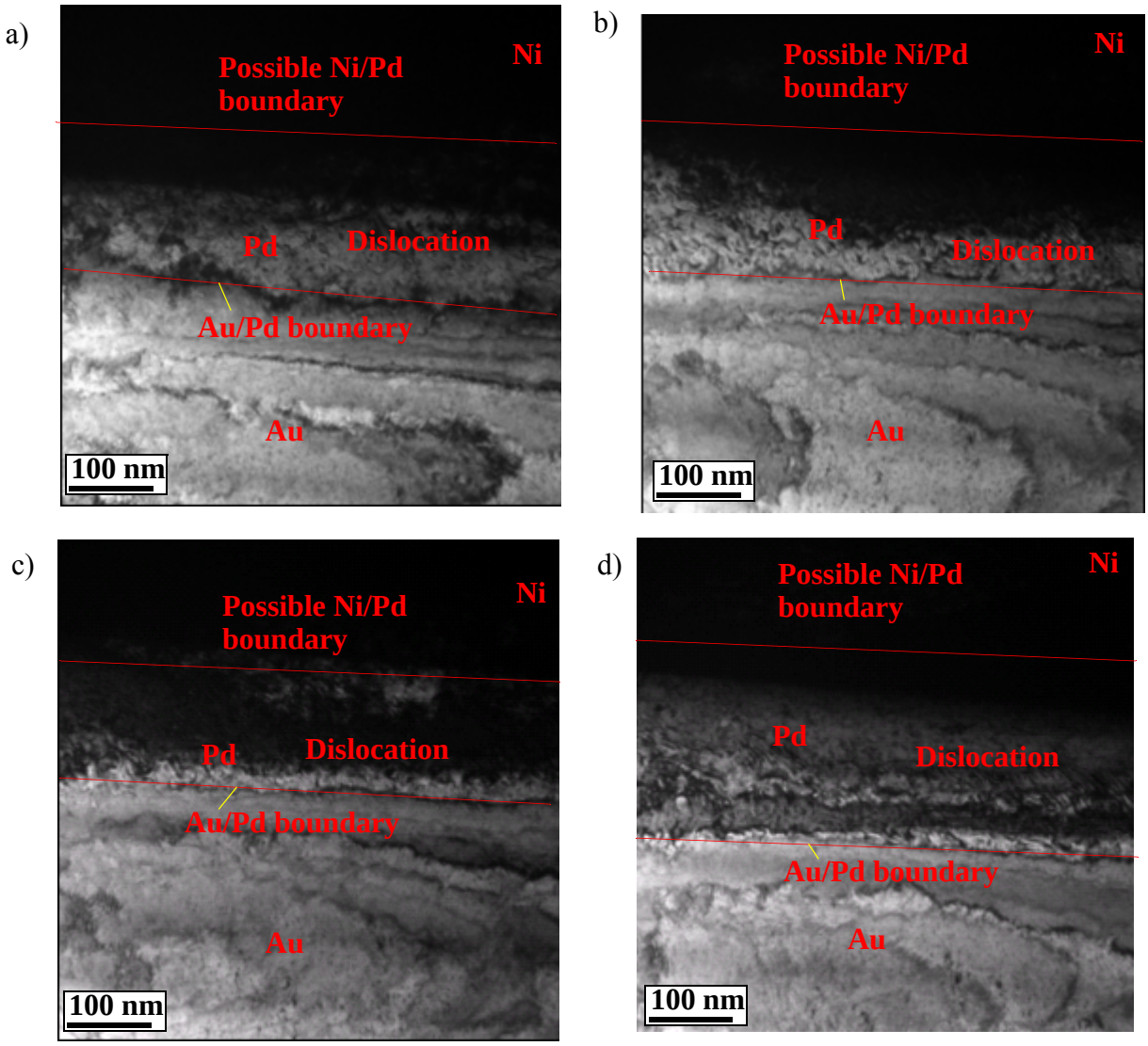

Figure 41 TEM image near the Au/Pd region at magnifications shown at various (a, b, c, d) tilt angle

material such as oxide, in the system, and the surface is free of impurities. Similar to the previous analysis, there is no observable evidence of IMC formation near the Au/Pd interface. However, At the regions near the Au/Pd interface, there is a visible concentration of about 0.1 μm of Au present on the Pd side.

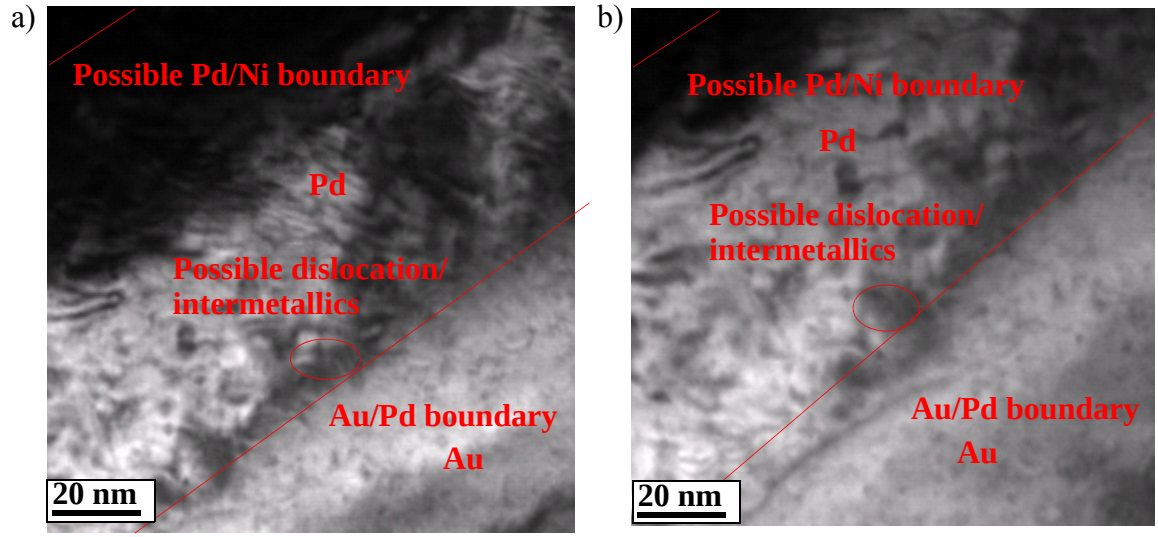

Figure 42 Detailed TEM image near the Au/Pd region at magnifications shown in a) and b), zoom of a)

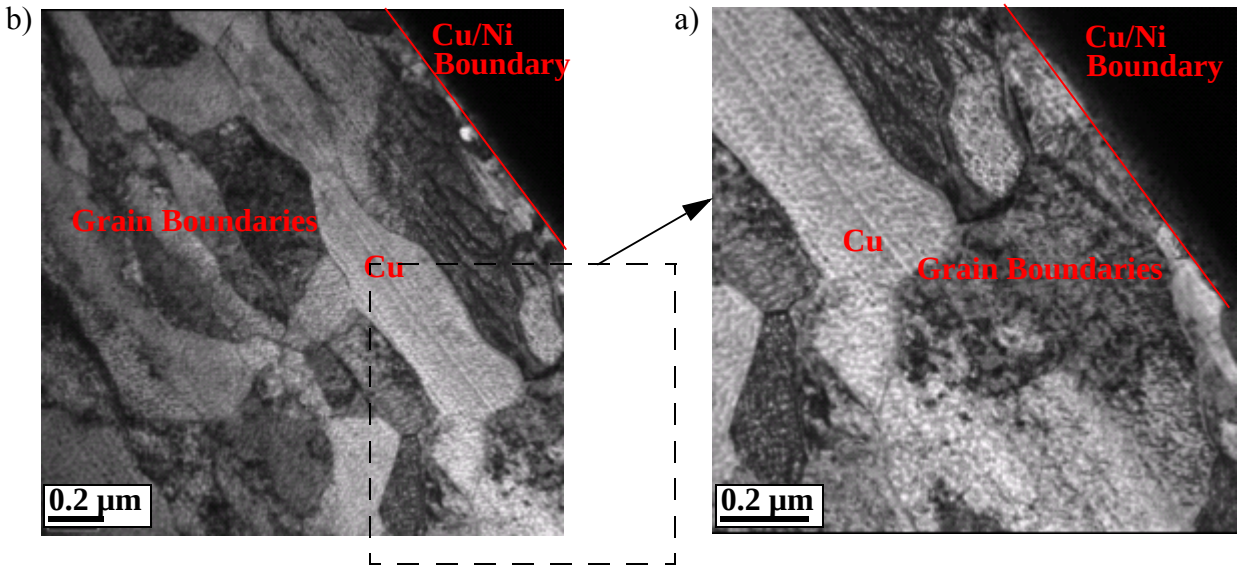

Figure 43 TEM image near the Cu region at magnifications various tilt angle (a, b)

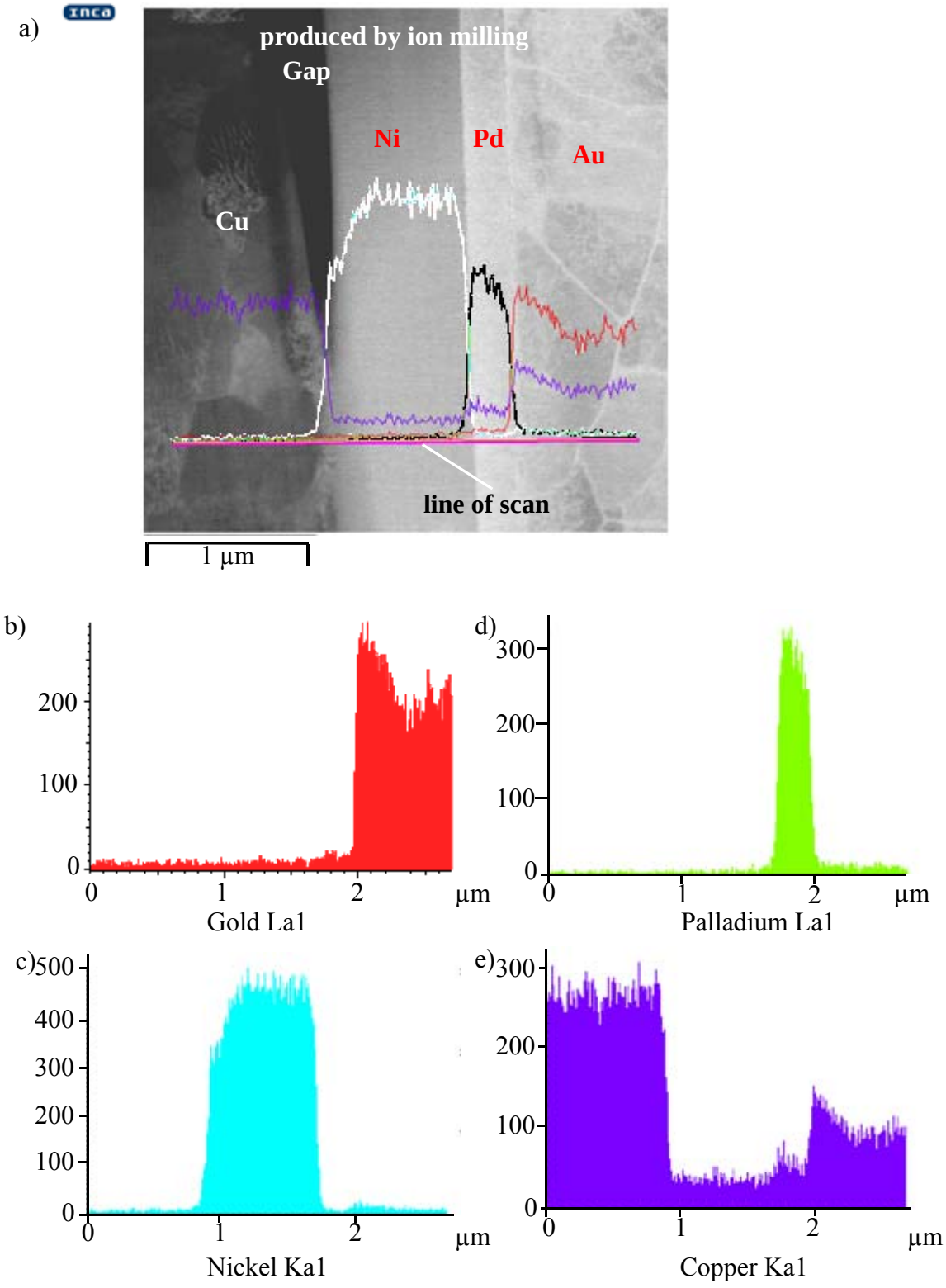

Figure 44 EDX line scan across the a) Pd/Ni/Cu/Au metallic layers for x ray spectra of b) Au, c) Ni, d) Pd, and e) Cu.

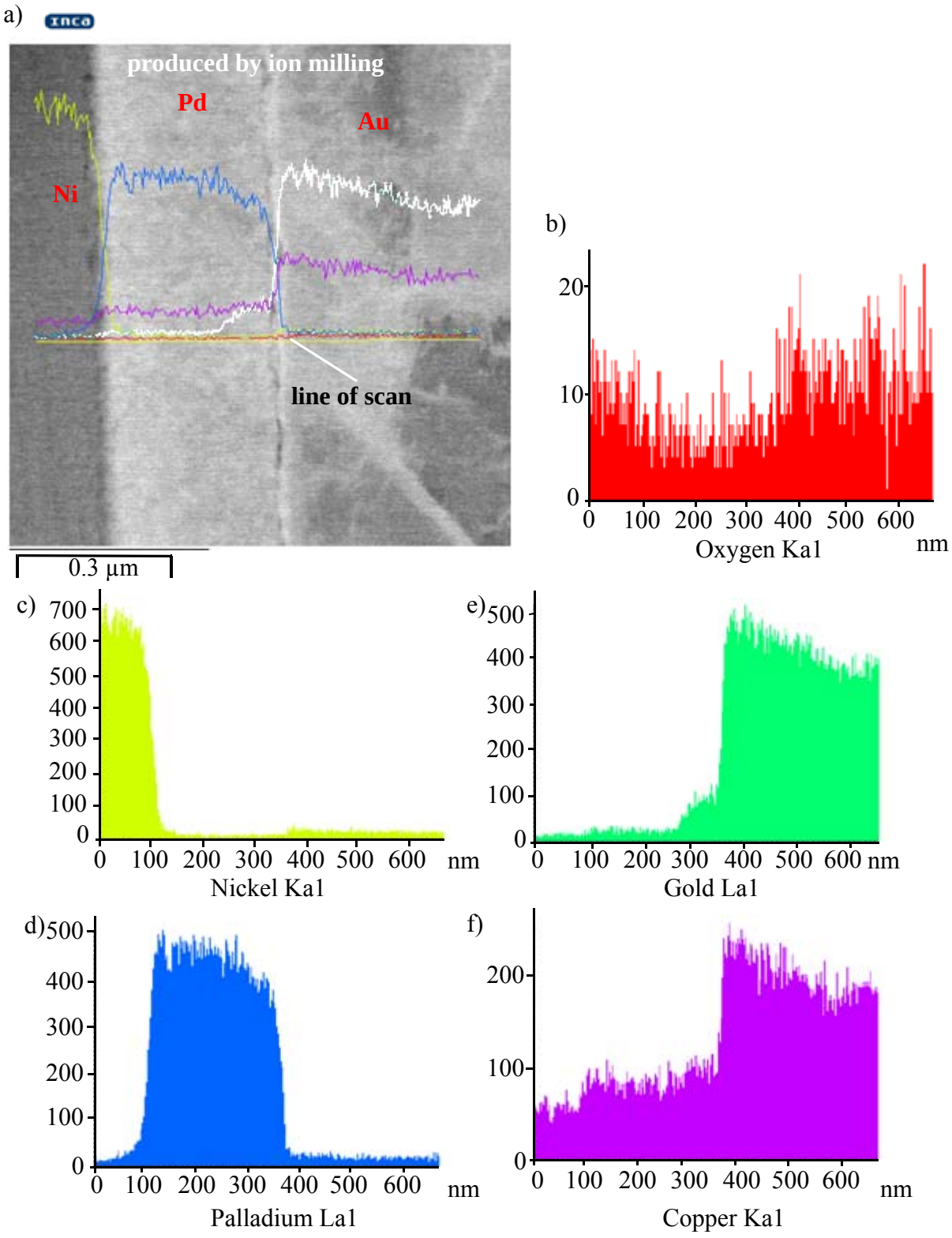

Figure 45 EDX line scan across the a) Au/Pd/Ni metallic layers for x ray spectra of b) O, c) Ni, d) Pd, e) Au and f) Cu.

5.2.4 Discussion

For the nanohardness results, between 0 to 0.4 µm away from the Pd/Au interface, the variation in the magnitude of the nanohardness is due to the small distance to the interface causing a "proximity effect" in which the adjacent harder material raises the perceived hardness of the adjacent softer material. Therefore, the nanohardness technique is not applicable in determining a correlation between diffusion and/or IMC formation near the interfaces in this process.

Due to the limitation in the resolution of the SEM, no conclusive results for the presence of IMC, voids, or interdiffusion can be drawn.

Diffusion from Au to Pd observed in the TEM-EDS analysis has been reported previously [29]. However, The depth of diffusion from Pd to Au is expected to be about 10-15 % higher than that of from Au to Pd. Diffusion from Pd to Au is not observed in this study. The overall chemical analysis indicates lack of impurities across all interfaces, which could attribute to the increase in bondability of the ball bonds post aging.

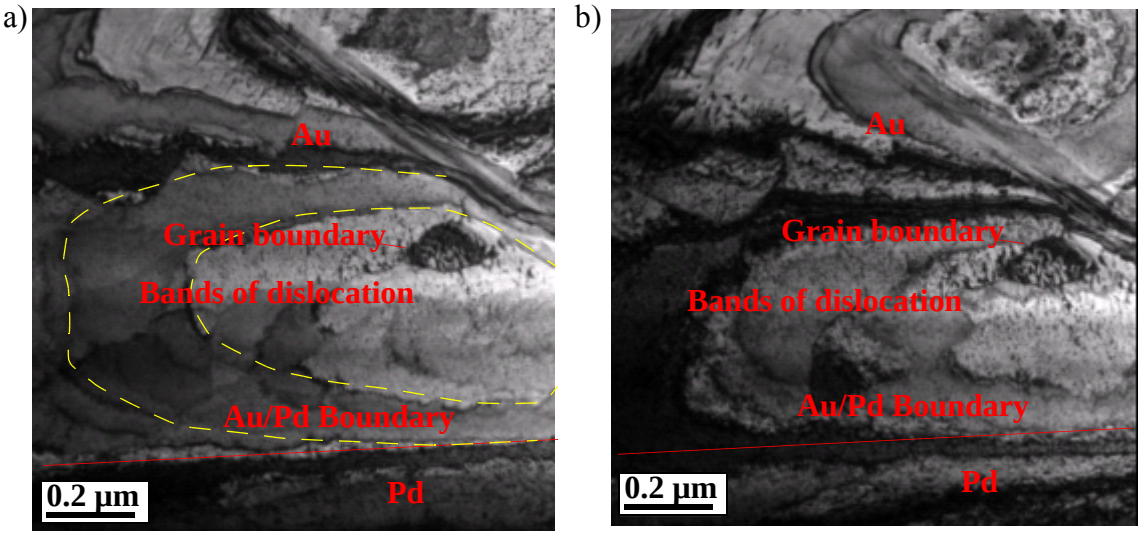

Figure 46 TEM image near the Au region at magnifications various tilt angle (a, b)

The lack of IMC formation from the SEM and TEM analysis is confirmed by the TEM-EDS analysis.

The difference of the dislocation shape between the Au/Pd and the Ni/Cu interface is likely due to the bonding process parameters affecting area near the Au/Pd interface, where repeated cycles of US motion result in dislocations shape subjected to repeated bending. The decrease in the amount of grain boundaries observed near the Pd/Au interface compared with the Ni/Cu interface indicates lack of Cu migration at the Au/Pd interface, which would degrade the bondability [54, 56].

The presence of Cu in the Ni and Pd region in the TEM-EDS analysis can be attributed to noise from the sample holder, which is made of Cu. The high Cu concentration in the Au wire is possibly due to a combination of noise, and error in the calculation of the x-ray spectra as Au and Cu have lattice parameters 4.08 Å, and 3.62 Å, respectively.

5.3 Summary

Based on shear testing results, the *SS* are higher for ball bonds aged for 200 h at 250 °C compared with that of the as bonded and aged for 50 h. No evidence of IMC formation and oxide were observed with the SEM, TEM, and nano-hardness techniques in the study. There is an indication of Au diffusion into Pd, which can correlate to the increase in bondability for ball bonds after aging. The nature of the chemical bond between Au and Pd is confirmed to be metallic.

6. Reliability Study Through Contact Resistance Monitoring

The contact resistance of the ball bonds is monitored for reliability analysis to confirm the previous results from the cross section analysis. A better understanding of the Au/Pd interface during aging is obtained. If formation of IMC or interdiffusion occurs during aging, a rise of the contact resistance is expected.

6.1 Experimental

The contact resistance (R_c) is measured by the standard 4-wire resistance measurement method illustrated in Figs. 47a and 47b in top view and side view, respectively. A second wire is attached to the ball bond using a modified bonding process with an US parameter reduced by at least 90 % resulting in a cold weld between the two Au balls, produced mainly by plastic deformation. Constant current I_c is fed via the second wire through the ball bond. At the same time, the voltage difference (V_L-V_H) is measured between the ball bond and substrate, where V_L and V_H are explained in Fig. 47b. R_c is calculated using Ohm's law by dividing the voltage difference by the applied current. The four wire configuration eliminates the wire loop resistance from the measurement.

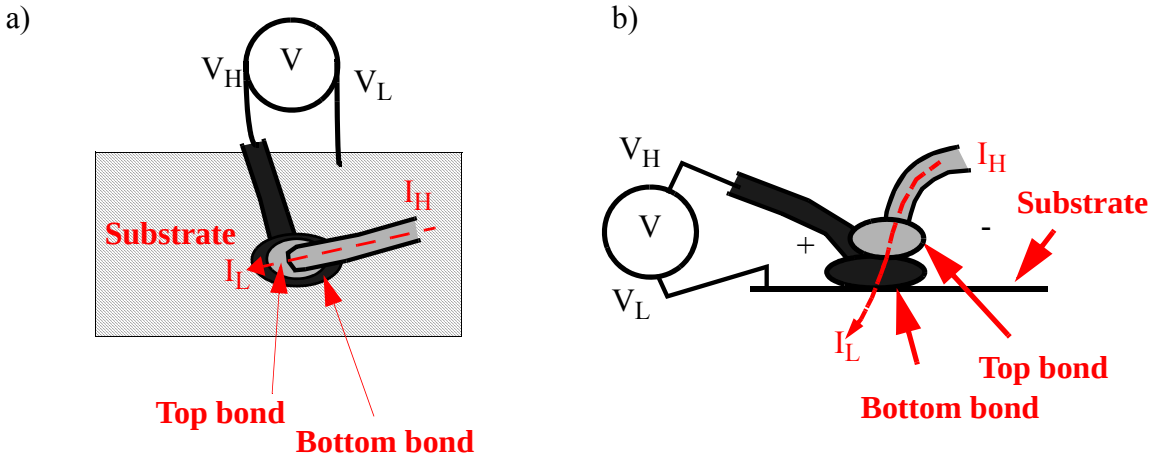

Figure 47 a) Top view and b) side view of the 4-wire contact resistance measurement method.

The same method has been used previously [42] for a similar experiment with an Au ball bond to a standard Al metallization.

The baseline substrate sample used in the contact resistance measurement during aging is denoted as sample 0. Sample 0 was plated with the optimum parameters and cut using a precision cutter to dimensions that fit on the diepad of the 28 pin chip package. The mounting of the Pd/Ni/Cu substrate on the package was performed using a thermally conductive silver epoxy cured at room temperature for 24 h. Figure 48 shows a photo of the assembly after mounting. The bonding diagram for the resistance measurement process is illustrated in Fig. 49. In total, 38 wire bonds are made. The pin configuration and its corresponding functionality are shown in Fig. 49. Pin 4 and pin 19 are used for I_L and V_L, respectively. Additional wires are bonded for the two pins as a precaution against premature failure. The remaining 26 pins are used to bond 13 sets of double bonds, with each set corresponding to V_H (bottom bond) and I_H (top bond). A maximum of 13

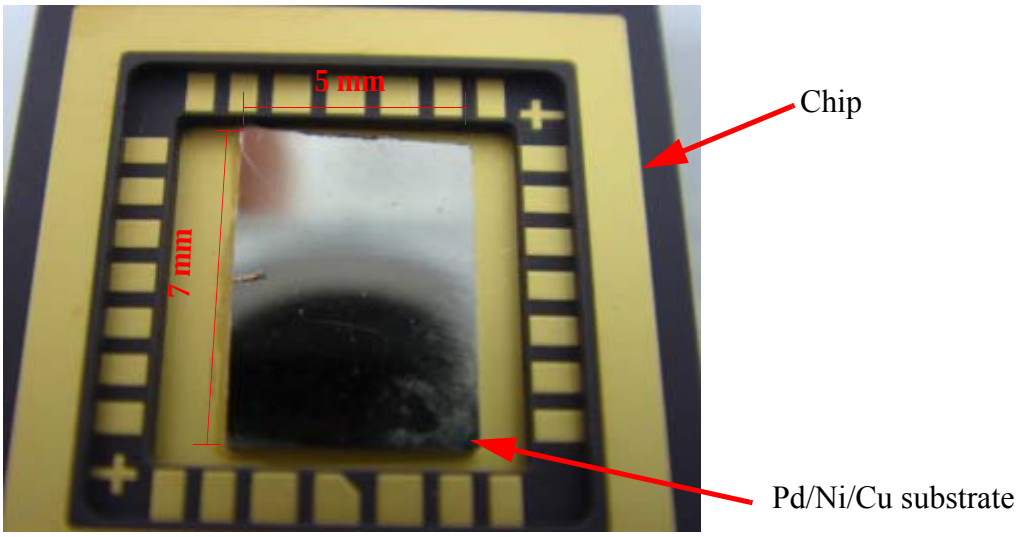

Figure 48 Photo of plated substrate after cutting and curing on the 28-pin chip package.

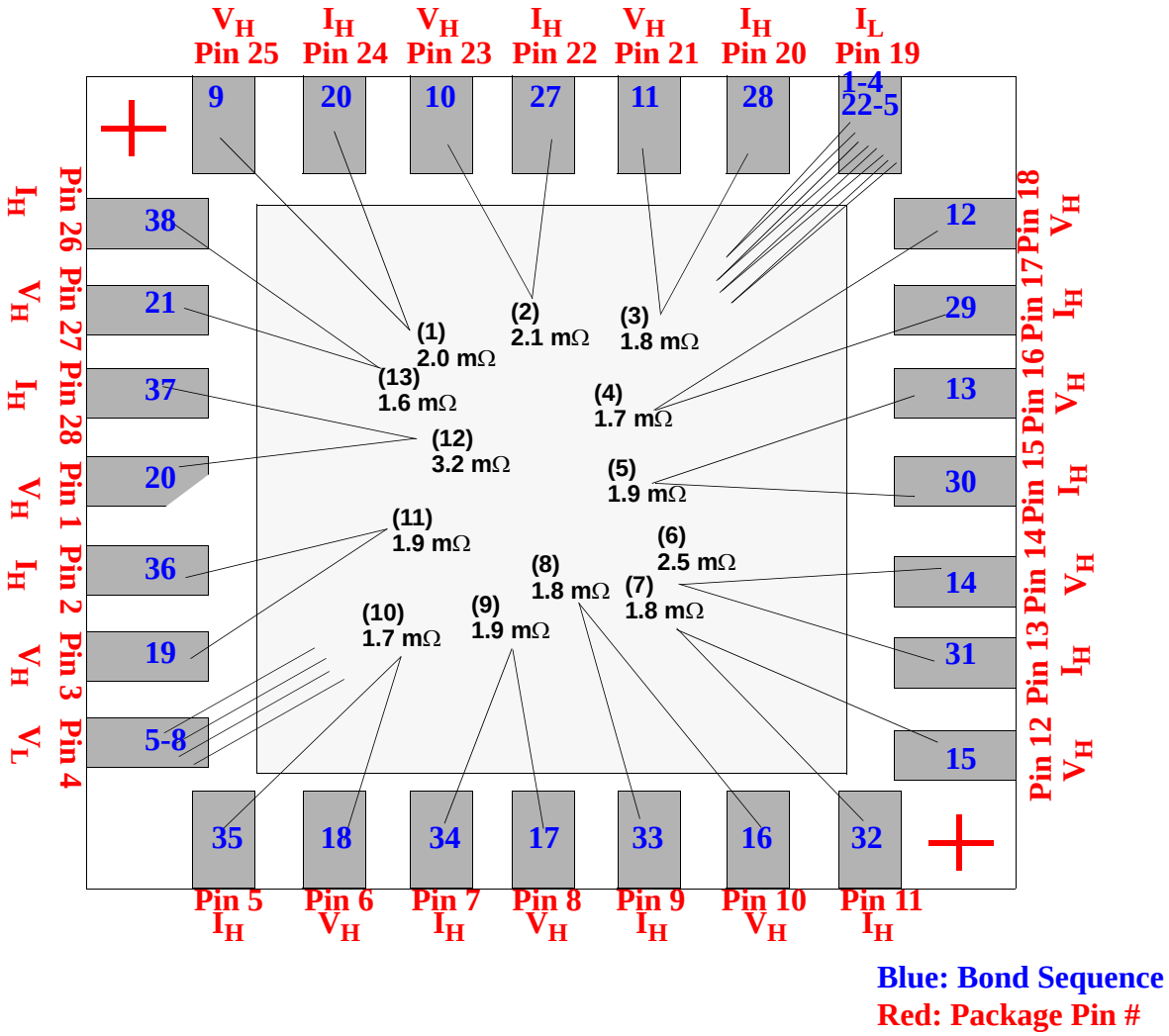

Figure 49 Bonding diagram for Pd/Ni/Cu on the 28-pin package (filename of bonding recipe: "YAN_INT1.REC".

sample resistance measurements can be generated from the 13 double bonds. The sample ball bond number is given in parentheses in Fig. 49. Below the ball bond number, there is the actual contact resistance measured at ambient temperature. The number given inside the package terminals in blue color indicates the sequence in which the bond is made on the wire bonder. The bottom ball bond parameter and the crescent bond parameters were taken from previous optimization processes for the baseline sample. Table 12 lists the top ball bond parameters. The IF and US for

the top ball bond are much lower than those used for the bottom ball bond to prevent the bottom ball bond from lift off by e.g. ultrasonically induced fatigue. A negative value for the "neck angle correction" parameter is used to obtain the desired loop shapes. Figures 50a and 50b show the actual chip during and after the wire bonding process.

High temperature solder consisting Pb and Ag, supplied by Kester Solder, Neuensalz, Germany, is used to join the leads of the package to a high temperature flat band cable supplied by Tyco Electronics, Berwyn, USA, and thereby to the multiplexer unit and the multimeter, supplied by Keithley Instrument, Cleveland, USA. The multiplexer is used to sequentially measure the 4-wire

Table 12: Top ball bond and other parameters for double ball bond process.

IF (mN)	BF (mN)	US (%)	BT (ms)	T (°C)	Loop Height (µm)	Neck Angle Correction
550	240	3	20	220	200	-0.826

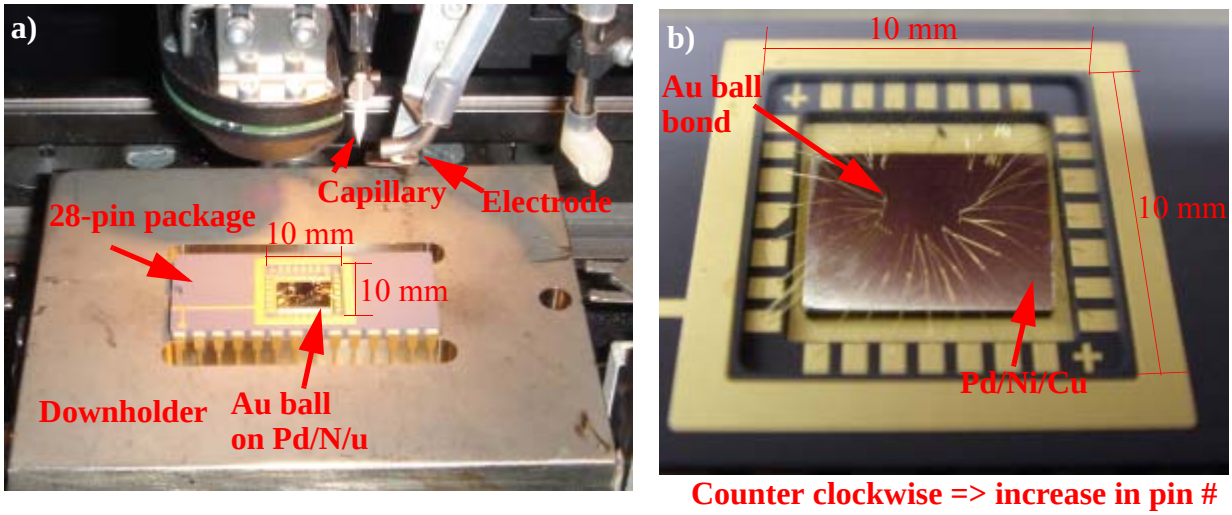

Figure 50 Photo of Au ball bonding process a) during and b) after bonding on Pd/Ni/Cu for contact resistance measurement.

resistance of each of the 13 available bonds via the multimeter. The computer, controlled by a custom made program (programming language is Matlab^{TM}) given in Appendix A (INSERT PROGRAM), switches the multiplexer and records the readings from the multimeter. The multimeter is used in the 4-wire resistance measurement mode, supplying a test current of I_c = 0.1 mA. The process is repeated for all 13 contact resistance measurements. Before starting the measurements, the chip is placed inside an oven (Omegalux, NJ, USA) where it remains at room temperature for 1 h to obtain reference measurements. The temperature next to the chip is measured by a Pt100 resistive temperature detector with a standard accuracy of ≈ ±4 K at 250 °C. Along with the contact resistance samples, the Pt100 unit is placed inside the oven, and the resistance is recorded using a DAQ unit and the same custom made program. The overall wiring diagram of the setup is illustrated in Fig. 51.

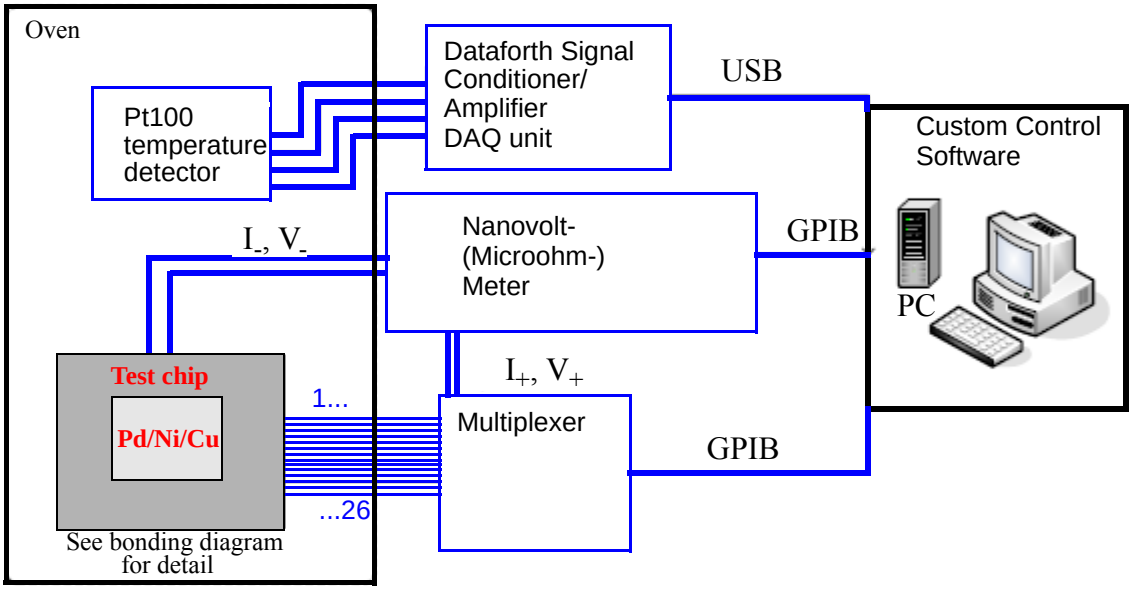

Figure 51 Wiring diagram for contact resistance measurement process of Au ball bonds to Pd/Ni/Cu substrate while in oven.

6.2 Results

The three process phases discussed are (I) heat-up, (II) aging, and (III) cool-down. The contact resistance rises with change in temperature in the heat-up phase until the target temperature of 250 °C is reached. The contact resistance saturating to a steady state value is observed in phase II. In the third phase, the oven is turned off and temperature drops to room temperature. The oven is turned on shortly again to obtain data for post aging temperature coefficient (*TC)* calculation.

Before phase (I), initial resistance measurements are made for reference at room temperature outside the oven by directly connecting each sample to the multimeter (bypassing the multiplexer) with results shown in Table 13. These measurements are then repeated with the samples connected to the multiplexer. Both results are identical, which indicates that the multiplexer does not add any offset to the R_c measurements. The actual temperature at the time for which the R_c was taken is also recorded in terms of resistance by the Pt100. The Pt100 resistance is converted back to temperature by

$$R = R_0 \cdot (1 + a \cdot T + b \cdot T^2) \qquad (1)$$

where $R_0 = 100\ \Omega$ is the resistance at 0 °C, $a = 3.9083 \cdot 10^{-3}\ K^{-1}$ and $b = -5.775 \cdot 10^{-7}\ K^{-2}$ are constants [57].

After 1 h of measurements at room temperature, the oven is reprogrammed to 50 °C and 100 °C, each for 30 min. Results from these additional temperature levels are used to calculate the *TC* of the R_c,

Table 13: Contact resistance reading for 13 sets of double ball bonds at ambient temperature.

Ball bond #	Contact Resistance (mΩ)	Ambient Temperature (°C)
1	2.04	26.2
2	2.12	26.2
3	1.756	26.2
4	1.738	26.3
5	1.879	26.3
6	2.538	26.4
7	1.80	26.4
8	1.81	26.2
9	1.934	26.2
10	1.708	26.2
11	1.893	26.2
12	3.188	26.3
13	1.596	26.0

$$TC(T) \equiv \frac{\frac{dR}{dT}}{R(T)} \qquad (2)$$

where T is the temperature and $R(T)$ is the resistance as a function of T [43]. The average TC at 20°C is 0.0022 K^{-1} with a standard deviation of 0.0001 K^{-1}, which is exactly the same as the TC post aging. The measured TC of R_c is lower compared to that of standard Au (0.003715K^{-1}) and Pd (0.0038K^{-1}). The value $R_{ref}=R(T_{ref})$ serves as comparison value between the magnitude of the contact resistance before and after aging. It is defined by

$$R_{ref} = \frac{R_x(T)}{1 + TC_{ref}(T_x - T_{ref})} \quad (3)$$

where $R_x(T)$ is the contact resistance with respect to temperature T_x, TC_{ref} is the temperature coefficient at T_{ref}, and T_x and T_{ref} = 20 °C are the actual and reference temperature, respectively [43]. The reference resistance before (R_{ref}^{pre}) and after (R_{ref}^{post}) aging, and the average and standard deviation of the contact resistance during aging are shown in Table 14. The median change is -6 %. As seen in Table 14, $R_{ref}^{pre} > R_{ref}^{post}$ for all 13 bonds after 287 h at 250°C.

Table 14: Comparison between R_c at different stages of aging for baseline sample.

Ball Bond	Before aging R_{ref}^{pre} (mΩ)	During Aging Average R_c (mΩ)	During Aging Resistance STDEV (mΩ)	After aging R_{ref}^{post} (mΩ)	Difference before and after (%)
1	2.00	2.7	0.01080	1.78	-11.04
2	2.15	2.9	0.02113	1.90	-11.62
3	1.70	2.4	0.00321	1.60	-5.92
4	1.70	2.4	0.00320	1.67	-1.76
5	1.83	2.6	0.03198	1.76	-3.82
6	2.40	3.1	0.01583	2.10	-12.5
7	1.75	2.3	0.00520	1.68	-4.00
8	1.70	2.5	0.02162	1.66	-2.35
9	1.73	2.5	0.00571	1.63	-5.78
10	1.77	2.4	0.02524	1.75	-1.13
11	1.84	2.5	0.01098	1.72	-6.52
12	3.12	3.8	0.04480	2.14	-31.41
13	1.57	2.2	0.00244	1.48	-5.73

Figure 52 represents in situ measurements of $R_c(t)$ of the bond with least change (bond #10), most change (bond #12) and typical change (bond #9) during aging. The thermal noise observed in Fig. 52 could be a due to random variations in the measured voltage caused by random movement of the electrons jolted around by thermal energy during the aging process. Figures 53a, 53b and 53c show SEM images of the double ball bonds #9, #10 and #12, respectively in top and side views. The shape of the ball bonds and the wire loops are similar to those observed on standard Al

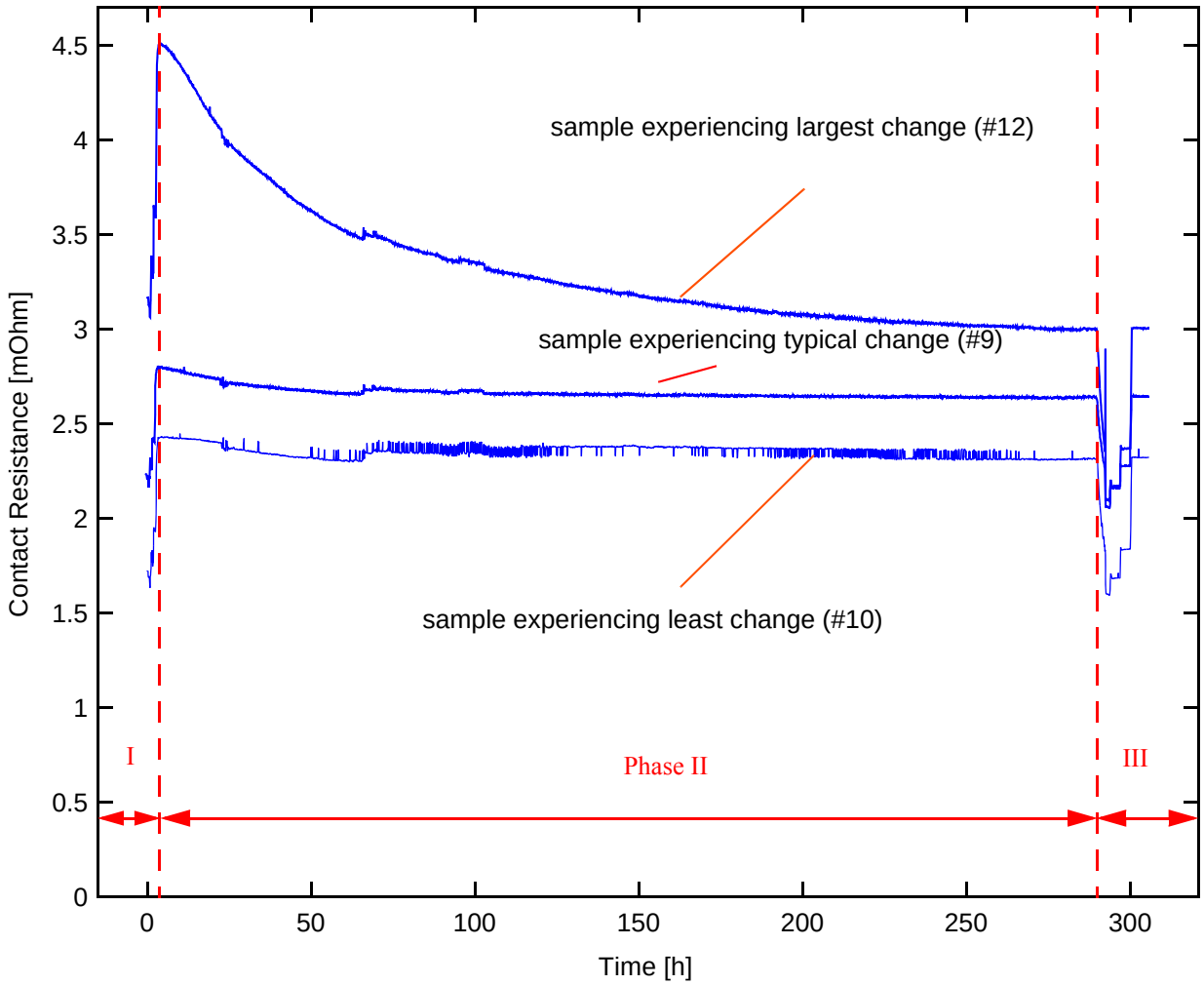

Figure 52 Contact resistance measurement test for largest change and least change in resistance for coupon with R_a of 0.08 µm. T = 250 °C during phase II.

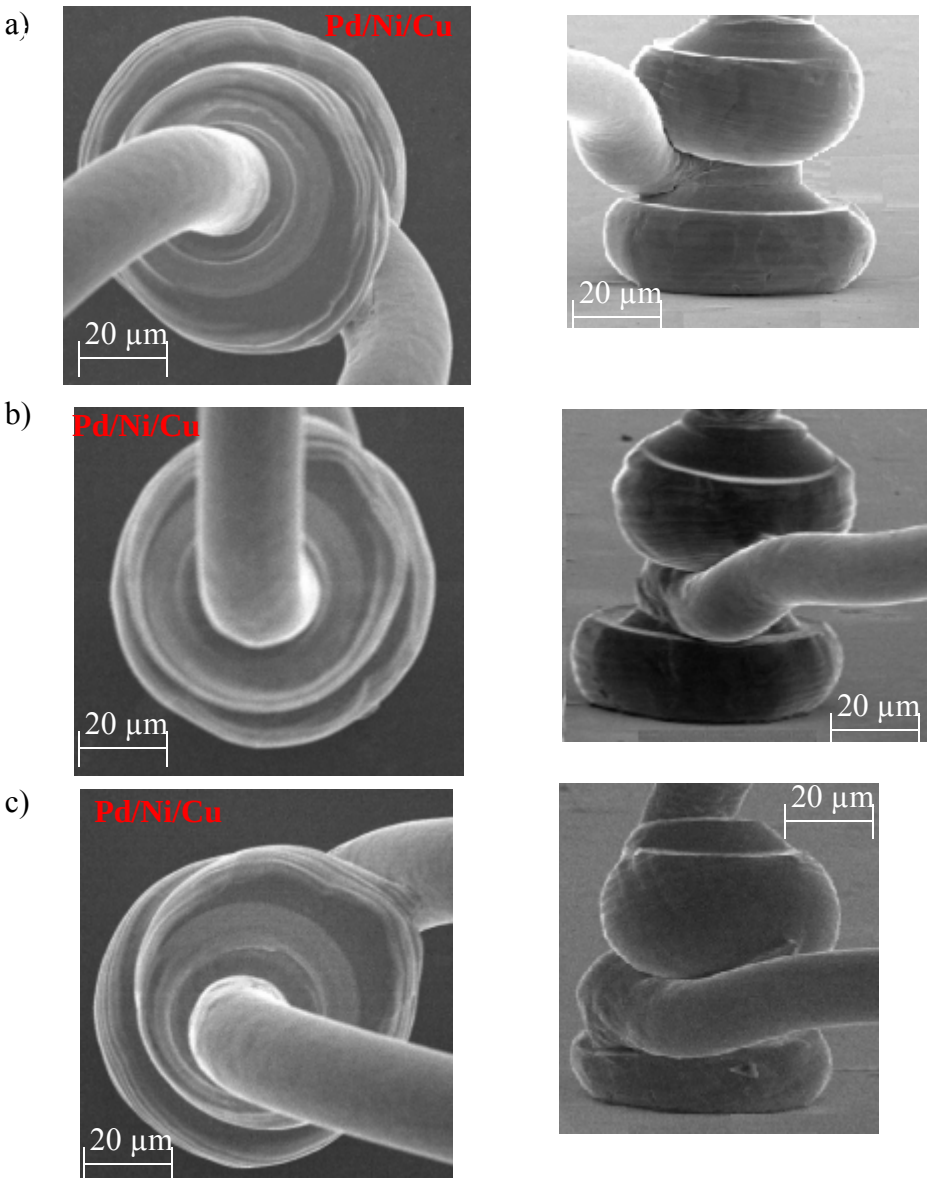

Figure 53 SEM images of double ball bond for a) largest R_c change (bond #12), b) the typical change (bond #9) and c) least change (bond #10) in i) top and ii) side view for coupon with R_a of 0.08 µm.

chips. The R_c measurements of the remaining samples are shown in Fig. 54. For these bonds, R_c does not rise during aging. On the contrary, R_c drops as observed for all 13 samples. The drop is strongest in the first 100 h of aging. The subsequent 100 h of aging shows a slower drop before R_c reaches a steady state value in some cases.

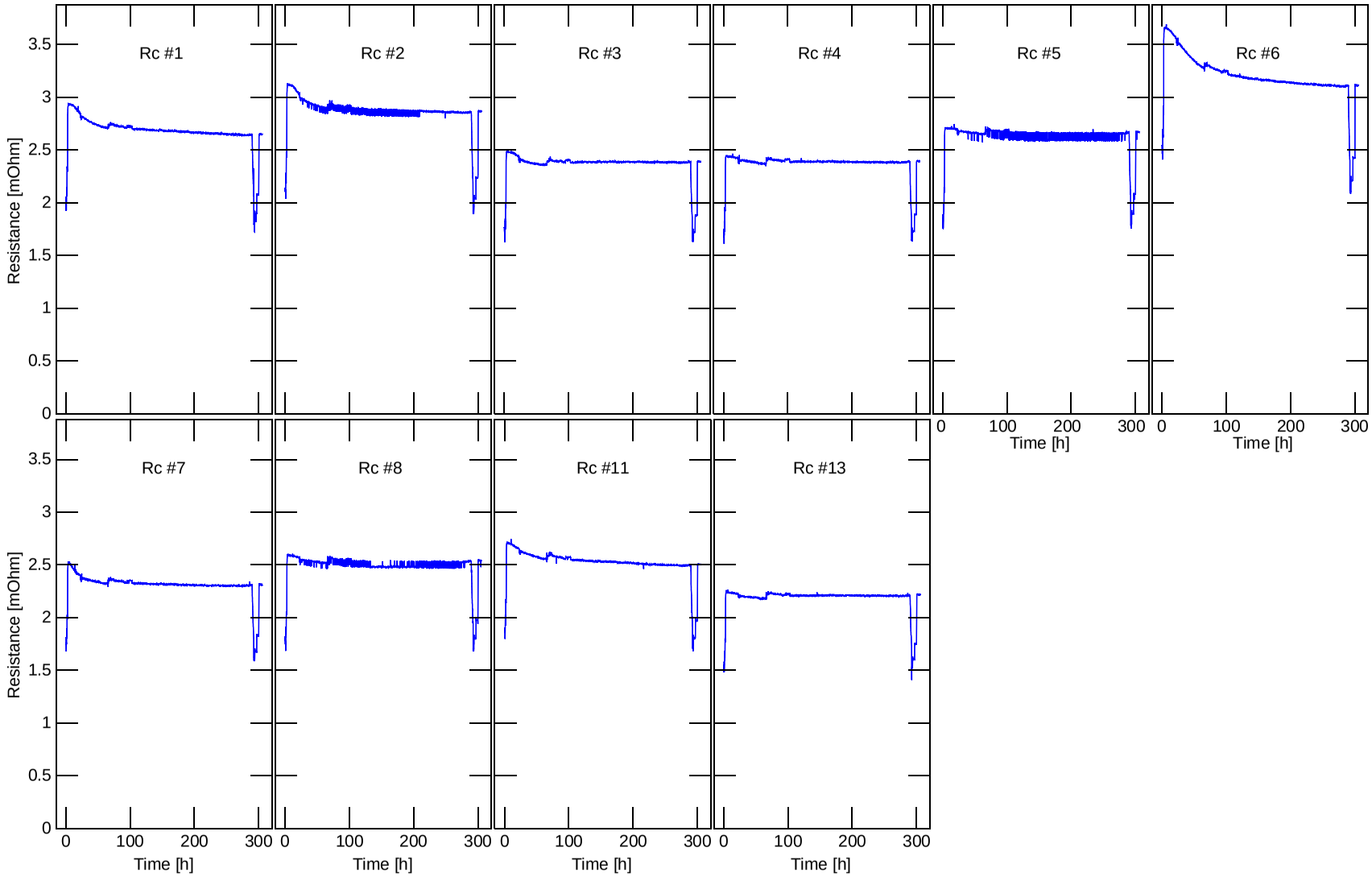

Figure 54 Contact resistance measurements for ball bond numbers 1-8, 11, and 13 through the 287 h aging at 250 °C for coupon with R_a = 0.08 µm.

6.3 Discussion

Logie et al. [44] reported an increase in resistivity that occurs from pure Au or Pd to AuPd alloys at liquid nitrogen point (77.2 K) as shown in Fig. 55. To correlate the results with the experiment conducted, if IMC formation was to occur, R_c is expected to increase similarly to that repeated in [44]. As R_c does not rise during aging, this indicates little or no IMC formation. The negligible variation between pre and post aging *TC* also reconfirms the lack of substantial IMC.

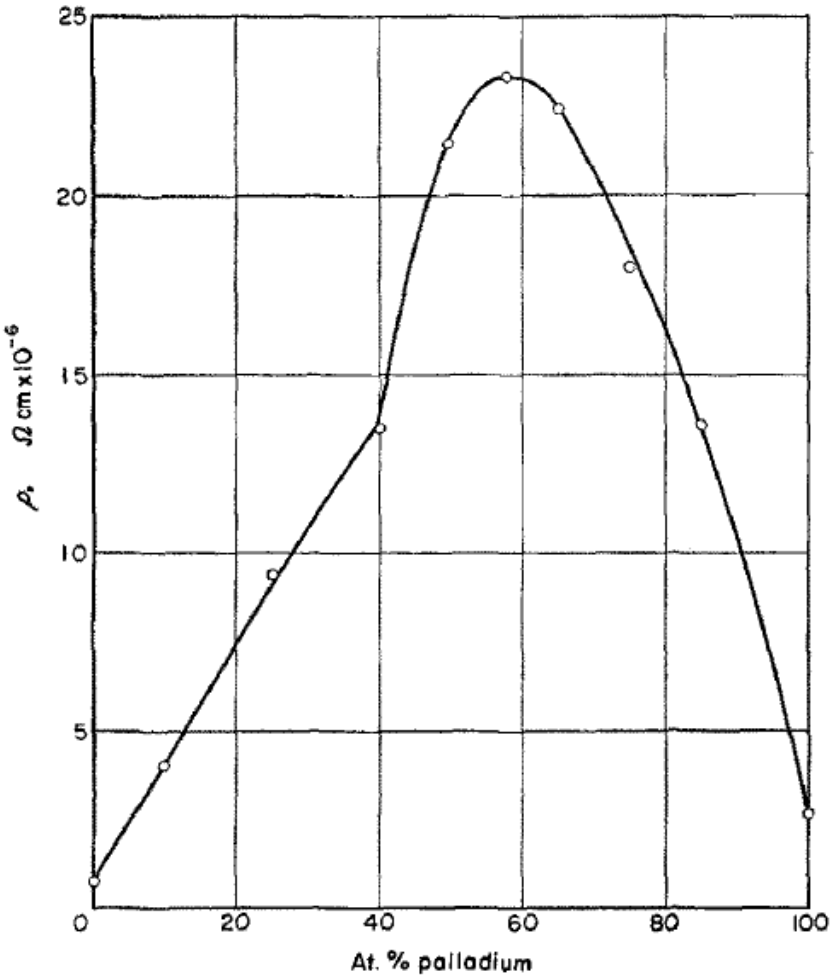

Figure 55 Resistivity of undeformed Au-Pd alloys at liquid nitrogen temperature (77.2 K) [44].

The findings here directly correlate with those of the destructive analysis where no IMC formation was observed.

The amount by which R_c decreases varies between ball bonds. The ball bonds with higher initial R_c show a greater drop during aging. R_c is affected by interfacial gaps (unbonded area) that are nanoscopic in size and located at different locations of the bonded interface. The amount of such gaps varies between the ball bonds. During aging, the gaps possibly experience a gradual filling by Pd or Au atoms diffusing into them as shown in the TEM-EDS analysis in chapter 5. Bonds starting with a relatively large amount of interfacial gaps (higher contact resistance) would experience substantial gap filling and therefore a relatively large decrease in R_c. Over time, the rate of decreases declines as less gap and dislocations are available near the contact zone to be filled.

6.4 Summary

The in-situ contact resistances of ball bonds are measured while they are aged at 250 °C over 250 h. No evidence of IMC formation has been found. For the baseline sample, R_c does not increase during aging period. In contrast, it tends to drop. This indicates the electrical integrity of the interconnections is maintained. In general, the reliability of the baseline sample show signs of improvement over the standard Au-Al process, where IMC formation and R_c rise are known at lower temperature and time used in this process.

7. Roughness Modulation

The roughness of the metallization is modulated to investigate the overall process quality and to analyze possible correlations between this adhesion modulator and the Au/Pd ball bond process.

7.1 Experiment

Excessive roughness has been found to influence the quality of the wirebond [35]. A typical bonding substrate has a roughness R_a much smaller than the diameter of the bond [52]. For too large R_a, the bondability is degraded as the asperities on the surface are too large to be broken down during the process. An upper limit for R_a of 0.5 μm is chosen in this study, which is at the upper end of the values used in typical wire bonding processes.

Three coupons are produced with roughness types and values different from those of the polished baseline sample. The roughness is introduced on the Cu before plating and the plated Ni and Pd roughnesses rare within 5 % of that of Cu. The electroless Ni and electrolytic Pd processes developed previously were used for the roughened samples. The plating parameters remain the same for regardless of the coupon roughness.

Three different processes are used to vary the roughness of the coupons. The first coupon (sample 1) used in the process is directly used after shipping. The R_a is about 0.2 μm and is directional due to the pre-rolling process of the Cu foil before shipment. The second coupon (sample 2) is mechanically scratched by 600 grit sand paper in one direction for five minutes. The R_a of the scratched coupon is about 0.4 μm and is conformal to the direction of the scratches. Figure 56a shows the photo of samples 1 and 2 with increase in R_a compared with Fig. 56b and 56c for the baseline and standard Ag substrate used in the laboratory. The coupons are mounted on a 90° stub with carbon tape for handling purposes.

The last coupon is sandblasted with glass beads between 170 µm to 325 µm, supplied by Flex-O-Lite, St. Louis, USA. Sandblasting is performed with the minimum recommended allowable pressure of 15 psi over 5 s with the sandblast machine supplied by Ritchey Supply Ltd, Vancouver, Canada, shown in Fig. 57a. A sandblasted sample (sample 3) is shown in Fig. 57c. The R_a of sample 3 is 0.5 µm. During sandblasting, the sandblast gun is held at a 45° angle, and about 5 cm away from the coupon. The coupon is fixed to the stub by carbon tape similar to the two previous

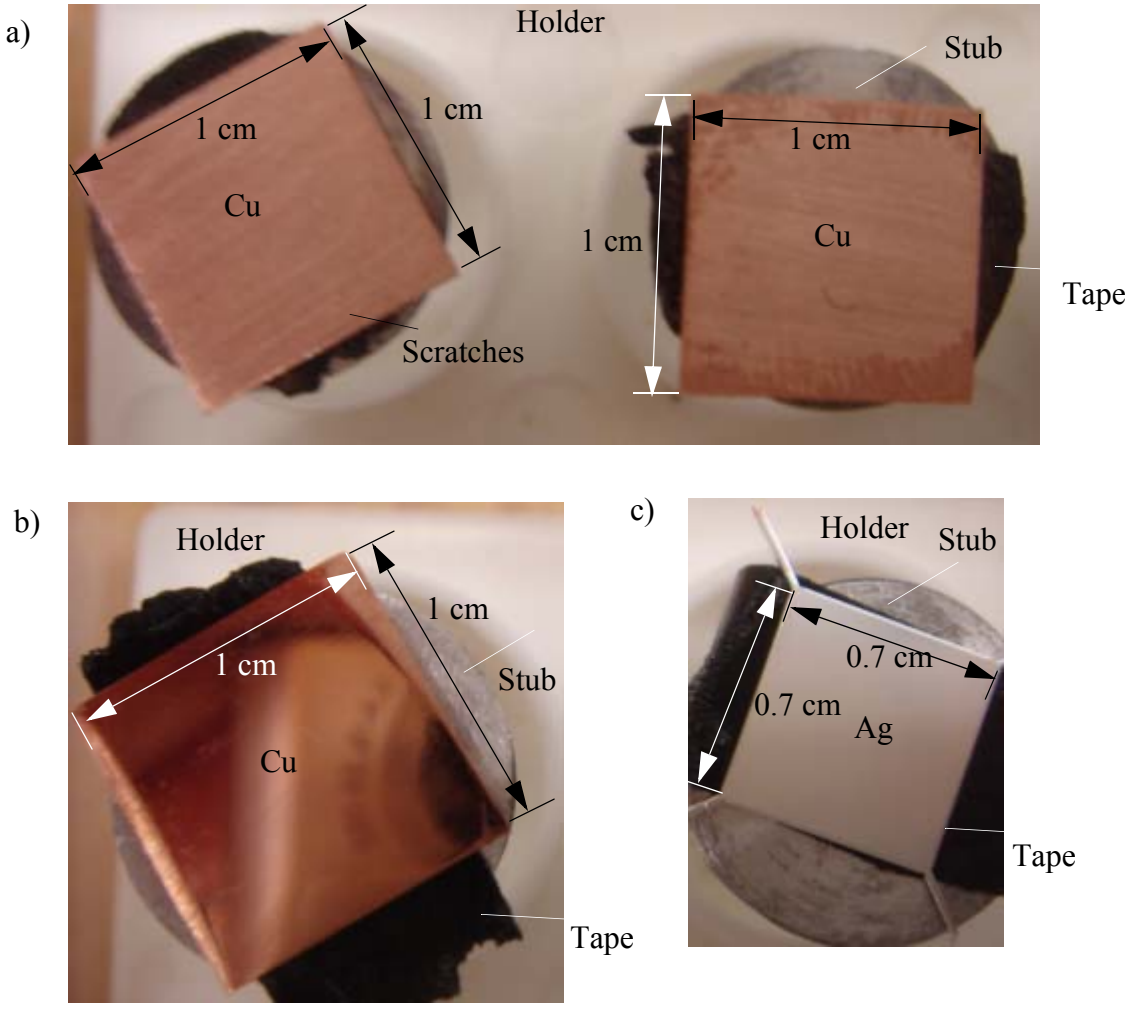

Figure 56 Roughness measurement samples of a) Cu after sanding with 500 grid sand paper, b) Cu after standard grinding and polishing, and c) standard Ag bondpad.

coupons. The operation ensures consistent results if repeated under the same conditions. Both pressure and time are directly correlated to R_a and ensure uniform distribution of the bead across the surface of the coupon in the process. Lower pressure or time values cannot ensure an uniform bead distribution with this machine, and therefore, lower values of R_a cannot reliably be achieved with the existing setup. The sandblast process introduces random roughness in contrast to the previous two samples. The abrasive used in the process is shown in Fig. 57c. The sandblast machine is replenished periodically when the bead are used up or after long storage.

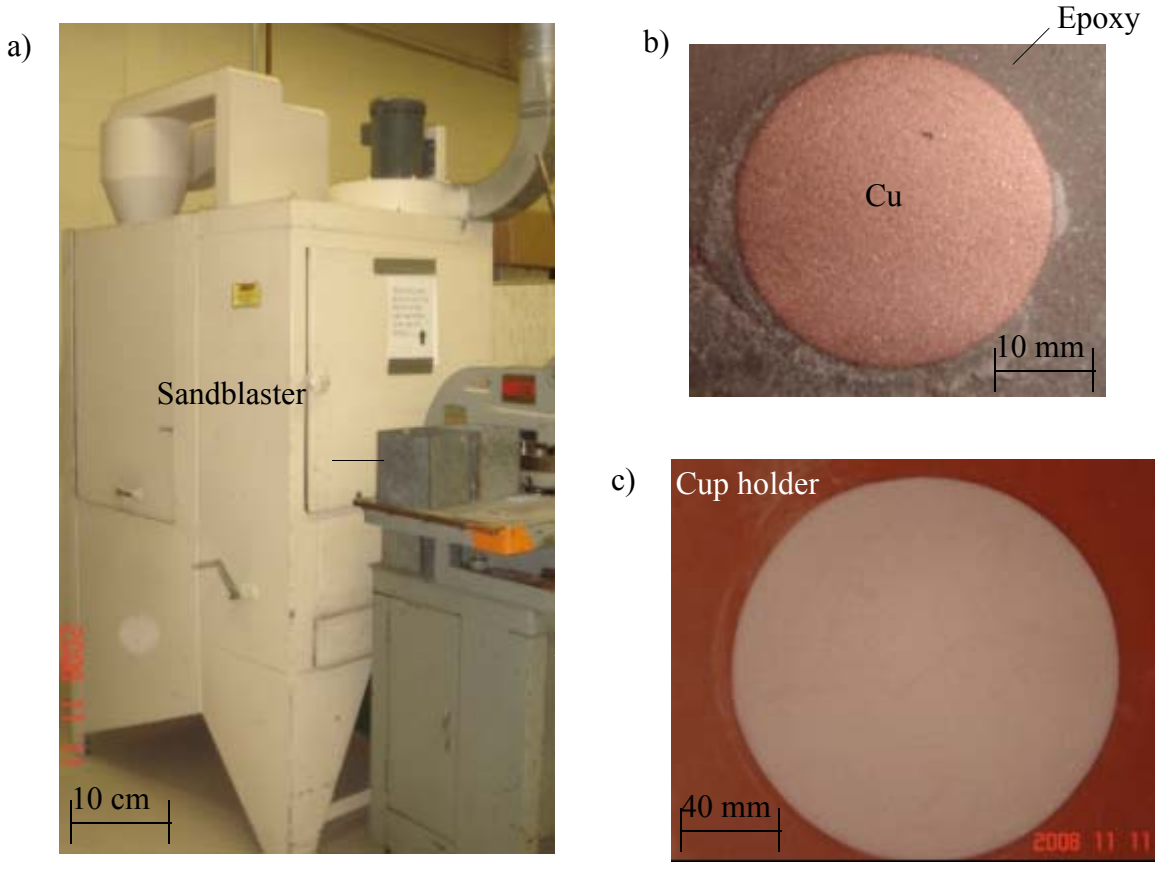

Figure 57 Overview of sandblasting a) machine, b) sample, and c) fine bead.

Before and after adding roughness to the Cu coupons, the samples are cleaned and stored in the same manner as the baseline samples.

The optical profiler is used to measure and analyze the magnitude and direction of the roughness, respectively. Figure 58a and 58b show the optical image and R_a measurement of the original baseline sample. Figures 59a, 59b, and 59c show optical images for sample 1, 2 and 3, respectively. Figures 59d, 59e and 59f show the corresponding optical profiler R_a measurements.

7.2 Wire Bonding Process Adjustments

The same ball bond optimization procedure used previously for the baseline sample was applied on the different roughness substrates. The optimized ball bonding factors are shown in Table 15. The optimized US parameter is reduced in the rage of 4 % to 18 % for depending on the roughness of the samples. while the remaining parameters are mostly the same. The average FAB diameters measured for the rough samples were lower than those of the baseline sample as shown in Fig. 60a. The other responses include average MBD and BH values shown in Figs. 60b and 60c,

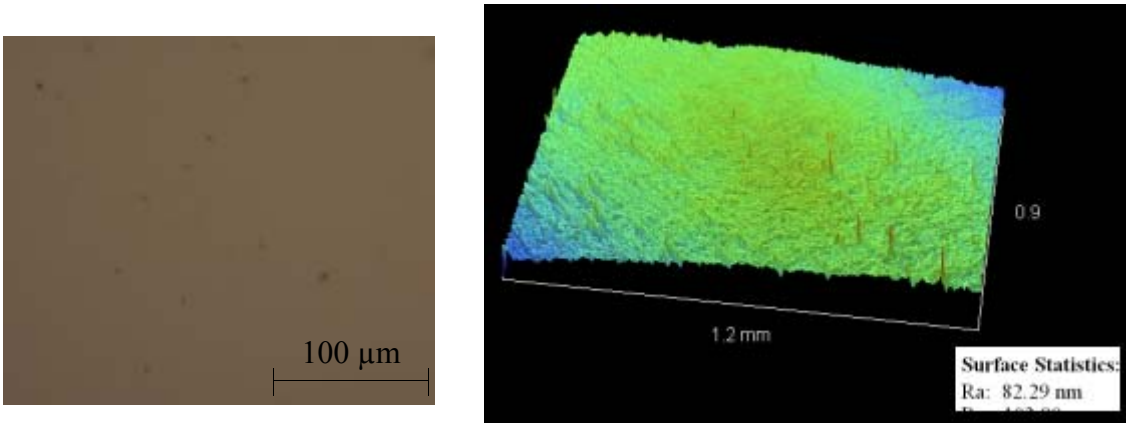

Figure 58 Optical microscope image of a) polished baseline sample with b) optical profiler roughness measurement

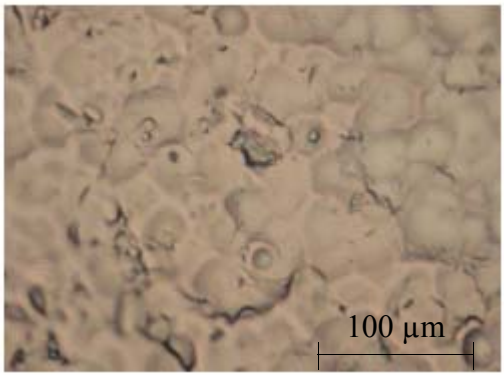

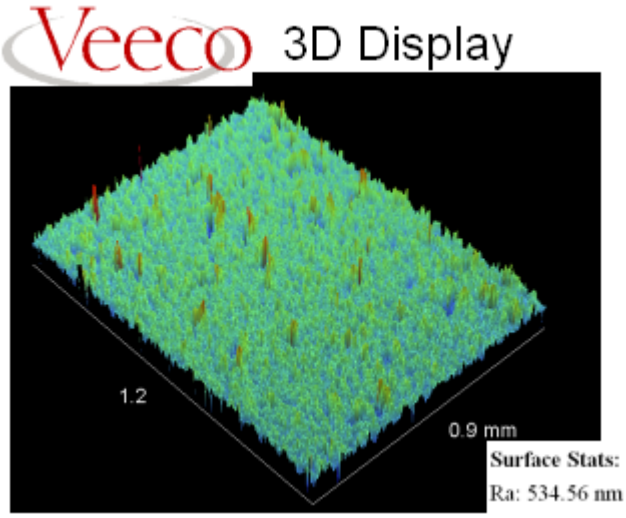

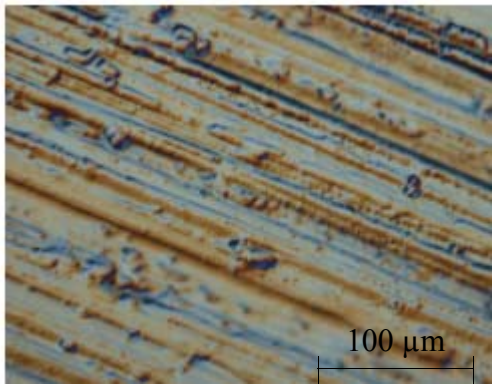

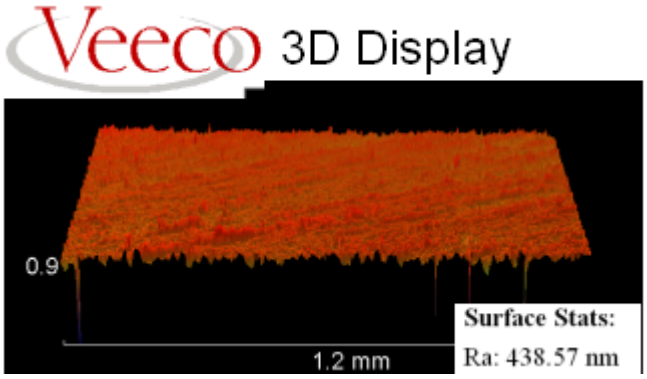

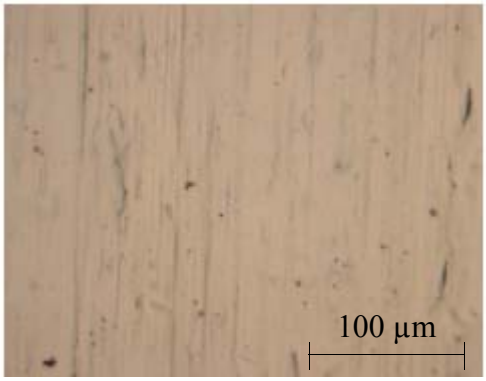

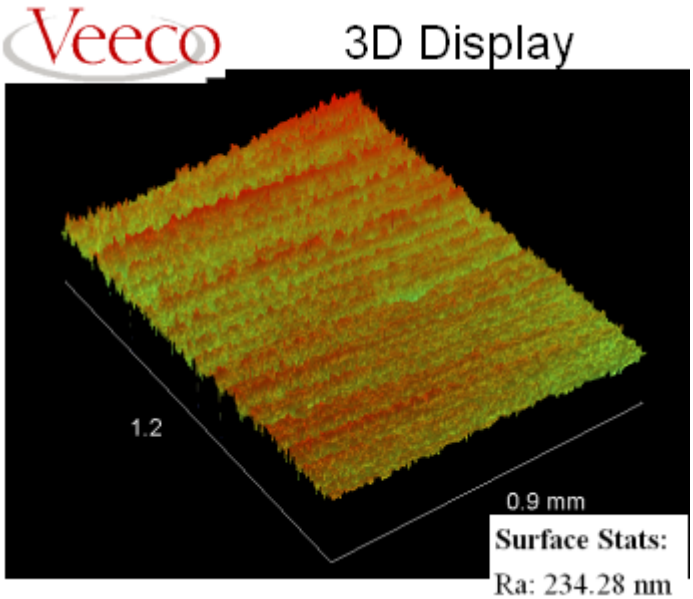

Figure 59 Optical microscope image and corresponding optical profiler measurement of a), d) sandblasted, b), e) sandpaper, and c), f) as shipped Pd/Ni/Cu coupon

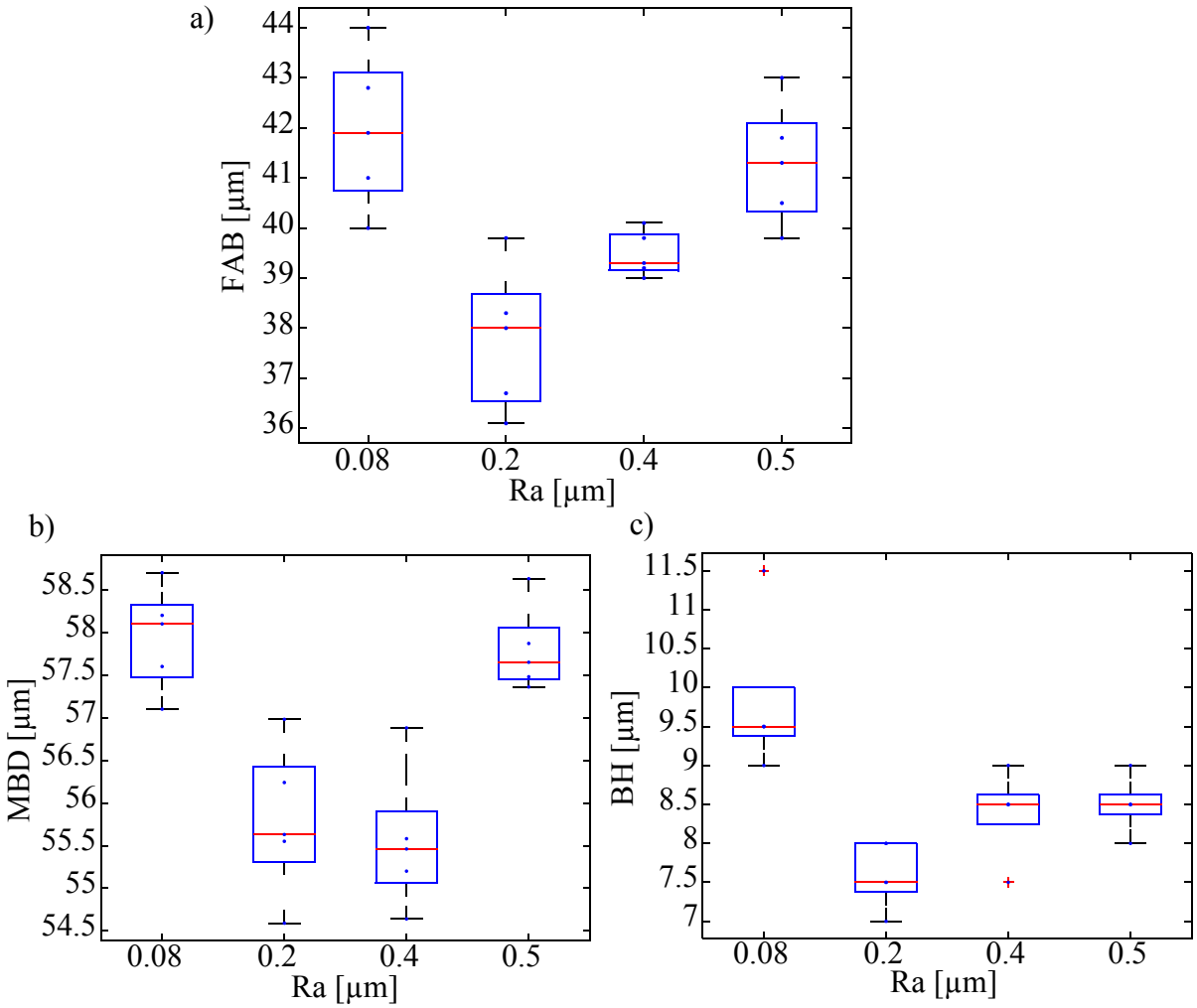

Figure 60 Variation in a) FAB, b) MBD, and b) BH with respect to change in roughness of Pd/Ni/Cu

Table 15: Ball bonding parameters with various roughness substrate

Sample	Ra (µm)	IF (mN)	BF (mN)	US (%)	BT (ms)	T (°C)
0	0.08	950	240	36	20	220
1	0.2	850	240	28	20	220
2	0.4	650	240	22	20	220
3	0.5	950	240	18	20	220

respectively. The baseline sample has the largest MBD and BH, resulting MBD and BH vary from 55 to 58 µm and 8 to 10 µm, respectively, and are within the specified ranges. The maximum *SS* obtained with the roughened samples increases with R_a, but is not higher than that obtained with the baseline sample. Similar to the baseline sample, the shear occurs at the ball for all roughened samples. The optimized *SS* for various roughness values are shown in Fig. 61. The *SS* increases with roughness for R_a above 0.08 µm. The average *SS* of Au ball bonds on the sandblasted specimen is comparable with that of polished baseline sample, while the other specimens have a relatively lower *SS*.

7.3 Non-Destructive Analysis

For comparison with the in situ R_c measurements of the baseline sample, sample 2 was aged over 200 h at 250 °C. The *TC* at the reference temperature of 20 °C is about 5.8% higher after aging. Figure 62a shows R_c of ball bonds #13, #8 and #6 with the most, typical and least change, respec-

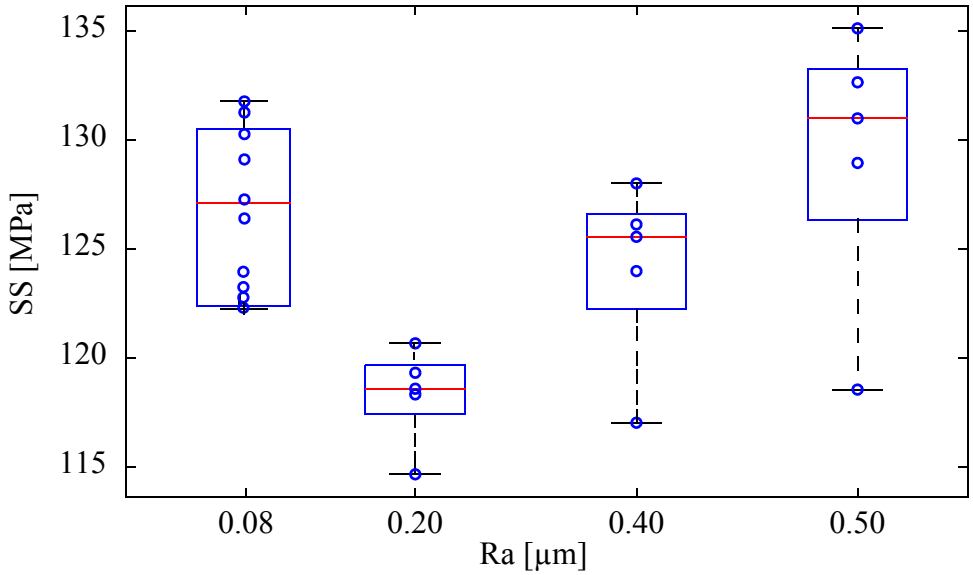

Figure 61 Au ball bond shear strength variation with roughness

tively. The cool down phase results are not shown. The heat up phase is similar to the baseline sample and shown in Fig. 65b, where an increase in R_c from increase in temperature occurs. During the aging phase, the R_c can increase as indicated clearly for ball bonds #13, This trend is opposite to that of the ball bonds on the baseline sample. Figure 63 shows the R_c of the remaining ball bonds. R_c increases for all thirteen ball bonds. Table 16 lists the comparison between R_c at different stages of the aging process.The R_{ref}^{pre} is below that of the R_{ref}^{post} for all thirteen ball bonds shown in Table 16. The median change is 5 %.

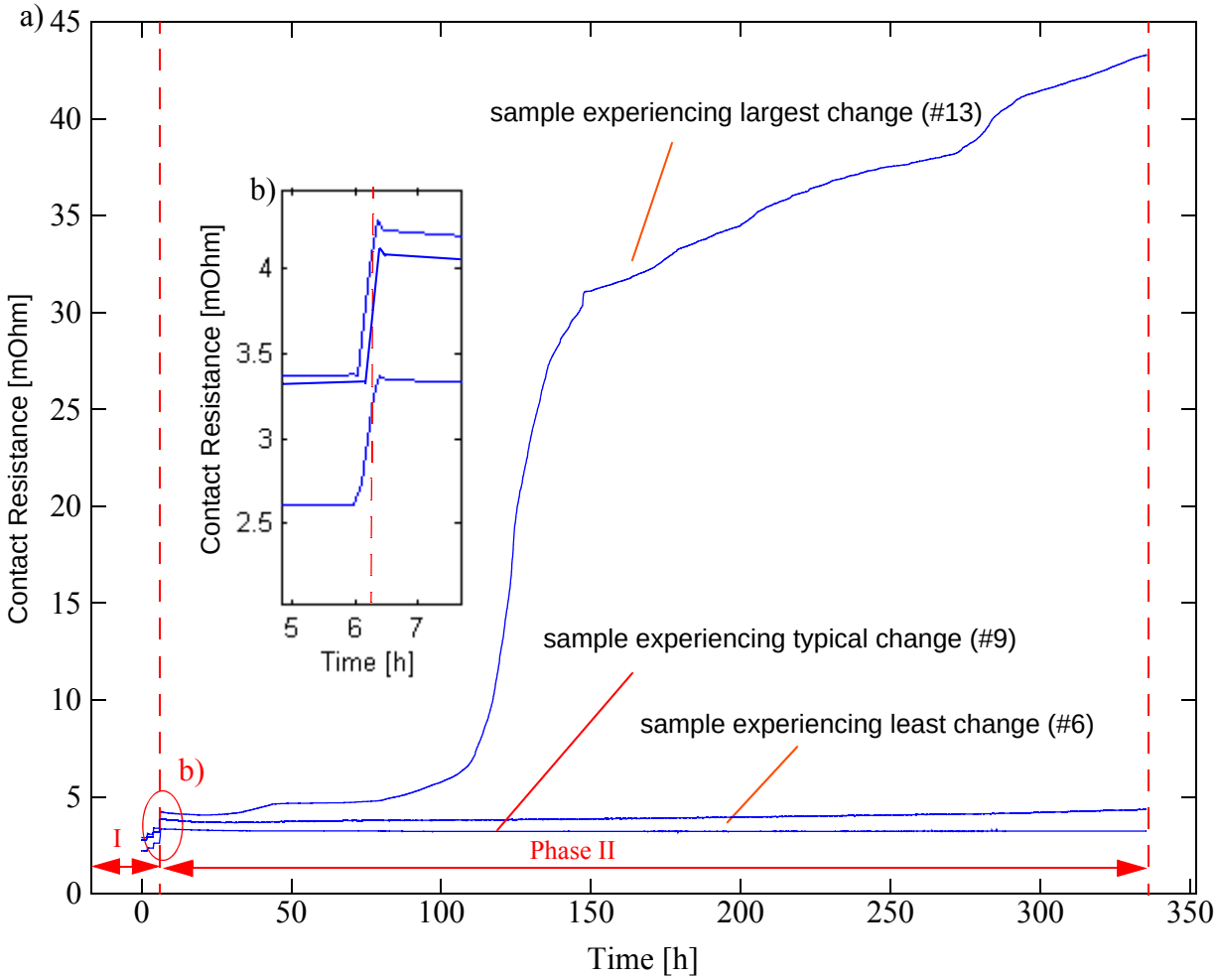

Figure 62 Contact resistance measurements for coupons with R_a of 0.4 µm. T = 250 °C during phase II.

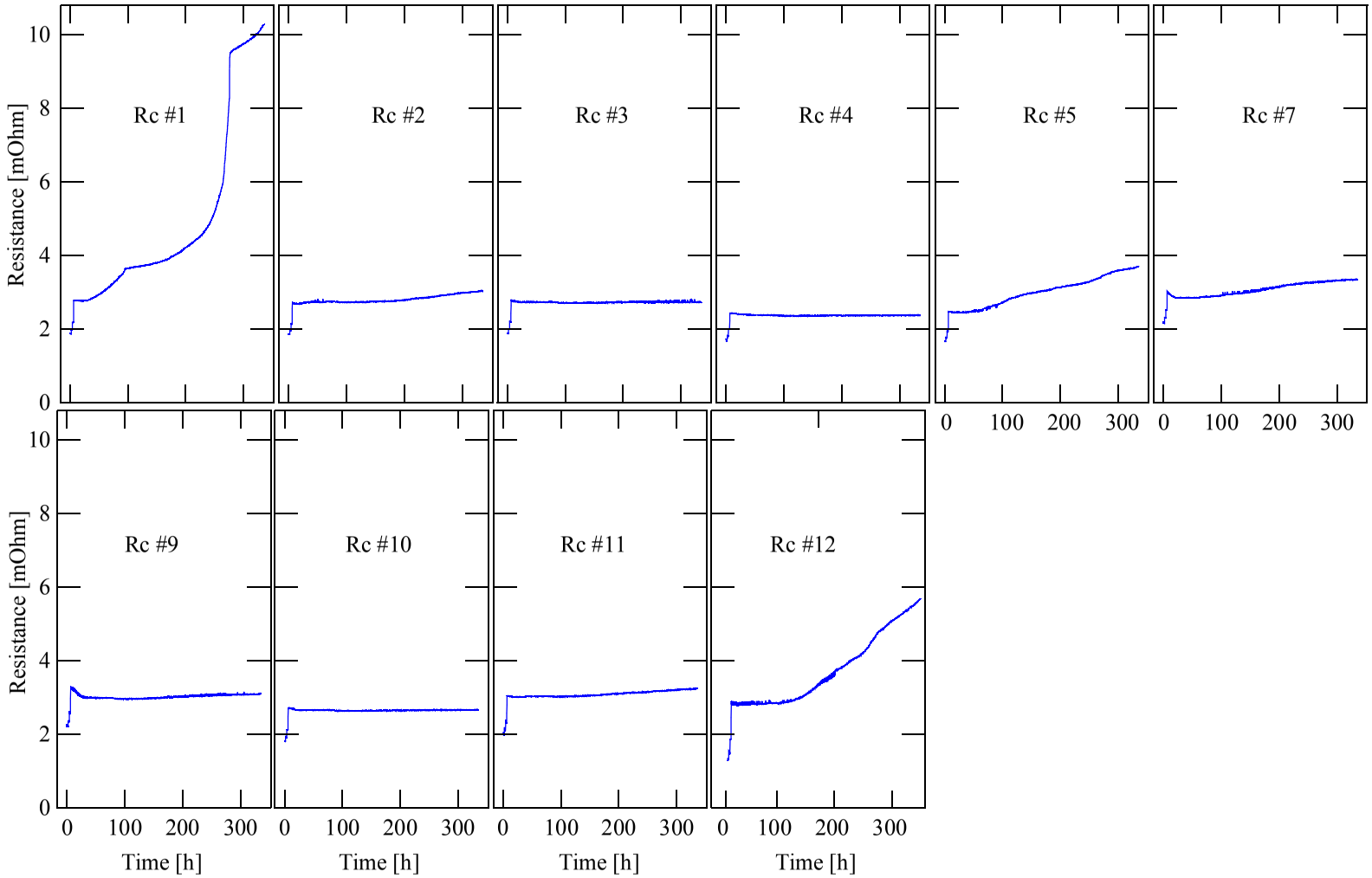

Figure 63 Contact resistance measurements for ball bonds 1-7, and 7-12 through 287 h aging at 250 °C.for coupon with R_a of 0.4 µm.

Same contact resistance measurement is repeated for the two remaining roughened samples. In order to measure the R_c for both samples during aging simultaneously using one multiplexer, six ball bonds were made for each of the two remaining roughened samples. Figure 64 shows the variation in R_c for the six ball bonds on sample 3. The six ball bonds shown in Fig. 64 contain the largest change (ball bond #3), typical (ball bond #5) and least change (ball bond #4) in R_c for sample 3. All six ball bonds shows the same trend, where R_c increases during aging. Similar to

Table 16: Comparison between contact resistance at different stages of aging for R_a= 0.4 µm sample (sample 2).

Ball Bond	Before aging R_{ref}^{pre} (mΩ)	During Aging Average Resistance (mΩ)	During Aging STDEV Resistance (mΩ)	After aging R_{ref}^{post} (mΩ)	Difference before and after (%)
1	1.73	5.2	2.4	7.32	323
2	1.80	2.8	0.11	2.04	13.3
3	1.83	2.7	0.05	1.88	2.73
4	1.64	2.4	0.04	1.68	2.44
5	1.62	3.1	0.37	2.43	50.0
6	2.11	3.2	0.06	2.15	1.90
7	2.23	3.1	0.18	2.34	4.93
8	2.10	3.1	0.16	2.35	11.9
9	2.04	3.0	0.07	2.09	2.39
10	1.71	2.6	0.05	1.79	4.68
11	2.05	3.1	0.9	2.11	2.93
12	1.92	3.5	5.7	3.05	58.8
13	1.82	26.6	146.1	32.63	1690

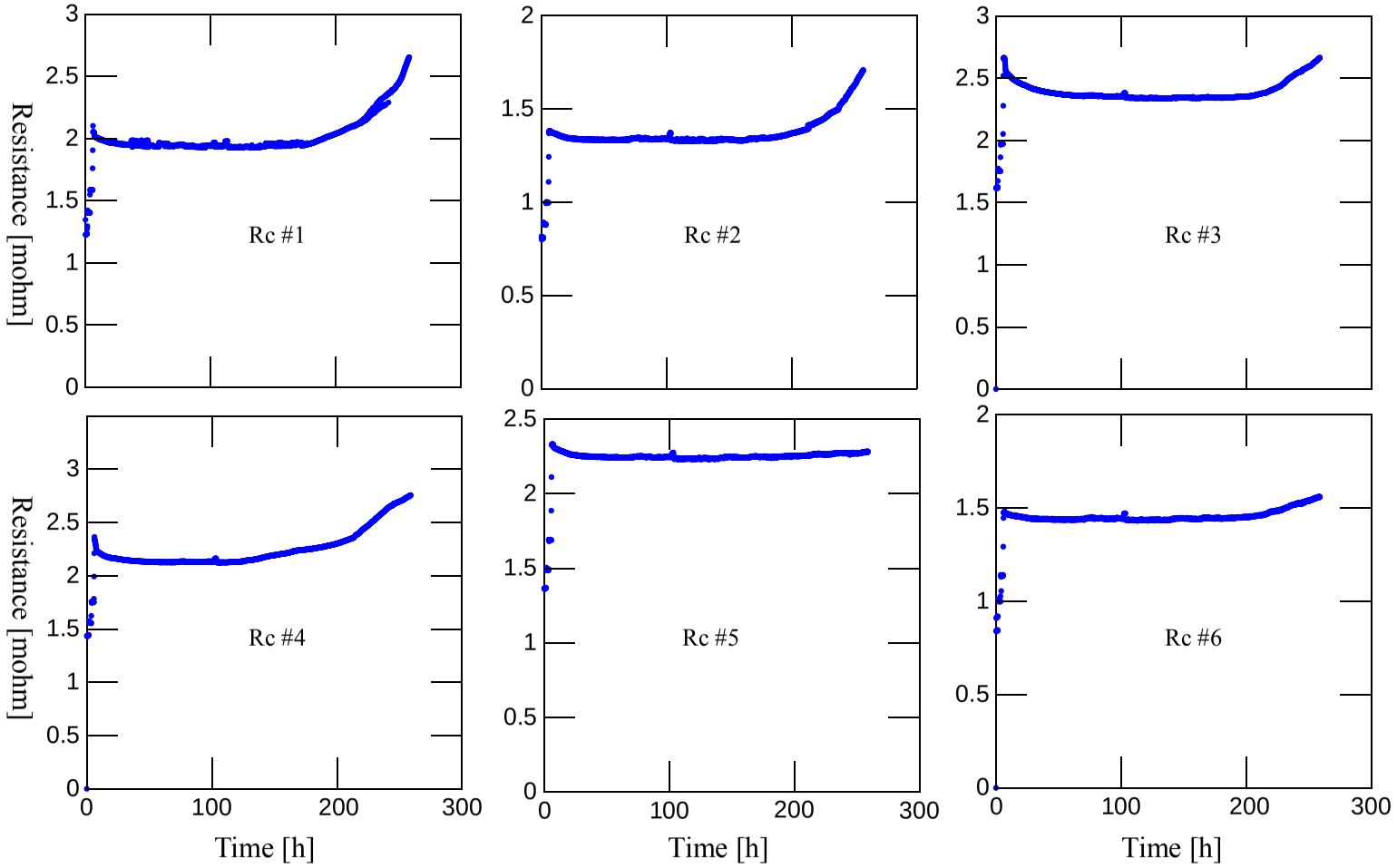

Figure 64 Contact resistance measurements for 6 ball bond through 287 h aging at 250 °C.for coupon with R_a of 0.5 µm.

sample 2, an increase in R_c with increase in temperature is observed in the first stage. During the second stage, the peak temperature of 250 °C is reached, and R_c continue to rise for all six ball bonds. Table 17 shows the R_{ref}^{pre} and R_{ref}^{post} for the six ball bonds on sample 3. The median change is 14 %. As expected, the increase in reference resistance is observed for all six ball bonds. The during aging average and standard deviation of the contact resistance are shown in Table 17.

Figure 65 shows the R_c trend for the six ball bonds on Pd/Ni/Cu on sample 6. The R_c for half the ball bonds (#6, #1 and #3) do show increase with aging time. Ball bond #6, #4 and #1 represents the largest, typical and least change in R_c, respectively. The slope of R_c during aging is less than those of sample 2 and 3. The other half (#2, #4 and #5) of the ball bonds indicate R_c trend similar to that of the baseline sample, where R_c does decreases after aging. The Table 18 shows the R_{ref}^{pre} and R_{ref}^{post} before and after aging, and the average and standard deviation of R_c during aging. The

Table 17: Comparison between contact resistance at different stages of aging for R_a= 0.5 µm sample (sample 3).

Ball Bond	Before aging R_{ref}^{pre} (mΩ)	During Aging Average Resis-tance (mΩ)	During Aging STDEV Resis-tance (mΩ)	After aging R_{ref}^{post} (mΩ)	Difference before and after (%)
1	2.14	2.2	0.21	2.40	12.1
2	1.42	1.5	0.11	1.86	31.0
3	2.62	2.5	0.25	3.08	17.6
4	2.33	2.5	0.14	2.71	16.3
5	2.14	2.5	0.051	2.26	5.61
6	1.58	1.5	0.065	1.73	9.49

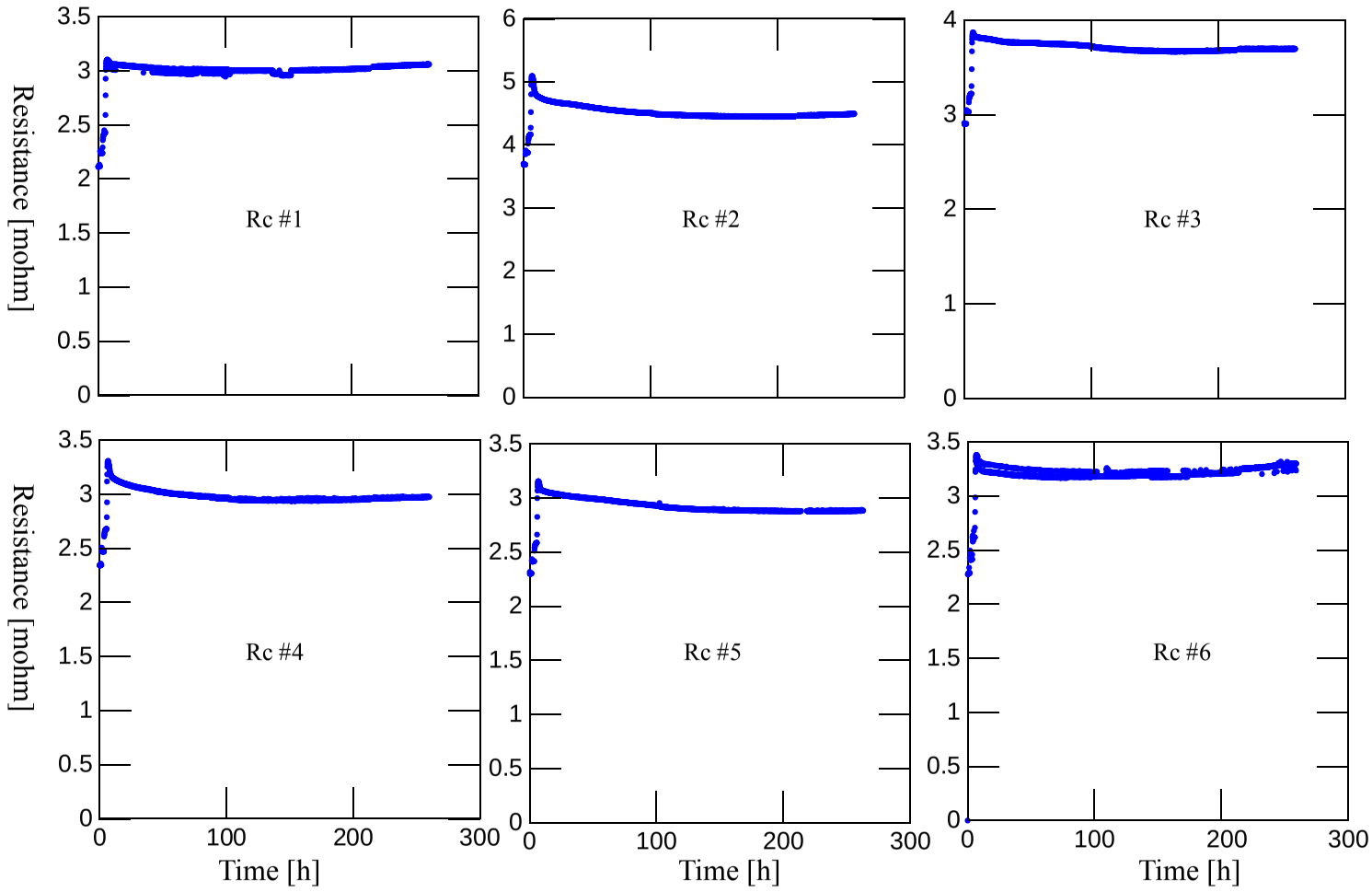

Figure 65 Contact resistance measurements for 6 ball bond through 287 h aging at 250 °C.for coupon with R_a of 0.2 µm.

median change is 0.4 %. Form the analysis observed so far, a direct correlation between the substrate roughness and percentage of ball bonds with increase in R_c can be drawn.

7.4 Destructive Analysis

The same sample preparation of the baseline sample is used for the roughened samples. Figures 66a and 66b show the optical micrographs of cross sections of ball bonds on the as received and the sandblasted samples, respectively, before aging. The different metallic layers are characterized by the difference in contrast in the figures. The asperities from the increase in roughness are visible on the sandblasted sample, and can be seen more clearly in regions away from the bonded area.

7.5 Discussion

A possible reason for the difference in FAB diameters between the roughened and baseline samples is that the wire tail produced by the wedge bond on the samples can have a different shape resulting in a different amount of material pick-up [45] than that produced on the baseline sample.

Table 18: Comparison between contact resistance at different stages of aging for R_a= 0.2 µm sample (sample 1).

Ball Bond	Before aging R_{ref}^{pre} (mΩ)	During Aging Average Resistance (mΩ)	During Aging STDEV Resistance (mΩ)	After aging R_{ref}^{post} (mΩ)	Difference before and after (%)
1	3.23	3.0	0.082	3.34	3.40
2	3.96	4.5	0.13	3.86	-2.52
3	3.44	3.9	0.14	3.58	4.07
4	2.70	3.0	0.069	2.63	-2.59
5	2.38	3.0	0.082	2.31	-2.94
6	2.83	3.3	0.11	3.04	7.42

The amount of material pick-up on the wire tail has an effect on the diameter of the FAB subsequently formed.

With regard to *SS* variation in the bonding process, no reliable value for standard deviation derived from such low sample sizes, the t-test shows the increase in *SS* from ball bonds on the baseline sample to that of sample 8 is not significant. The maximized *SS* of all roughened coupons are comparable to the standard Au ball bond *SS* of 110 MPa.

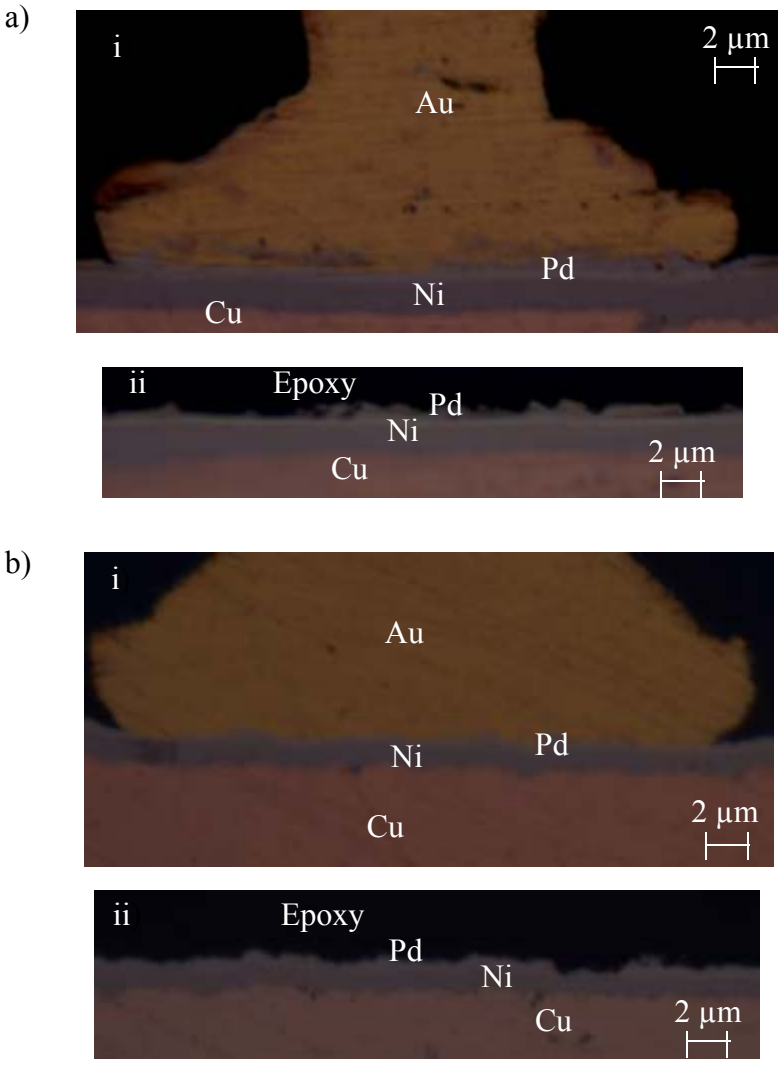

Figure 66 Cross section of ball bonds on Pd/Ni/Cu with roughness of a) 0.2 µm and b) 0.5 µm before aging i) at the ball bond and ii) away from ball bond.

The increase in R_c and R_{ref} from pre to post aging for the roughened samples can be correlate to possible voids, IMC formation at the interfaces and/or impurities from the roughness particles, which grow with increase in temperature, reducing the contact area between the Au ball and Pd/Ni/Cu surface, but further cross section analysis is required to give more conclusive details supporting the claim.

The reliability of the Au/Pd process with increase in R_a in this study remains an improvement over the Au/Al process, where R_c grows linearly at 250 °C, and does not saturate with time [55]. However, compared to the baseline sample, the reliability of the roughened sample is degraded.

7.6 Summary

The roughness of the Pd/Ni/Cu substrate as shipped from manufacturer are varied by scratching, sandblasting and mechanically polishing. The sandblast sample has a random roughness of 0.5 µm, while the as received and scratched sample have directional roughness of 0.2 µm and 0.4 µm, respectively.

Bonding optimization made on the various roughened samples shows an increase in the US for successful bonding on roughened substrates. The final *SS* increases with R_a for the roughened sample, and remains comparable to that of the standard Au-Al process.

The R_c of the roughened samples shows increase with aging time, which is the opposite trend to that of the baseline samples. The median and percentage of ball bonds for the R_c increase directly correlate with substrate roughness.

No conclusive evidence is available to justify the increase in R_c for the roughened samples as additional destructive analysis to investigate voids and/or IMC formation at the cross section is planned.

8. Conclusions

The Ni and Pd plating processes developed in this project can be used to coat Cu base material to produce substrates for bonding process studies. Methods to produce roughness variations of the substrates are developed using sandblasting or sandpaper processes, and produce surface modulation suitable for the bonding process studies. The standard ball bonding optimization procedure described was applicable for all produced Pd/Ni/Cu substrates, resulting in mostly uniform bond strength and geometry. The shear strength and shape of the ball bonds are comparable to those typically obtained for Au ball bonds on Al metallization.

Ball bonds were made and aged by high temperature storage. For the aging temperature and duration chosen, TEM analysis indicates some Au diffusion into the Pd layer. SEM, TEM, nanohardness, and contact resistance measurements showed no evidence of intermetallics and void formation at the Au/Pd interface. However, intermetallics and voids may occur when aging at higher temperature or for longer durations. With a low enough roughness, lack of interfacial impurities, and the similarity in lattice structure and constant between Au and Pd, the nature of the bond is determined to be a chemical bond of metallic type.

This study confirms that the bondability and reliability of the Au to Pd system are superior to those of the standard Au to Al system, i.e., the overall electrical integrity of the interconnection is enhanced. Increasing the roughness does not improve the Au to Pd reliability. However, the amount of ultrasound required for successful bonding is reduced.

References

[1] Harman G *"Wire-bonding in microelectronics materials process reliability and yield",* McGraw-Hill Publishers, NY, 1990

[2] Karpel, A., Gur, G., Atzmon Z., and Kaplan, W. D., "*Microstrctural evolution of gold-aluminum wire-bonds",* Journal of Mater Sci., Feb 2007, pp. 2347-2357

[3] Hang *et al.* "*Growth behavior of Cu/Al compounds and cracks in copper ball bonds during isothermal aging",* Microelectronics, Mar 2007, pp. 416-424

[4] Deley, M., and Levine, Lee., "*The Emergence of High Volume Copper Ball Bonding",* SEMICON West Conference, Jan 2004

[5] Shah *et al. "Reduction of Underpad Stress in Thermosonic Copper Ball Bonding",* IEEE, 2008, pp. 2123-2131

[6] Tan, C. W., and Daud, A. R., *"Bond pad cratering study by reliability tests",* Journal of Material Science, Nov 2004, pp. 309-314

[7] Shingo, K., Nonaka, T., and Mizoguchi, A., *"The Development of Cu Bonding Wire With Oxidation-Resistant Metal Coating",* IEEE, May 2006, pp. 227-232

[8] Yamada *et al. "Reliability of wire-bonding and solder joint for high temperature operation of power semiconductor device",* Microelectronics Reliability, Dec 2007, pp. 2147-2151

[9] Jun-hui, L., Lei, H., and Jue Z., *"Atomic Diffusion Properties in Al/Ni & Au/Al Bond Interface",* IEEE, Jun 2005, pp463-466

[10] Long Z., Han L., Wu, Y., and Zhong, J., *"Study of Temperature Parameter in Au-Ag Wire Bonding",* IEEE, Jul 2008, pp. 221-227

[11] Snugovsky, P., Arrowsmith P., and Romansky M., *"Electroless Ni/Immersion Au interconnects" Investigation of black pad in wire bonds and solder joints",* Journal of Electronic Materials, Jul 2007, pp. 1262-1270

[12] Fan, C., Abys, A. J., and Blair, A., *"Gold and aluminum wire bonding to palladium surface finishes",* MCB University Press, Mar 1999, pp. 23-27

[13] Fan, C. *et al. "Gold Wire Bonding To Nickel/Palladium Plated Leadframes",* Plating & Surface Finishing, Jul 2001 pp. 54-58

[14] Okamoto, H., and Massalski, T. B., *"Phase Diagrams of Binary Gold Alloys",* ASM International, 1987.

[15] Arthur, S., *"Chemical vapor deposition for microelectronics: principles, technology, and applications",* Noyes Publications, 1987

[16] Kiyotaka, W., *"Handbook of sputter deposition technology: principles, technology, and applications",* Noyes Publication, 1992

[17] Schlesinger, M., and Paunovic, M., *"Modern Electroplating",* John Wiley & Sons, 2000

[18] Tromans, B., *"The Canning Handbook On Electroplating",* Canning Limited, 1978

[19] Gawrilov, G. G., *"Chemical (Electroless) Nickel-Plating",* IPortcullis Press, 1979

[20] Brugger, R., *"Nickel Plating",* Robert Draper Ltd, 1970

[21] Mayer, M., Schwizer, J., *"Ultrasonic Bonding: Understanding How Process Parameters Determine the Strength of Au-Al Bonds",* Proc. of International Symposium on Microelectronics, 2002, pp. 626-631

[22] *"Method and apparatus for adjusting plating solution flow characteristics at substrate cathode periphery to minize edge effect",* U.S. Patent 5000827

[23] Shigolev, P. V., *"Electrolytic and chemical polishing",* Tel-Aviv, 1974

[24] Liang, H., Craven, D., *"Tribology In Chemical-Mechanical Planarization"* CRC Press, 2005

[25] Hansen, M., *"Constitution of Binary Alloys",* McGraw-Hill, 1901, pp.224

[26] Wire Bond Shear Test Method, Electronics Industries Alliance/JEDEC Standard EIA/JESD22-B116, 1998, PP. 7-8.

[27] Shah, A., Mayer, M., Zhou, Y., and Hong, S. J., *"In-situ Ultrasonic Force Signals during Low Temperature Thermosonic Copper Wire Bonding using Piezo-resistive Microsensors. Microelectronics Engineering",* 85(9) 1851-1857.

[28] Ratchev, P., Stoukatch, S., and Swinnen, B., *"Mechanical reliability of Au and Cu wire bonds to Al, Ni/Au and Ni/Pd/Au capped Cu bond pads"*, Microelectronic Reliability, Dec, 2005, pp.1315-1325.

[29] Poate, J. M., Turner, P., A., and DeBonte, W., J., *"Thin-film interdiffsuion. I. Au-Pd, Pd-Au, Ti-Pd, Ti-Au, Ti-Pd-Au, and Ti-Au-Pd",* J. Appl. Phys., Oct, 1975, pp. 4275-4283

[30] Murakami, M., deFontaine, D., and Fodor, J., *"X-ray diffraction study of interdiffusion in bimetallic Au/Pd thin films",* AIP, Mar 1976, pp. 2850-2857

[31] Zeng *et al. "Kirkendall void formation in eutectic SnPb solder joints on bare Cu and its effect on joint reliability",* Journal of Applied Physics, Dec 2004, pp.024508-1-8

[32] Klengel *et al. "Intermetallic Compound Formation in Au/Al Thermosonic Wire Bonding During High Temperature Annealing at 150°C as a Function of Wire Material",* IEEE, 2006, pp. 370-376

[33] Chang *et al. "Intermetallic Growth of Wire-bond at 175°C High Tempearture Aging",* Journal of Electronic Materials, 2001, pp. 1171-1178

[34] Chang *et al. "Wire-Bond Void Formation During High Temperature Aging",* IEEE 2004, pp. 155-161

[35] Kim, J., and Au B. P. L., *"Effects of Metallizatin Characteristics on Gold Wire Bondability of Organic Printed Circuit Boards",* Journal of Electronic Materials, 2001, pp. 1001-1011

[36] Zhang *et al. " Interface roughness effects on the performance of magnetic tunnel junctions",* Thin Solid Films, Feb 2007, pp. 3941-3945

[37] Electroless Ni plating kit datasheet, Cadwell Inc.

[38] Electro Pd plating, *"Pallaspeed technical datasheet",* Technic Inc.

[39] C. J. Hang *et al., "Online hardness characterization of novel 2-mil copper bonding wires",* Proceedings of ASME InterPACK'07 Conference, 2007.

[40] Samsonov G.V. (Ed.) in *Handbook of the physicochemical properties of the elements*, IFI-Plenum, New York, USA, 1968.

[41] Chang *et al*, "*Wire-Bond Void Formation During High Temperature Aging*", IEEE Transactions on Components and Packaging Technologies, vol. 27, no. 1, pp. 155-160, March 2004.

[42] Mayer M., *"Non-Desctructive Monitoring of Au Ball Bond Stress During High-Temperature Aging",* Electronic Components and Technology Conference, 2008, pp. 1762-1768.

[43] Mayer M., "*Microelectronic Bonding Process Monitoring by Integrated Sensors",* PhD Dissertation ETH No. 13685, Physical Electronics Laboratory, ETH Zurich, Switzerland, 2000

[44] Logie *et al*, *"Effect of Plastic Deformation on resistivity of Gold-Palladium Alloys",* Acta Metallurgica, Aug, 1996, pp. 707-714.

[45] Lee *et al*, "*Silver Pick-Up during Tail Formation and Its Effect on Free Air Ball in Thermosonic Copper Ball Bonding*", Proc. ECTC, 2008.

[46] Breach, C. D. and Wulff, F.,*"New Observations on Intermetallic Compound Formation in gold ball bonds: general growth pattern and identification of two forms of Au_4Al",* Microelectronics Reliability, Apr, 2004, pp.973-981.

[47] Bielmann *et al, "The H2 Plasma Treatment on Silver Contacts: Impact on Wire Bonding Performance",* Journal of Electric Materials, May, 2002, pp.1316-1320

[48] Petzold *et al, "Surface oxide films on Aluminum bondpads: Influence on thermosonic wire-bonding behavior and hardness",* Microelectronics Reliability, Oct, 2000, pp.1515-1520

[49] Krzanowski E. J. and Murdeshwar N., *"Deformation and Bonding Processes in Aluminum Ultrasonic Wire Wedge Bonding",* Journal of Electronic Materials, Apr, 1990, pp.919-928

[50] Murali S, Srikanth N, and Vath C. J., *"Effect of wire size on the formation of itnermetallics and Kirkendall voids on thermal aging of thermosonic wire bonds",* Materials Letters, Jun, 2004, pp. 3096-3101

[51] Flis J. and Duquette D. J., *"Initiation of Electroless Nickel Plating on Copper, Palladium Activated Copper, Gold, and Platinum"* Electrochemical Science and Technology, Feb, 1984, pp. 254-260

[52] Pecht, M. *"Handbook of Electronic Package Design",* CRC, 1991

[53] McGuire G. E., Jones, J. V. and Dowell H. J., *"The Auger Analysis of Contaminants that Influence the Thermocompression Bonding of Gold"*, Thin Solid Films, Apr. 1997, pp. 59-68

[54] Lin *et al. "Surface topographical characterization of silver-plated film on the wedge bondability of leaded IC packages",* Microelectronics Reliability, Jan. 2003, pp. 803-809

[55] Caers *et al. "Conditions for Reliable Ball-Wedge Copper Wire Bonding",* IEEE Japan Int'l Electronics Manufacturing Technology Symposium, 1993, pp. 312-315

[56] Lin *et al. "The evaluation of copper migration during the die attach curing and second wire bondign process",* Proceedings of the IEEE ECTC, 2002

[57] Pt100 Platinum Resistance Thermometers datasheet, Pico Technology.

Appendix A

Matlab program “Rc Resistance Measurement_YH.m” for measuring contact resistances of the samples in the study.

```
Desired_Alpha_Temps = [20 50 100 200 250];
cutoff = 4*3600;%time then data goes unreliable
cutoff_post = 293.7*3600; %after ageing when data becomes reliable again
cutoff_post2 = 301*3600;
POSTCOMPLETED = 0;

%DELETE---------------
    a1 = 295*3600; a2 = 296.5*3600;     %50 deg post ageing
    b1 = 298*3600; b2 = 299.5 * 3600;   %100 deg post ageing
    c1 = 302*3600; c2 = 304.5*3600;      %250 deg post ageing

    d1 = 0.5; d2 = 1.5*3600; dd1=1;         %20 deg pre ageing
    e1 = 2.6*3600; e2 = 3.7*3600;           %50 deg pre ageing
    f1 = 4.4*3600; f2 = 6*3600;             %100 deg pre ageing
    g1= 10*3600; g2 = 300*3600;             %250 deg pre ageing
    s=[];
    spre=[];
% END DELETE

open('sandpaper_ambient_temp__20090209T160045.mat');


%1 - Find Average Slope between temp and res
slopes = [];%avg slope for each sample
for j = 1:13;%cycle thru all bond pairs
    num_meas = length(y((1:1:end),1,j)/3600); %how many measurements taken
    %cycle thru and get slope at each increment
    Slope = []; %add each incremental slope to array and take mean after
    for i = 1:num_meas-1
        %DELETE -------------
            if y(i,1,j)<d1; dd1 = i; end
            if y(i,1,j)<d2; dd2 = i; end
            if y(i,1,j)<e1; ee1 = i; end
            if y(i,1,j)<e2; ee2 = i; end
            if y(i,1,j)<f1; ff1 = i; end
```

```
            if y(i,1,j)<f2; ff2 = i; end
            if y(i,1,j)<g1; gg1 = i; end
            if y(i,1,j)<g2; gg2 = i; end
        %END DELETE
        if y(i,1,j)<cutoff; %only take readings from before PT breaks
            DR = y(i+1,3,j)-y(i,3,j);
            DT = y(i+1,2,j)-y(i,2,j);
            if DT > 0 || DT< 0; %To avoid dividing by 0
                Slope = [Slope abs(DR/DT)]; %Add to collection of slopes
            end;
        end
    end
    %DELETE
        T20 = mean(y(dd1:dd2,2,j)); R20 = mean(y(dd1:dd2,3,j));
        T50 = mean(y(ee1:ee2,2,j)); R50 = mean(y(ee1:ee2,3,j));
        T100 = mean(y(ff1:ff2,2,j)); R100 = mean(y(ff1:ff2,3,j));
        T250 = mean(y(gg1:gg2,2,j)); R250 = mean(y(gg1:gg2,3,j));
        s11 = (R100-R50)/(T100-T50); s22 = (R250-R50)/(T250-T50); %s33 = (R50-
R20)/(T50-T20);
        %spre = [spre (s11+s22+s33)/3]; s_cur = (s11+s22+s33)/3;
        %spre = [spre (s11+s22)/2]; s_cur = (s11+s22)/2;
        spre = [spre s11]; s_cur = s11; % Changed to get rid of s12 because
drift occurs
    %DELETE
    slopes = [slopes mean(Slope)]; %mean slope for each sample
end
slopes = spre;
m = mean(slopes)

%2. Given Average Slope, Find Average Intercept
inters = [];%avg Intercept for each sample
for j = 1:13;%cycle thru all bond pairs
    num_meas = length(y((1:1:end),1,j)/3600); %how many measurements taken
    %cycle thru and get slope at each increment
    Intercept = []; %add each incremental slope to array and take mean after
    for i = 1:num_meas-1;
        if y(i,1,j)<cutoff; %only take readings from before PT breaks
            b = y(i,3,j)-slopes(j)*y(i,2,j);
            Intercept = [Intercept abs(b)];
        end
    end
```

```
    inters = [inters mean(Intercept)];
end

b = mean(inters) %mean intercept for each sample

%3. Calculate Coefficient for desired temperatures
ALPHAS = []; %Individual Alpha for each sample at each desired temp
ALPHAS_dev = [];
Avg_ALPHAS = []; %Avg Alpha for each desired temp
Alpha_STD = [];% stdev for each group of ALPHAS per temperature


for i = 1:length(Desired_Alpha_Temps);
    for j = 1:13
       ALPHAS (i,j) =  slopes(j)/(slopes(j)*Desired_Alpha_Temps(i)+inters(j));
        %ALPHAS_dev (i,j) = [
    end
    Avg_ALPHAS = [Avg_ALPHAS m/(m*Desired_Alpha_Temps(i) + b)];
    Alpha_STD = [Alpha_STD std(ALPHAS(i,:))];
end

% GET avg resistance and std res of resistance
Avg_RES_250 = [];
STD_PER_SAMPLE_250=[];

for j = 1:num_meas
    if y(j,1,1)< (30*3600); t_30 = j; end
    if y(j,1,1)< (250*3600); t_250 = j; end
end

for i = 1:13
    Avg_RES_250 = [Avg_RES_250 mean(y((t_30:end),3,i))];
    STD_PER_SAMPLE_250=[STD_PER_SAMPLE_250 std(y((t_30:end),3,i))];
end
    Avg_RES_250_std = std(Avg_RES_250)



%REPEAT FOR POST AGEING:!------------------------
if POSTCOMPLETED == 1
```

```
s=[];
slopes_post = [];%avg slope for each sample
for j = 1:13;%cycle thru all bond pairs
    num_meas = length(y((1:1:end),1,j)/3600); %how many measurements taken
    %cycle thru and get slope at each increment
    Slope_post = []; %add each incremental slope to array and take mean after
    for i = 1:num_meas-1
        %DELETE -------------
            if y(i,1,j)<a1; aa1 = i; end
            if y(i,1,j)<a2; aa2 = i; end
            if y(i,1,j)<b1; bb1 = i; end
            if y(i,1,j)<b2; bb2 = i; end
            if y(i,1,j)<c1; cc1 = i; end
            if y(i,1,j)<c2; cc2 = i; end
        %END DELETE
        if y(i,1,j)>cutoff_post && y(i,1,j)<cutoff_post2; %only take readings
from before PT breaks
            DR_post = y(i+1,3,j)-y(i,3,j);
            DT_post = y(i+1,2,j)-y(i,2,j);
            if DT_post > 0 || DT_post< 0; %To avoid dividing by 0
                Slope_post = [Slope_post abs(DR_post/DT_post)]; %Add to
collection of slopes
            end;
        end
    end
    %DELETE-----------
        T50 = mean(y(aa1:aa2,2,j)); R50 = mean(y(aa1:aa2,3,j));
        T100 = mean(y(bb1:bb2,2,j)); R100 = mean(y(bb1:bb2,3,j));
        T250 = mean(y(cc1:cc2,2,j)); R250 = mean(y(cc1:cc2,3,j));
        s1 = (R100-R50)/(T100-T50); s2 = (R250-R50)/(T250-T50); s = [s
(s1+s2)/2]; s_cur = (s1+s2)/2;
        %b1 = (R50-s_cur*T50); b2 =
    %END DELETE
    slopes_post = [slopes_post mean(Slope_post)]; %mean slope for each sample
end
slopes_post = s;
m_post = mean(slopes_post)

%2. Given Average Slope, Find Average Intercept
inters_post = [];%avg Intercept for each sample
for j = 1:13;%cycle thru all bond pairs
```

```
    num_meas = length(y((1:1:end),1,j)/3600); %how many measurements taken
    %cycle thru and get slope at each increment
    Intercept_post = []; %add each incremental slope to array and take mean
after
    for i = 1:num_meas-1;
        if y(i,1,j)>cutoff_post && y(i,1,j)<cutoff_post2; %only take readings
from before PT breaks
            b_post = y(i,3,j)-slopes_post(j)*y(i,2,j);
            Intercept_post = [Intercept_post abs(b_post)];
        end
    end

    inters_post = [inters_post mean(Intercept_post)];
end

b_post = mean(inters_post) %mean intercept for each sample

%3. Calculate Coefficient for desired temperatures
ALPHAS_post = []; %Individual Alpha for each sample at each desired temp
ALPHAS_dev_post = [];
Avg_ALPHAS_post = []; %Avg Alpha for each desired temp
Alpha_STD_post = [];% stdev for each group of ALPHAS per temperature


for i = 1:length(Desired_Alpha_Temps);
    for j = 1:13
        ALPHAS_post (i,j) =
slopes_post(j)/(slopes_post(j)*Desired_Alpha_Temps(i)+inters_post(j));
        %ALPHAS_dev_post (i,j) = [
    end
   Avg_ALPHAS_post = [Avg_ALPHAS_post m_post/(m_post*Desired_Alpha_Temps(i) +
b_post)];
    Alpha_STD_post = [Alpha_STD_post std(ALPHAS_post(i,:))];
end
end

%OUTput Data
%ALPHAS
%ALPHAS_post
%Avg_ALPHAS
%Avg_ALPHAS_post
%Alpha_STD
```

```
%Alpha_STD_post

%Calculate Reference Resistances
Rref_pre_20 = [];
Rref_post_20 = [];
Rref_pre_50 = [];
Rref_post_50 = [];
Rref_pre_100 = [];
Rref_post_100 = [];

    for j = 1:13
        for i = 1:num_meas-1

                if y(i,1,j)<d1; dd1 = i; end
                if y(i,1,j)<d2; dd2 = i; end
                if y(i,1,j)<e1; ee1 = i; end
                if y(i,1,j)<e2; ee2 = i; end
                if y(i,1,j)<f1; ff1 = i; end
                if y(i,1,j)<f2; ff2 = i; end
                if y(i,1,j)<g1; gg1 = i; end
                if y(i,1,j)<g2; gg2 = i; end

                if y(i,1,j)<a1; aa1 = i; end
                if y(i,1,j)<a2; aa2 = i; end
                if y(i,1,j)<b1; bb1 = i; end
                if y(i,1,j)<b2; bb2 = i; end
                if y(i,1,j)<c1; cc1 = i; end
                if y(i,1,j)<c2; cc2 = i; end
        end
            T20 = mean(y(dd1:dd2,2,j)); R20 = mean(y(dd1:dd2,3,j));
            T50 = mean(y(ee1:ee2,2,j)); R50 = mean(y(ee1:ee2,3,j));
            T100 = mean(y(ff1:ff2,2,j)); R100 = mean(y(ff1:ff2,3,j));
            T250 = mean(y(gg1:gg2,2,j)); R250 = mean(y(gg1:gg2,3,j));

            Rref_pre_20 = [Rref_pre_20 R50/(1+ALPHAS(1,j)*(T50-20))];
            Rref_pre_50 = [Rref_pre_50 R100/(1+ALPHAS(2,j)*(T100-50))];
            Rref_pre_100 = [Rref_pre_100 R250/(1+ALPHAS(3,j)*(T250-100))];

            if POSTCOMPLETED == 1
            T50post = mean(y(aa1:aa2,2,j)); R50post = mean(y(aa1:aa2,3,j));
            T100post = mean(y(bb1:bb2,2,j)); R100post = mean(y(bb1:bb2,3,j));
```

```
            T250post = mean(y(cc1:cc2,2,j)); R250post = mean(y(cc1:cc2,3,j));

            Rref_post_20 = [Rref_post_20 R50post/(1+ALPHAS_post(1,j)*(T50-
20))];
            Rref_post_50 = [Rref_post_50
R100post/(1+ALPHAS_post(2,j)*(T100post-50))];
            Rref_post_100 = [Rref_post_100
R250post/(1+ALPHAS_post(3,j)*(T250post-100))];
            end
    end
if POSTCOMPLETED == 1
AvgRref_post = mean(Rref_post_50)
StdRref_post = std(Rref_post_50)
end
AvgRref_pre = mean(Rref_pre_50)
StdRref_pre = std(Rref_pre_50)


save(['Statistics.mat'])
```